3. DESIGN OF STRUCTURES, COMPONENTS, EQUIPMENT, AND SYSTEMS

3.7 SEISMIC DESIGN

3.7.1 SEISMIC INPUT

3.7.1.1 Design Response Spectrum

The soil at the site is a thick (900+ feet) deposit of well-graded dense sand, of essentially uniform properties. The design basis earthquake (DBE) is postulated to occur near the site (5 miles), and the accelerations are postulated to be quite high (0.67g). Because of these site-specific characteristics, the site tends to amplify long-period motions, and to attenuate short-period motions. These site-specific characteristics were accounted for in site-specific analyses, as discussed in appendix 2.5B. In brief, the design spectrum was developed by requiring it to fit over the peaks of the surface response spectra developed from site-specific analyses for input earthquake acceleration time histories scaled to produce a 0.67g ground surface acceleration. Further, the severity of the acceleration time history fitted to the design spectrum (paragraph 3.7.1.2), was compared to that of many recorded acceleration time histories using several measures of severity and was found to be significantly more severe. The measures of severity included: spectral amplification ratio, spectral intensity, pulse distribution, impulse, kinetic energy, and Housner severity parameters. Details of analyses and results of the severity comparison study are presented in appendix 2.5B. The resulting site-specific design spectrum for horizontal motions is shown in figure 3.7-1.

The spectrum of figure 3.7-1 is applicable to both horizontal components. The vertical-motion spectrum has the same shape, but is 2/3 times the horizontal, as also shown in figure 3.7-1. The operating basis earthquake (OBE) response spectra have the same shape but are one-half times those for the DBE, shown in figure 3.7-1.

The site-specific spectral shapes of figure 3.7-1 are valid for damping values other than 2%, but the spectral values are altered based on amplification factors suggested by Newmark and Hall[1] normalized to a value of 3.5 at 2% damping as follows:

	Factor by which to multiply 2% spectral value of acceleration control points	
Damping	A (T = 0.2s)	B (T = 1.0s)
0	1.49	1.49
0.5	1.34	1.34
1	1.20	1.20
2	1.00	1.00
5	0.63	0.63
7	0.46	0.46
10	0.40	0.40

3.7.1.2 Design Basis Earthquake Acceleration Time History

The 80-second duration DBE acceleration time history was developed from a simulated strong-motion record, synthesized by Jennings, Housner, and Tsai.[2] This simulated free-field strong-motion record was modified so that its response spectrum approximates the design response spectrum of figure 3.7-1. Modification of the simulated acceleration time history was accomplished for a response spectrum for 2% damping in 2 steps:

- The acceleration record was scaled linearly to g maximum- acceleration level, consistent with the zero-period acceleration of the design response spectrum.

- Using the spectrum-suppress and spectrum-raising iterative technique developed by Tsai,[3] the acceleration time history was modified until its spectrum appropriately matched the design spectrum (50 iterations were necessary).

The resulting acceleration time history is given in figure 3.7-2. The period intervals used for spectrum calculation are:

Period Range (s)	Oscillator Interval (s)
0.01 to 0.20	0.01
0.20 to 1.80	0.02
1.80 to 2.00	0.05

These period intervals were based on the listing of period intervals that was in common usage for spectrum calculation at the time the spectrum matching was completed. Specifically, the listing was published in a sub-routine of a lumped mass program developed at the University of California, Berkeley, for site response analyses.

The resulting spectra for the DBE time history are presented, along with the corresponding design response spectra, in figures 3.7-3 through 3.7-10.

The DBE acceleration time history of figure 3.7-2 is applicable to both horizontal components. The DBE acceleration time history for the vertical component has the same shape, but is times the horizontal.

3.7.1.3 Critical Damping Values

Damping values for the structures have been taken from reference 3 and the soil dampings, both hysteretic and spatial, have been calculated and measured. All safety-related structures will be founded in the San Mateo Formation sand, so only that material is considered here.

Hysteretic soil damping of the San Mateo Formation sand was measured directly in two ways: laboratory cyclic triaxial tests, and field in-situ wave-propagation tests. The details of the tests are presented in appendix 3.7C. The values used are given in figure 3.7-11. The appropriate strains to be used for DBE and OBE analyses shown on figure 3.7-11 were derived from finite-element analyses as described in appendix 3.7C.

Spatial soil dampings were calculated by elastic theory, using the expressions in table 3.7-1. The large-scale field tests were performed at the site to check the calculated values of spatial damping. These tests, which did verify the calculated values, are reported in detail in appendix 3.7C. The calculated values used are given in table 3.7-2. The values actually used were limited to 10% for the DBE analysis and to 8% for OBE analysis as indicated on table 3.7-3. Further the viscous damping values used for steel, prestressed concrete, and reinforced concrete are tabulated on table 3.7-3 and are equal to or less than those recommended in Regulatory Guide 1.61.

3.7.1.4 Supporting Media for Seismic Category I Structures

3.7.1.4.1 Soil Conditions

Soil conditions at the San Onofre site have been described in paragraphs 2.5.4.1 and 2.5.4.2. Briefly, the native soils at the site consist of approximately 70 feet of terrace deposits (from elevation 120 to 50), underlain by approximately 900 feet of San Mateo Formation sand which, in turn, is underlain by bedrock of the Capistrano Formation. The soils comprising the terrace deposits are predominantly clayey sands and silty clays. The San Mateo Formation sand is a very dense medium-to-coarse sand which exhibits some apparent cohesion and high shear strength due to efficient grain packing. The San Mateo Formation sand at the site is quite uniform, with no significant continuous layering, although occasional lenses of soils of different grain sizes do occur.

In the plant area, the soil has been excavated to between elevation +29 and -34 feet. Thus all Seismic Category I structures are founded on the San Mateo Formation sand.

3.7.1.4.2 Soil Properties

The static and dynamic properties of the San Mateo Formation sand are presented in paragraph 2.5.4.2. A general summary of the pertinent static and dynamic properties of the San Mateo Formation sand are summarized in table 3.7-4, and the variation of shear modulus and hysteretic damping with strain and confinement is presented in figure 3.7-12 for this material.

A summary of relevant foundation and structure characteristics for the various Seismic Category I structures is presented in table 3.7-5.

The stiffness parameters used for the design of Seismic Category I structures are presented in table 3.7-6. Details of the general procedures used in developing these stiffness parameters together with the evaluation of structural sliding of shallowly imbedded structures and design parameters for long critical ductways and piping are presented in appendix 3.7C.

Table 3.7-1
SPATIAL DAMPING PARAMETERS

Parameters	Mode of Motion			
	Vertical Translation	Horizontal Translation	Rocking	Twisting
Inertia	M, mass of foundation and machine	M, mass of foundation and machine	I_r, mass moment of inertia about rocking axis	I_t, mass moment of inertia about twisting axis
Equivalent[(a)] Radius	$r = \sqrt{\dfrac{BL}{\pi}}$	$r = \sqrt{\dfrac{BL}{\pi}}$	$r = \sqrt[4]{\dfrac{BL^3}{3\pi}}$	$r = \sqrt[4]{\dfrac{BL(B^2+L^2)}{6\pi}}$
Inertia[(b)] ratio	$B_v = \dfrac{(1-v)m}{4\rho r_e^3}$	$B_h = \dfrac{(7-8\nu)m}{32(1-\nu)\rho r_e^3}$	$B_r = \dfrac{3(1-\nu)I_r^{\cdot}}{8\rho r_e^5}$	$B_t = \dfrac{I_t}{\rho r_e^5}$
Effective inertia for design	m	m	$I_r^{\cdot} = \eta_r I_r$ (reference 4)	I_t
Spatial damping	$D_v = \dfrac{0.425}{\sqrt{B_v}}$	$D_h = \dfrac{0.288}{\sqrt{B_h}}$	$D_r = \dfrac{0.15}{(1+B_r)\sqrt{B_r}}$	$D_t = \dfrac{0.50}{1+2B_t}$

(a) For square or rectangular footing -

B = width of foundation in plan (parallel to axis of rotation)

L = length of foundation in plan (perpendicular to axis of rotation)

(b) where:

r_e = effective radius = 0.6r for translation modes

r_e = effective radius = 0.8r for rotational modes

v = Poisson's ratio = 0.35

ρ = unit mass density of soil, k-slug/ft^3

η_r = a factor to account for inertial effects[(4)]

Table 3.7-2

SUMMARY OF TOTAL DAMPING VALUES
CALCULATED FOR SEISMIC CATEGORY I STRUCTURES (Sheet 1 of 2)

Structure	Spatial Damping (%)	Hysteretic Damping (%)		Total Damping[a] (%)	
		DBE	OBE	DBE	OBE
Containment	D_v=40 D_h=24 D_r=9 D_t=(b)	12.5	10	D_v=52.5 D_h=36.5 D_r=21.5 D_t=(b)	50 34 19 (b)
Auxiliary Building	D_v=56 D_h=34 D_{rxx}=22 D_{ryy}=16 D_t=15	12.5	10	D_v=68.5 D_h=46.5 D_{rxx}=34.5 D_{ryy}=27.5 D_t=27.5	66 44 32 26 25
Intake Structure	D_v=51 D_h=31 D_{rxx}=21 D_{ryy}=22	12.5	10	D_v=63.5 D_h=31.5 D_{rxx}=33.5 D_{ryy}=34.5	61 41 31 32
Fuel Handling Building	D_v=32 D_h=19 D_{rxx}=11 D_{ryy}=11 D_t=(b)	12.5	10	D_v=44.5 D_h=31.5 D_{rxx}=17.5 D_{ryy}=23.5 D_t=(b)	42 29 15 21 (b)

(a) Definitions:

D_v = Damping for translation in vertical direction
D_h = Damping for translation in horizontal direction
D_{rxx} = Damping for rocking about x axis
D_{ryy} = Damping for rocking about y axis
D_t = Damping for twisting about vertical axis

(b) Available structural data insufficient to develop these values

Table 3.7-2

SUMMARY OF TOTAL DAMPING VALUES
CALCULATED FOR SEISMIC CATEGORY I STRUCTURES (Sheet 2 of 2)

Structure	Spatial Damping (%)	Hysteretic Damping (%)		Total Damping[a] (%)	
		DBE	OBE	DBE	OBE
Safety Equipment Building	D_v=47	12.5	10	D_v=59.5	57
	D_h=41			D_h=53.5	51
	D_{rxx}=(b)			D_{rxx}=(b)	(b)
	D_{ryy}=(b)			D_{ryy}=(b)	(b)
	D_t=(b)			D_t=(b)	(b)
Electrical and Piping Gallery Structure	D_v=47	12.5	10	D_v=59.5	57
	D_h=29			D_h=41.5	39
	D_{rxx}=23			D_{rxx}=35.5	33
	D_{ryy}=25			D_{ryy}=37.5	35
	D_t=14			D_t=26.5	24
Condensate and Refueling Tank Enclosure Structure	D_v=49	12.5	10	D_v=61.5	59
	D_n=30			D_n=42.5	40
	D_{rxx}=14			D_{rxx}=26.5	25
	D_{ryy}=19			D_{ryy}=31.5	29
	D_t=13			D_t=25.5	23
Diesel Generator Building	D_v=46	12.5	10	D_v=58.5	56
	D_n-28			D_n=40.5	38
	D_{rxx}=8			D_{rxx}=20.5	18
	D_{ryy}=12			D_{ryy}=24.5	22
	D_t=10			D_t=22.5	20

Reviews were made for the use of soil structure interaction parameters developed for various Seismic Category I structures, as outlined in section 5.0 of appendix 3.7C. Table 3.7-7 lists the various structures for which these reviews were made. Reviews for other structures are made on an ongoing basis as their designs progress.

Table 3.7-3
DAMPING VALUES (%) USED FOR SEISMIC CATEGORY I STRUCTURES (Sheet 1 of 2)

Building	OBE					DBE				
	Soil	Steel	Reinforced Concrete	Prestressed Concrete	Subsystems	Soil	Steel	Reinforced Concrete	Prestressed Concrete	Subsystems
Containment	8	NA	4	2	1[b]	10	NA	7	5	2[b]
Auxiliary building	8	3-4	3	NA	2[c]	10	5	6	NA	5[c]
Fuel handling building	8	3-4	3	NA	2[c] [d]	10	5	6	NA	5[c]
Electrical and piping gallery structure[a]	NA	NA	NA	NA	NA	10	NA	7	NA	NA
Safety equipment building[a]	NA	NA	NA	NA	NA	10	0	7	NA	NA

[a] Separate OBE analysis was not performed. OBE response was taken to be 60% of DBE response based on results of analyses on other structures.

[b] See table 3.7-22 for values used in NSSS analysis.

[c] Damping values used for subsystem analyses of steel beam-column framing systems.

[d] Damping values used for the liquid content in the fuel pool.

[e] Damping values are for the liquid content in the tanks.

Table 3.7-3
DAMPING VALUES (%) USED FOR SEISMIC CATEGORY I STRUCTURES (Sheet 2 of 2)

Building	OBE					DBE				
	Soil	Steel	Rein-forced Concrete	Pre-stressed Concrete	Sub-systems	Soil	Steel	Rein-forced Concrete	Pre-stressed Concrete	Sub-systems
Condensate and refueling tank enclosure structure	8	NA	3	NA	[e]	10	NA	7	NA	1[e]
Diesel generator building	8	NA	4	NA	NA	10	NA	7	NA	NA

Amended: May 2007 TL: E041430

Table 3.7-4

SUMMARY OF PROPERTIES OF SAN MATEO FORMATION SAND

Property	Value
In-situ total unit weight	130 lb/ft^3
Unified soil classification	well-graded sand (SW)
Angle of internal friction	41°
Effective cohesion[a]	700 lb/ft^2
Shear wave velocity at low strain[b]	930 ft/s
Shear modulus at low strain[b]	3500 k/ft^2

(a) Back calculated from stability analysis of existing slopes using $\phi = 41°$, assuming slope-stability safety factor of unity.

(b)
- For strain on the order of 10^{-4}%.
- For near-surface material, i.e., upper 15 feet.
- The effect of strain and confinement (or depth) on modulus and hysteretic damping are summarized in figure 3.7-12.

3.7.2 SEISMIC SYSTEM ANALYSIS

Seismic Category I structures, systems, and components are classified consistent with the recommendations of NRC Regulatory Guide 1.29 as discussed in section 3.2. The above are analyzed for earthquake conditions, the DBE and the OBE as described in subsections 2.5.2 and 3.7.1.

3.7.2.1 Seismic Category I Structures

3.7.2.1.1 Seismic Analysis Methods for Structures

In the analysis of Seismic Category I structures, two distinct objectives must be satisfied:

A. Development of in structure seismic response characteristics when necessary for use in the analysis and design of Seismic Category I systems, equipment, and components.

B. Determination of stress distributions within the various structures resulting from the design criteria free-field seismic input for use in the design of Seismic Category I structures.

Table 3.7-5

SUMMARY OF STRUCTURAL DIMENSIONS

Structure	Foundation Dimension (ft)	Foundation Embedment [a] (ft)	Total Height (ft)
Containment	92 radius	9[b]	184' - 9"
Auxiliary building	221 x 280	30[d]	~94
Intake structure	226 x ~280[c]	30 - 60	~60
Fuel handling building	Irregular 87 x 134	19.5 avg	106
Safety equipment building	Irregular 74 x 174	10 - 50	70
Electrical and piping junction gallery structure	Irregular 67 x 86	~35	54[e]
Condensate and refueling tank enclosure structure	Irregular 98 x 137	4	44 (average)
Diesel generator building	91 x 60	5 ft 6 in.	40 ft 10 in.
Box conduit	41 x 160	23[f]	23
Auxiliary intake structure	Irregular 27 x 20	~27[g]	38
Circular conduit	20 OD x 24	~20[h]	~20

(a) Embedment is based on the area of foundation walls in contact with soil.
(b) Irregular, varies from 9 feet at the base-slab to 43.5 feet at the base of tendon galleries.
(c) Intake structure foundation is common to two units.
(d) East wall only.
(e) Nominal height, Unit 2 access way has a height of 101 feet.
(f) Structure is completely buried, with depth of cover from 6 ft to 15 ft.
(g) Conduit portion of structure is completely buried, with a minimum depth of cover of 4 ft.
(h) Structure is completely buried, with a minimum depth of cover of 4 ft.

Table 3.7-6
SUMMARY OF VALUES OF STIFFNESS PARAMETERS FOR SEISMIC CATEGORY 1 STRUCTURES

Structure	Stiffness Parameter	Horizontal	Component Value		Twisting	Depth[(a)] (ft)
			Vertical	Rocking		
Containment	K	500G	600G	1.9×10^6G	4.25×10^6G	50
Auxiliary Building	C[(b)]	1.0	0.81	0.66	0.41	37
Intake Structure	K avg. Values	1180G	570G	3.2×10^6G	--	47
Fuel Handling Building	C	2.3	0.98	1.08[(c)] 0.84[(d)]	1.19	35
Safety Equipment Building	K	1340G[(e)] 1240G[(f)]	450G	5.6×10^5G[(d)] 12.4×10^6G[(c)]	3.5×10^6G	30
Electrical and Piping Gallery Structure	K	435G	230G	3.7×10^5G[(c)] 2.1×10^5G[(d)]	3×10^5G	20
Condensate and Refueling Tank Enclosure Structure	K	496G	376G	5.6×10^5G[(d)] 7.5×10^5G[(c)]	1×10^6G	32
Diesel Generator Building	K	289G	199G	1.3×10^5G[(d)] 1.9×10^5G[(c)]	2.5×10^5G	40

(a) Depth = depth below foundation for calculating strain-compatible values of shear modulus G, using figure 3.7-12
(b) $C = C_1C_2$ where C_1 = stress-distribution factor
C_2 = embedment factor
(c) Rocking about short axis
(d) Rocking about long axis
(e) Along long axis
(f) Along short axis

Amended: May 2007 TL: E041420

Table 3.7-7

REVIEW OF INTERACTION PARAMETERS FOR SEISMIC CATEGORY I STRUCTURES

Structure	Parameters Developed	Date of Transmission of Parameters	Review of Use of Parameters
Containment	Stiffness and damping	12 Feb 1973	23 Oct 1973
Auxiliary Building	Stiffness and damping	12 Feb 1973	19 Nov 1973
	Sliding potential	20 Feb 1973	23 Feb 1972
Intake structure	Stiffness and damping	4 Dec 1973	15 Jan 1974
	Critical instantaneous displacement profile	7 Sep 1973	15 Jan 1974
Fuel handling building	Stiffness and damping	11 Sep 1974	(a)
Safety equipment building	Stiffness and damping	21 Mar 1974	(a)
Electrical and piping gallery structure	Stiffness and damping	11 Dec 1974	21 Mar 1975
Condensate and refueling tank enclosure structure	Stiffness and damping	10 Nov 1976	(a)
Diesel generator building	Stiffness and damping	24 June 1977	(a)

(a) Review was made on an on-going basis.

3.7.2.1.1.1 General Methods

Two separate analytical procedures are employed to satisfy the above requirements. A time history analysis is used to develop in structure response data, and a modal response spectra analysis is used to develop stress distributions within the various structures. The mathematical idealization of the structural characteristics of the various Seismic Category I structures was accomplished by either a lumped-parameter beam-stick model or a three-dimensional finite-element model. The general analytical methods and modeling techniques used in these analyses are discussed in Bechtel Topical Report BC-TOP-4A.[5]

Variations in the application of specific details are discussed in the next paragraph and in the applicable sections of this document. The seismic design criteria input is defined in terms of the OBE and DBE design response spectra (paragraph 3.7.1.1), the free-field time history records (paragraph 3.7.1.2), and the soil-structure interaction parameters (paragraph 3.7.1.4).

The seismic ground acceleration was defined as the free-field motion at the ground surface. This motion was applied as input at the foundation level without modification or reduction for embedment depth. Such free-field motion would be exhibited by an embedded basemat of mass-density similar to the soil if the basemat were detached from the superstructure response interaction. The corresponding input for the mathematical models used in the dynamic structural analyses was applied at the base of dimensionless soil-structure-interaction springs attached to the foundation basemat of each structure. The equations of motion used in the dynamic analyses were formulated to represent the above definition of input motion whereby the basemat without super-structure would track the free field motion. A more detailed description is given in Section 3.6 of reference 6.

Structural damping values are defined in table 3.7-3 and soil-damping characteristics in tables 3.7-2 and 3.7-3.

Incorporation of damping into the seismic analyses was accomplished in two ways. For the lumped-parameter time history analyses, the nonproportional damping technique discussed in reference 7 was used. For the three-dimensional finite-element analyses, the composite modal damping technique as described in sections 3.2 and 3.3 of reference 5 was used.

Depending upon the degree of embedment, the soil-structure interaction effects are represented either by the lumped-parameter approach using strain-dependent soil springs or by the series combination of a finite-element soil grid multipoint, constrained to a set of discrete springs resulting in the equivalent soil-structure interaction parameters as prescribed by the project geotechnical consultant. A more complete description of this subject is provided in paragraph 3.7.2.1.4.

General considerations for structural and response coupling, the minimum number of mass points, and the number of degrees-of-freedom per mass point are described in Section 3.2 of reference 5.

Consideration of maximum relative displacements of Seismic Category I structures is provided by means of a supplementary three-dimensional finite-element analysis of the entire power block area. By means of this analysis, a more realistic assessment of the phase relationship between the response of the various structures can be determined. A more detailed description of the modeling technique can be found in paragraph 3.7.2.1.3.10. Intra building relative support displacements were established in accordance with Section 5.3 of reference 5.

Significant effects such as piping interactions, external structural restraints, and hydrodynamic effects are included in the analysis.

3.7.2.1.1.2 Methods Employed in the Analysis of the Intake Structure

Two independent analyses are performed to develop seismic-induced stress distributions within the intake structure. The first, a dynamic equivalent static load analysis, is used to establish member sizes and define reinforcement requirements, while the second, a more rigorous pseudo-dynamic instantaneous displacement profile analysis (refer to section 3.5 and appendix H of appendix 3.7C) is used as a check to verify the magnitude and distribution of the forces and moments from the first analysis. Refer to paragraph 3.7.2.1.10 for a detailed description of each analysis. These two analyses are justified in lieu of a seismic system dynamic analysis, since the structure is very rigid in both vertical and horizontal directions due to its numerous piers and partition walls, and being a nearly buried structure filled with water during normal operation, the mass and inertial characteristics of the structure are similar to those of the displaced soil.

3.7.2.1.1.3 Methods Employed in the Analysis of the Offshore Circular Conduits

The intake conduits consist of 20-foot outside diameter pipe segments, 24 feet in length, connected by bell and spigot joints that were designed to accommodate the maximum rotation and translation resulting from the DBE ground motion. Because the joints are designed to articulate and are incapable of transferring tension, and the conduits are completely bedded in the select gravel backfill and formational material, the conduits as a whole are fully compliant with the ground motion. Longitudinal bending stresses cannot be transferred from segment to segment, and lateral shear stresses between the conduits cannot develop since continuity will be maintained in the formation during a DBE (refer to figure 3.7-13 for an illustration of the conduit behavior during a seismic event). The analysis of individual pipe segments for longitudinal bending and shear is discussed below. The maximum rotations and translations were calculated using the critical instantaneous displacement profile (CIDP) (refer to appendix 3.7C) and verified using the methodology outlined in the BC-TOP-4 Section 6.0, Analysis of Long Buried Structures.

The seismically-induced transverse stresses on the pipe sections were determined by modeling the pipe as a closed ring and inputting the seismic accelerations statically to the structure as equivalent inertia loads (refer to paragraph 3.7.2.1.10 for a detailed description of the equivalent static analysis methodology). Calculation of the transverse stresses on the pipe section adjacent to the box conduit at the interface included the additional soil pressure resulting from the differential displacement of the conduit at the interface. Corresponding stresses from the vertical and two horizontal seismic loadings are combined by taking the square root of the sum of the squares (SRSS) of the individual seismic stresses.

Longitudinal bending and shear stresses in the individual pipe sections are calculated using the BC-TOP-4 methodology. This methodology assumes that a long, flexible pipeline will be bent to conform with the seismic wave shape. In this case, the intake pipe segments are rigid with respect to longitudinal bending and will not comply individually with the calculated curvature. The relative soil displacement over the 24-foot pipe segment from the calculated radius of curvature is not sufficient to mobilize additional soil pressure. Thus, there are essentially no longitudinal bending or shear stresses in the individual pipe segments.

The offshore circular conduits interface with the box conduit structure approximately 160 feet seaward of the permanent seawall. The first circular conduit segment is a starter section, 8 feet in length, which is embedded 2 feet into the box conduit. Because the box conduit is a relatively rigid structure and will not comply with the ground motion, the structure will displace differentially with respect to the soil and the circular conduit segments. The starter section and first 24-foot pipe segment will be subjected to longitudinal bending and shear stresses induced by the soil contact stresses resulting from the differential displacement of the conduit with respect to the soil. Differential displacement was calculated using the BC-TOP-4 methodology, and the corresponding soil pressures were provided by Woodward-Clyde Consultants.

The method of analysis used for the offshore circular conduits is justified in lieu of a seismic system dynamic analysis for the following reasons: (1) the pipes are completely buried structures filled with water, the mass and inertial characteristics are similar to those of the displaced soil and no significant soil structure interaction will be experienced; (2) the pipe sections are adequately modeled as a beam in the longitudinal direction and a closed ring in the transverse direction.

3.7.2.1.1.4 Methods Employed in the Analysis of the Box Conduit

The box conduit is analyzed and designed for static and equivalent dynamic loads, using the finite element model of the conduit cross-section shown in figure 3.7-14. The model is constructed using beam elements to model the conduit and soil springs to simulate the stiffness of the soil around the box conduit. The seismically-induced stress distributions for the transverse direction are determined by inputting the maximum unamplified free field accelerations statically to the structure as equivalent inertia loadings (refer to paragraph 3.7.2.1.10 for a detailed description of the equivalent static analysis).

A separate lumped mass model, representing the conduit structure acting as a longitudinal beam supported by a continuous elastic media, is used to determine the stresses in the longitudinal direction and to check the adequacy of the longitudinal reinforcing steel. Seismically-induced displacements, determined by the critical instantaneous displacement profile, are applied to the three major axes of the structure to determine the longitudinal stresses. (The critical instantaneous displacement profile is discussed in detail in appendix 3.7C.)

The method of analysis used for the box conduits is justified in lieu of a seismic system dynamic analysis for the following reasons: (1) the box conduit structure is a completely buried structure filled with water under normal operating conditions; the mass and inertial characteristics are similar to those of the displaced soil, and no significant soil structure interaction will be experienced; (2) the overall simplicity of the structural models; the conduit can be adequately modeled in the transverse direction using the finite element model with beam elements, and modeled in the longitudinal direction by the lumped mass model as a beam supported by a continuous elastic media.

3.7.2.1.1.5 Methods Employed in the Analysis of the Auxiliary Intake Structure

The seismically-induced stress distributions within the auxiliary intake structure are calculated using an equivalent static analysis. Seismic accelerations are input statically into the structure as equivalent inertia loadings (refer to paragraph 3.7.2.1.10 for a detailed description of the equivalent static analysis methodology). The corresponding stresses from the vertical and the two horizontal seismic loadings are combined by taking the square root of the sum of the squares (SRSS) of the individual seismic stresses. In addition to the structural inertia loadings, hydrodynamic and soil loadings induced by the earthquake were considered in the seismic analysis. Three wave loading conditions were also calculated independently. Normal storm waves are assumed to be concurrent with seismic loadings. They were not included in stress comparisons because the independent calculation showed that they were negligible compared to the seismic stresses. Maximum storm waves produce lower stresses than seismic loadings and are considered independently since they represent an unrelated extreme event. Tsunami loadings are seismically induced but do not occur for at least 5 minutes following the earthquake and are thus nonconcurrent.

The equivalent static analysis is justified in lieu of seismic system dynamic analysis based on the overall simplicity of the structural model. The riser is modeled as a rigid cantilever beam element supported on a rigid buried base. The pipe section can be analyzed as a standard frame element, with the stresses determined by conventional methodology employing analytical techniques based on the principles of virtual work. Soil structure interaction will not be significant because of the use of the select gravel backfill material, the rigidity of the structure, and the similar mass densities of the structure and the backfill.

3.7.2.1.1.6 Mathematical Models

Refer to figures 3.7-15 through 3.7-30 for either a pictorial representation or an actual sketch of the mathematical model of each Seismic Category I structure. A complete description of the formulation of the mathematical models and their use is provided in paragraph 3.7.2.1.3.

3.7.2.1.2 Natural Frequencies and Response Loads

A summary of natural frequencies and modal characteristics is given in tables 3.7-8 through 3.7-14. Selected total response, determined by seismic analyses for each Seismic Category I structure, is given in figures 3.7-31 through 3.7-36, and tables 3.7-15 through 3.7-20. The response spectra at selected plant elevations with major equipment and equipment support points for each structure are given in appendix 3.7A.

The results of the analyses show that the structural response is dominated by the soil-structure interaction modes. Likewise, the effects of the strain-dependent soil springs are clearly shown by the frequency shift between the DBE and OBE results.

The typical in structure response spectra shown in appendix 3.7A represent an envelope of the response for a given coordinate direction resulting from the square-root-of-the-sum-of-the-squares (SRSS) combination of the response produced from the vertical excitation and a single-axis horizontal excitation.

For the fuel handling building, the first seven modes correspond to fluid oscillation in the spent fuel pool and exhibit little fluid-structure interaction. The summation of participation factors for these modes were less than 8%.

Table 3.7-8
CONTAINMENT STRUCTURE (SHELL AND INTERNAL STRUCTURE) DBE ANALYSIS SUMMARY OF FREQUENCIES AND MODAL CHARACTERISTICS OF LUMPED-PARAMETER COUPLED MODELS

Mode No.	Model Parallel to Hot Leg			Model Perpendicular to Hot Leg		
	Frequency (Hz)	Participation Factor (%)	Critical Damping (%)	Frequency (Hz)	Participation Factor (%)	Critical Damping (%)
1	1.40	76.8 H[a]	9.82	1.40	77.1 H	9.82
2	2.16	90.3 V[b]	9.97	2.16	90.3 V	9.97
3	2.63	15.5 H	9.90	2.63	15.8 H	9.91
4	9.72	1.4 H	5.61	10.89	0.8 H	5.59
5	12.45	0.0 H	3.83	16.48	0.0 H	2.22
6	13.40	0.03 H	4.29	16.51	0.8 H	2.91
7	17.65	0.0 H	2.55	18.45	2.2 V	4.87
8	18.58	2.3 V	4.93	20.04	0.0 H	5.29
9	18.61	1.5 H	5.74	21.06	1.9 H	5.70

(a) H = Horizontal mode

(b) V = Vertical mode

Amended: May 2007 TI: E041420

Table 3.7-9
AUXILIARY BUILDING
SUMMARY OF FREQUENCIES AND MODAL CHARACTERISTICS OF THE LUMPED-PARAMETER GEOMETRICALLY COUPLED MODEL

Mode No.	Frequency (Hz)	Critical Damping (%)	Participation Factors, DBE (%)			Type of Main Response[a]
			Horizontal -X	Horizontal -Y	Vertical-Z	
1	1.50	9.95	56.9	0.4	1.1	H_x, T_z, R_y
2	1.57	9.95	0.3	57.1	14.3	H_y, V_z, R_x
3	1.79	9.95	4.4	1.6	0.1	H_y, H_x, T_z, R_y
4	1.83	9.97	1.3	13.9	74.6	V_z, H_y, H_x
5	2.35	9.98	35.6	0.3	0.8	H_x, V_z, R_y, T_z
6	2.55	9.99	0.2	25.6	8.7	H_y, V_z, R_x
7	15.41	6.05	0.6	0.0	0.0	
8	16.32	6.05	0.0	0.6	0.1	
9	17.04	6.03	0.4	0.0	0.0	
10	22.43	6.01	0.01	0.2	0.0	

[a] Direction of main response given in order of importance for first six modes according to the following notation:

H_x = Horizontal translation along X-axis
H_y = Horizontal translation along Y-axis
V_z = Vertical translation along Z-axis
R_x = Rotation about X-axis
R_y = Rotation about Y-axis
T_z = Torsion about Z-axis

Table 3.7-10[a]

FUEL-HANDLING BUILDING SUMMARY OF FREQUENCIES AND MODAL CHARACTERISTICS OF THE LUMPED-PARAMETER GEOMETRICALLY COUPLED MODEL

Mode[b] No.	Frequency (Hz)	Critical Damping (%)	Participation Factor, DBE (%)			Type of Main Response[c]
			Horizontal-X	Horizontal-Y	Vertical-Z	
8	2.38	9.79	0.0	48.6	3.9	H_y, V_z, R_x
9	2.58	9.87	41.9	0.2	10.0	H_x, V_z, R_y
10	2.99	9.98	6.1	2.7	83.9	V_z, H_x, R_y
11	4.57	9.77	4.0	0.6	0.4	H_x, H_y, T_z
12	5.53	9.94	37.4	0.5	1.3	H_x, V_z, R_y
13	5.85	9.87	0.4	38.1	0.6	H_y, V_z, R_x
14	18.80	6.20	0.2	0.2	0.0	
15	21.77	6.11	0.5	0.3	0.0	
16	22.34	6.17	0.2	0.7	0.0	
17	28.57	6.05	0.1	0.9	0.0	
18	31.98	6.06	1.0	0.0	0.0	
19	36.48	6.02	0.0	0.0	0.0	

(a) See Table 3.7-20A for additional modal importance for characteristics information.

(b) The model has seven degrees of freedom associated with fluid mass. The first seven modes correspond to fluid oscillations exhibiting little fluid-structure interaction. The tabulated participation factors do not add up to 100% due to the exclusions of the first seven modes.

(c) Direction of Main Response given in order of 8-13 modes according to the following notation:

H_x = Horizontal translation along X-axis
H_y = Horizontal translation along Y-axis
V_z = Vertical translation along Z-axis
R_x = Rotation about X-axis
R_y = Rotation about Y-axis
T_z = Torsion about Z-axis

Table 3.7-11
SAFETY EQUIPMENT BUILDING
SUMMARY OF FREQUENCIES AND MODAL CHARACTERISTICS OF THREE-DIMENSIONAL FINITE-ELEMENT MODEL

Mode No.	Frequency (Hz)	Modal Damping (%)	Participation Factor, DBE (%)			Type of Main Response[a]
			Horizontal-X	Horizontal-Y	Vertical-Z	
1	2.39	10	46.69	0.78	1.35	H_x, R_y, T_z
2	3.22	10	1.01	0.89	92.43	V_z, H_x, R_x
3	4.12	10	2.22	0.37	0.26	H_x, H_y, R_y
4	5.05	10	0.68	68.55	1.85	H_y, V_z, R_x
5	7.31	10	36.64	3.13	1.16	H_x, H_y, R_y
6	8.85	10	5.84	21.89	1.87	H_y, H_x, R_x
7	12.69	7	3.19	0.95	0.16	
8	13.59	7	3.04	0.62	0.24	
9	15.62	7	0.55	1.96	0.47	
10	17.68	7	0.14	0.87	0.21	

[a] Direction of Main Response given in order of importance for first six modes according to the following notation:

H_x = Horizontal translation along X-axis
H_y = Horizontal translation along Y-axis
V_z = Vertical translation along Z-axis

R_x = Rotation about X-axis
R_y = Rotation about Y-axis
T_z = Torsion about Z-axis

Table 3.7-12
ELECTRICAL AND PIPING GALLERY STRUCTURE
SUMMARY OF FREQUENCIES AND MODAL CHARACTERISTICS OF THREE-DIMENSIONAL FINITE-ELEMENT MODEL

Mode No.	Frequency (Hz)	Modal Damping (%)	Participation Factors, DBE (%)			Type of Main Response[a]
			Horizontal-X	Horizontal-Y	Vertical-Z	
1	2.09	10	2.858	16.967	3.934	H_y, R_x, T_z
2	2.40	10	11.686	4.634	13.512	V_z, H_x, R_y
3	3.28	10	14.502	0.265	16.172	V_z, H_x
4	3.81	10	1.408	5.801	1.115	H_y, R_x, T_z
5	4.82	10	10.959	5.765	4.840	H_x, R_y
6	5.27	10	4.207	10.839	2.752	H_y, T_z
7	8.12	7	0.526	0.745	1.346	
8	9.01	7	0.038	0.691	1.265	
9	10.19	7	0.016	0.393	0.018	
10	11.67	7	0.313	0.231	0.071	

[a] Direction of main response given in order of importance for the first 6 modes according to the following notation:

H_x = Horizontal translation along X-axis
H_y = Horizontal translation along Y-axis
V_z = Vertical translation along Z-axis

R_x = Rotation about X-axis
R_y = Rotation about Y-axis
T_z = Torsion about Z-axis

Table 3.7-13
CONDENSATE AND REFUELING TANK ENCLOSURE STRUCTURE SUMMARY OF FREQUENCIES AND MODAL CHARACTERISTICS OF THREE-DIMENSIONAL FINITE-ELEMENT MODEL (Sheet 1 of 2)

Mode[a] No.	Frequency (Hz)	Modal Damping (%)	Participation Factors, DBE (%)			Type of Main Response[b]
			Horizontal-X	Horizontal-Y	Vertical-Z	
9	4.09	10	5.27	21.89	0.08	H_y, R_x, T_z
10	4.14	10	25.74	5.62	1.00	H_x, R_y, T_z
11	4.44	10	2.11	13.42	0.00	H_y, R_x
12	6.15	10	1.39	0.35	12.40	V_z, H_x
13	6.30	10	0.12	5.51	1.58	H_y, T_z

(a) The model has eight degrees of freedom associated with fluid mass. The first eight modes correspond to fluid oscillations exhibiting little fluid-structure interaction. The tabulated participation factors do not add up to 100% due to exclusions of the first eight modes.

(b) Direction of main response given in order of importance for 9-15 modes according to the following notation:

H_x = Horizontal Translation along X-axis
H_y = Horizontal Translation along Y-axis
V_z = Vertical Translation along Z-axis Rx
R_x = Rotation about X-axis
R_y = Rotation about Y-axis
T_z = Torsion about Z-axis

Table 3.7-13
CONDENSATE AND REFUELING TANK ENCLOSURE STRUCTURE SUMMARY OF FREQUENCIES AND MODAL CHARACTERISTICS OF THREE-DIMENSIONAL FINITE-ELEMENT MODEL (Sheet 2 of 2)

Mode[a] No.	Frequency (Hz)	Modal Damping (%)	Participation Factors, DBE (%)			Type of Main Response[b]
			Horizontal-X	Horizontal-Y	Vertical-Z	
14	6.39	10	4.26	2.23	8.06	Vz, Hx Ry
15	6.55	10	4.27	2.25	3.18	Hx, Ry, Tz
16	8.15	7	0.46	0.07	0.48	
17	9.07	7	0.48	0.46	1.27	
18	9.19	7	0.01	0.21	0.26	
19	9.25	7	0.24	0.18	0.77	
20	9.32	7	0.05	0.33	0.70	
21	9.43	7	0.14	0.38	0.49	
22	9.73	7	0.73	0.31	0.34	

Amended: May 2007 TL: E041420

Table 3.7-14
DIESEL GENERATOR BUILDING SUMMARY OF FREQUENCIES AND MODAL CHARACTERISTICS OF THE LUMPED-PARAMETER GEOMETRICALLY COUPLED MODEL

Mode No.	Frequency (Hz)	Critical Damping (%)	Participation Factors, DBE (%)			Type of Main Response[a]
			Horizontal-X	Horizontal-Y	Vertical-Z	
1	3.38	10	0.00	13.88	0.00	H_y, R_x
2	3.39	10	11.85	0.00	0.00	H_x, R_y
3	4.140	10	0.00	0.00	18.68	V_z, R_x, R_y
4	4.26	10	0.00	0.00	0.00	T_z, H_x, H_y
5	5.78	10	14.44	0.00	0.00	R_y, H_x
6	6.38	10	0.00	12.49	0.00	R_x, H_y
7	28.73	7	0.00	0.43	0.00	
8	33.59	7	0.34	0.00	0.00	
9	34.63	7	0.00	0.00	0.00	
10	42.23	7	0.00	0.07	0.00	

[a] Direction of main response given in order of importance for the first 6 modes according to the following notation:

H_x = Horizontal translation along x-axis
H_y = Horizontal translation along y-axis
V_z = Vertical translation along z-axis
R_x = Rotation about x-axis
R_y = Rotation about y-axis
T_z = Torsion about z-axis

Amended: May 2007 TL: E041420

Table 3.7-15
AUXILIARY BUILDING NODAL FORCES, ACCELERATIONS, AND DISPLACEMENTS FROM DBE ANALYSIS
(N-S AND VERTICAL EXCITATION)

Node[a] No.	Nodal Weight ($x 10^4$ k)	Forces[b] ($x 10^4$ k)			Accelerations[b] (ft/s^2)			Displacements[b] ($x 10^{-2}$ ft)			Displacements[b] ($x 10^{-4}$ rad)		
		F_x	F_y	F_z	$\ddot{u}_x$	$\ddot{u}_y$	$\ddot{u}_z$	u_x	u_y	u_z	θ_x	θ_y	θ_z
1	10.66	7.00	1.78	6.38	21.1	5.4	19.3	19.6	4.3	14.7	2.3	19.8	4.8
2	1.65	1.17	0.28	1.01	22.8	5.4	19.6	23.6	4.5	14.9	2.3	19.9	4.8
3	0.09	0.07	0.02	0.10	23.4	8.0	34.6	24.8	7.4	28.4	2.4	20.0	4.8
4	0.09	0.07	0.02	0.10	23.4	8.2	34.5	24.8	7.7	28.7	2.4	20.0	4.8
5	1.34	0.85	0.22	0.78	20.4	5.4	18.9	19.7	4.6	14.3	2.3	19.9	4.8
6	2.56	1.93	0.43	1.57	24.3	5.4	19.7	26.4	4.7	15.0	2.4	19.9	4.8
7	0.20	0.14	0.05	0.21	23.5	8.1	34.7	25.4	7.6	28.5	2.4	20.0	4.8
8	0.20	0.14	0.05	0.21	23.5	8.3	34.7	25.4	7.9	28.9	2.4	20.0	4.8
9	2.67	1.98	0.45	1.60	23.9	5.5	19.3	26.1	4.8	14.6	2.4	19.9	4.8
10	3.03	2.58	0.53	1.85	27.4	5.6	19.7	30.8	5.0	15.0	2.4	20.0	4.8
11	0.93	0.69	0.16	0.55	24.0	5.7	19.0	26.6	5.1	14.4	2.4	20.0	4.8
12	2.75	2.48	0.50	1.66	29.0	5.9	19.4	32.8	5.4	14.7	2.4	20.0	4.8
13	0.18	0.18	0.05	0.20	30.8	8.5	35.2	34.9	8.1	28.9	2.4	20.1	5.0
14	0.18	0.18	0.05	0.20	30.8	8.9	35.2	34.9	8.5	29.3	2.4	20.1	5.0

(a) Refer to figure 3.7-21 for node location.

(b) Nomenclature:

x, y, z = axes of coordinate system according to figure 3.7-19

F_i = translational force along I-axis

u_i = translational displacement along I-axis

θ_i = rotational displacement about I-axis

$\ddot{u}_i$ = translational acceleration along I-axis

Table 3.7-16
AUXILIARY BUILDING NODAL FORCES, ACCELERATIONS, AND DISPLACEMENTS FROM DBE ANALYSIS
(E-W AND VERTICAL EXCITATION)

Node[a] No.	Nodal Weight ($x\ 10^4$ k)	Forces[b] ($x\ 10^4$ k)			Accelerations[b] (ft/s^2)			Displacements[b] ($x\ 10^{-2}$ ft)			Displacements[b] ($x\ 10^{-4}$ rad)		
		F_x	F_y	F_z	$\ddot{u}_x$	$\ddot{u}_y$	$\ddot{u}_z$	u_x	u_y	u_z	θ_x	θ_y	θ_z
1	10.66	0.21	8.06	8.38	0.6	24.3	25.3	0.5	22.8	19.5	17.2	0.4	0.9
2	1.65	0.03	1.33	1.38	0.7	25.9	26.8	0.6	25.3	21.1	17.3	0.4	0.9
3	0.09	0.002	0.07	0.08	0.7	25.8	26.8	0.6	25.5	21.1	17.3	0.5	1.0
4	0.09	0.002	0.08	0.08	0.7	27.6	27.1	0.6	27.4	21.4	17.3	0.5	1.0
5	1.34	0.05	1.11	1.13	1.1	26.6	27.2	1.0	26.4	19.9	17.3	0.4	0.9
6	2.56	0.06	2.18	2.18	0.7	27.5	27.5	0.6	27.5	21.7	17.3	0.4	0.9
7	0.20	0.004	0.27	0.15	0.7	27.7	25.2	0.6	27.9	19.1	17.3	0.5	1.0
8	0.20	0.004	0.18	0.15	0.7	29.5	25.3	0.6	29.9	19.3	17.3	0.5	1.0
9	2.67	0.06	2.42	2.09	0.7	29.2	25.2	0.7	29.6	19.1	17.3	0.4	0.9
10	3.03	0.06	2.94	2.53	0.7	31.3	26.9	0.7	31.9	21.2	17.4	0.4	0.9
11	0.93	0.04	0.94	0.80	1.3	32.4	27.7	1.13	33.1	20.2	17.4	0.4	0.9
12	2.75	0.07	2.98	2.16	0.8	34.9	25.3	0.8	35.6	19.3	17.4	0.4	0.9
13	0.18	0.005	0.21	0.14	0.9	35.7	25.2	0.8	36.3	19.2	17.4	0.5	1.0
14	0.18	0.005	0.22	0.15	0.8	37.7	25.4	0.8	38.3	19.3	17.4	0.5	1.0

(a) Refer to figure 3.7-21 for node location.

(b) Nomenclature:

x, y, z = axes of coordinate system according to figure 3.7-19

F_i = translational force along I-axis

u_i = translational displacement along I-axis

θ_i = rotational displacement about I-axis

$\ddot{u}_i$ = translational acceleration along I-axis

Table 3.7-17
AUXILIARY BUILDING MAXIMUM CONNECTIVITY FORCES FROM DBE ANALYSIS (Sheet 1 of 3)

Connectivity (Nodes)[a]	N-S and Vertical Excitation						E-W and Vertical Excitation					
	Forces[b] (x 10^4 k)			Moments[b] (x 10^6 k-ft)			Forces[b] (x 10^4 k)			Moments[b] (x 10^6 k-ft)		
	F_x	F_y	F_z	M_x	M_y	M_z	F_x	F_y	F_z	M_x	M_y	M_z
1 - 2	8.31	1.96	5.89	1.79	6.10	3.21	0.14	10.79	8.21	4.46	0.19	0.15
1 - 3	0.00	0.00	0.12	0.06	0.16	0.00	0.00	0.00	0.06	0.03	0.09	0.00
1 - 4	0.00	0.00	0.12	0.06	0.16	0.00	0.00	0.00	0.06	0.03	0.09	0.00
1 - 5	3.35	0.60	3.36	3.21	4.24	3.26	0.24	3.18	5.22	5.46	0.16	0.45
1 - 6	1.18	0.24	0.61	0.47	0.59	1.47	0.07	1.34	1.77	2.36	0.05	0.14
1 – 10	0.15	0.05	0.14	0.16	0.50	0.19	0.007	0.29	0.53	0.71	0.01	0.02
2 - 3	0.16	0.18	0.53	0.03	0.58	0.19	0.005	0.87	0.34	0.10	0.37	0.95
2 - 4	0.16	0.20	0.57	0.03	0.63	0.22	0.01	1.01	0.39	0.11	0.43	1.12
2 - 5	0.50	0.03	0.19	0.12	0.07	0.33	0.02	0.13	0.25	0.16	0.08	0.05
2 - 6	6.50	1.33	4.21	0.30	3.50	0.52	0.15	7.48	5.90	1.10	0.13	0.23

(a) Refer to figure 3.7-21 for relative location of nodes

(b) Nomenclature:

x, y, z = axes of coordinate system according to figure 3.7-19

F_i = translational force along the I-axis

M_i = rotational force about the I-axis

Table 3.7-17
AUXILIARY BUILDING MAXIMUM CONNECTIVITY FORCES FROM DBE ANALYSIS (Sheet 2 of 3)

Connectivity (Nodes)[a]	N-S and Vertical Excitation						E-W and Vertical Excitation					
	Forces[b] (x 10^4 k) (x 10^4 k)			Moments[b] (x 10^6 k-ft) (x 10^6 k-ft)			Forces[b] (x 10^4 k) (x 10^4 k)			Moments[b] (x 10^6 k-ft) (x 10^6 k-ft)		
	F_x	F_y	F_z	M_x	M_y	M_z	F_x	F_y	F_z	M_x	M_y	M_z
3 - 5	0	0.002	0	0	0	0.002	0	0.002	0	0	0	0
3 - 6	0.11	0.16	0.50	0.03	0.55	0.18	0.004	0.80	0.30	0.05	0.33	0.87
3 - 7	0	0	0.06	0.04	0.007	0	0	0	0.03	0.02	0.003	0
4 - 5	0	0.002	0	0	0	0.002	0	0.002	0	0	0	0.002
4 - 6	0.11	0.18	0.54	0.03	0.58	0.20	0.008	0.94	0.35	0.05	0.38	1.01
4 - 8	0	0	0.06	0.04	0.007	0	0	0	0.03	0.02	0.003	0
5 - 6	1.41	0.13	0.81	0.59	0.83	1.13	0.09	0.62	1.18	0.85	0.05	0.13
5 - 7	0.18	0.05	0.44	0.23	0.56	0.11	0.007	0.25	0.36	0.18	0.44	0.27
5 - 8	0.18	0.06	0.46	0.24	0.58	0.11	0.02	0.28	0.37	0.18	0.45	0.30
5 - 9	1.30	0.19	1.45	1.65	1.31	1.77	0.11	1.09	2.46	2.81	0.03	0.19
6 - 7	0.12	0.18	0.59	0.23	0.65	0.21	0.004	0.88	0.34	0.14	0.38	0.97
6 - 8	0.12	0.18	0.60	0.23	0.64	0.21	0.01	0.91	0.35	0.14	0.38	0.98
6 - 9	6.90	1.17	3.79	1.69	2.88	3.23	0.16	6.66	5.24	2.36	0.07	0.11
6 – 10	0.47	0.10	0.20	0.17	0.20	0.44	0.02	0.58	0.62	0.53	0.01	0.04
7 - 9	0.21	0.19	0.75	0.13	0.83	0.21	0.009	0.97	0.40	0.12	0.44	1.04
7 – 10	0.15	0.001	0.15	0.13	0.20	0.17	0.01	0.008	0.13	0.13	0.17	0.03

Table 3.7-17
AUXILIARY BUILDING MAXIMUM CONNECTIVITY FORCES FROM DBE ANALYSIS (Sheet 3 of 3)

Connectivity (Nodes)[a]	N-S and Vertical Excitation						E-W and Vertical Excitation					
	Forces[b] (x 10^4 k)			Moments[b] (x 10^6 k-ft)			Forces[b] (x 10^4 k)			Moments[b] (x 10^6 k-ft)		
	F_x	F_y	F_z	M_x	M_y	M_z	F_x	F_y	F_z	M_x	M_y	M_z
8 - 9	0.21	0.20	0.76	0.13	0.83	0.21	0.009	1.01	0.41	0.13	0.45	1.09
8 – 10	0.15	0.001	0.16	0.14	0.20	0.17	0.006	0.008	0.13	0.14	0.18	0.01
9 – 10	5.16	1.14	3.43	1.07	3.25	2.20	0.13	6.65	4.53	1.89	0.10	0.23
9 – 11	0.78	0.11	0.82	0.95	0.71	1.06	0.04	0.68	1.31	1.57	0.03	0.07
10 – 11	1.10	0.20	0.55	0.39	0.60	0.70	0.03	1.19	0.74	0.54	0.01	0.04
10 – 12	2.25	0.57	1.42	0.72	1.22	1.42	0.07	3.40	2.01	0.97	0.05	0.13
10 – 13	0.10	0.00	0.15	0.13	0.22	0.10	0.004	0.002	0.08	0.07	0.11	0.006
10 – 14	0.09	0.00	0.16	0.14	0.23	0.10	0.01	0.002	0.09	0.08	0.12	0.01
11 – 12	1.19	0.15	0.81	0.66	0.80	0.81	0.04	0.94	1.19	1.00	0.05	0.07
12 – 13	0.07	0.06	0.10	0.04	0.12	0.13	0.03	0.28	0.09	0.07	0.10	0.33
12 – 14	0.07	0.07	0.12	0.03	0.13	0.14	0.02	0.32	0.11	0.08	0.12	0.36

Table 3.7-18
FUEL HANDLING BUILDING NODAL FORCES, DISPLACEMENTS, AND ACCELERATIONS FROM DBE ANALYSIS
(N-S AND VERTICAL EXCITATION)

Node[a] No.	Nodal Weight ($\times 10^4$ k)		Forces[b] ($\times 10^4$ k)			Accelerations[b] (ft/s^2)			Displacements[b]					
									($\times 10^{-2}$ ft)			($\times 10^{-4}$ rad)		
	Horiz. Trans.	Vert. Trans.	F_x	F_y	F_z	$\ddot{u}_x$	$\ddot{u}_y$	$\ddot{u}_z$	u_x	u_y	u_z	θ_x	θ_y	θ_z
1	1.63	2.02	1.51	0.04	1.44	29.8	0.8	22.9	3.87	0.20	6.49	0.7	12.8	0.7
2	0.96	0.83	0.79	0.03	0.59	26.5	0.9	22.9	5.40	0.31	6.54	0.7	12.8	0.8
3	0.73	0.55	0.56	0.02	0.40	26.0	1.2	23.1	7.21	0.42	6.58	0.7	12.9	0.8
4	0.86	0.84	0.72	0.04	0.60	26.9	1.6	23.1	9.49	0.56	6.59	0.7	13.0	0.8
5	0.44	0.44	0.50	0.03	0.32	36.5	2.2	23.1	13.74	0.81	6.60	0.7	13.1	0.9
6	0.30	0.30	0.41	0.02	0.21	44.2	2.6	23.2	16.17	0.95	6.63	0.7	13.1	0.9

(a) Refer to figure 3.7-22 for node location

(b) Nomenclature:

x, y, z = axes of coordinate system according to figure 3.7-20

F_i = translational force along I-axis

u_i = translational displacement along I-axis

θ_i = rotational displacement about I-axis

$\ddot{u}_i$ = translational acceleration along I-axis

Table 3.7-19
FUEL HANDLING BUILDING NODAL FORCES, ACCELERATIONS, AND DISPLACEMENTS FROM DBE ANALYSIS
(E-W AND VERTICAL EXCITATION)

Node[a] No.	Nodal Weight ($x 10^4$ k)		Forces[b] ($x 10^4$ k)			Accelerations[b] (ft/s^2)			Displacements[b] ($x 10^{-2}$ ft)			Displacements[b] ($x 10^{-4}$ rad)		
	Horiz. Trans.	Vert. Trans.	F_x	F_y	F_z	$\ddot{u}_x$	$\ddot{u}_y$	$\ddot{u}_z$	u_x	u_y	u_z	θ_x	θ_y	θ_z
1	1.63	2.02	0.08	1.51	1.33	1.6	29.7	21.1	0.46	4.02	6.03	16.3	1.5	0.7
2	0.96	0.83	0.07	0.77	0.54	2.2	25.9	21.1	0.70	6.29	6.02	16.6	1.5	0.7
3	0.73	0.55	0.06	0.56	0.38	2.9	24.6	22.2	0.95	8.71	6.19	16.9	1.5	0.7
4	0.86	0.84	0.10	0.72	0.55	3.8	27.4	21.0	1.24	11.92	5.98	17.1	1.5	0.7
5	0.44	0.44	0.07	0.56	0.29	5.3	41.1	21.2	1.77	17.59	6.02	17.3	1.6	0.7
6	0.30	0.30	0.06	0.47	0.19	6.2	51.3	21.2	2.07	20.86	6.01	17.3	1.6	0.7

(a) Refer to figure 3.7-22 for node location

(b) Nomenclature:

x, y, z = axes of coordinate system according to figure 3.7-20

F_i = translational force along I-axis

u_i = translational displacement along I-axis

θ_i = rotational displacement about I-axis

$\ddot{u}_i$ = translational acceleration along I-axis

Amended: May 2007 TI: E041420

Table 3.7-20
FUEL HANDLING BUILDING MAXIMUM CONNECTIVITY FORCES FROM DBE-ANALYSIS

Connectivity (Nodes)[a]	N-S and Vertical Excitation						E-W and Vertical Excitation					
	Forces[b] (x 10^4 k)			Moments[b] (x 10^6 k-ft)			Forces[b] (x 10^4 k)			Moments[b] (x 10^6 k-ft)		
	F_x	F_y	F_z	M_x	M_y	Mz	F_x	F_y	F_z	M_x	M_y	M_z
1 – 2	2.63	0.15	2.11	0.19	1.79	0.25	0.36	2.64	1.93	1.66	0.22	0.20
2 – 3	1.75	0.12	1.37	0.23	1.20	0.30	0.25	2.10	1.62	0.93	0.20	0.06
2 – 4	0.27	0.001	0.16	0.06	0.11	0.10	0.04	0.01	1.02	0.39	0.05	0.02
3 – 4	1.28	0.09	0.98	0.09	0.88	0.15	0.19	1.67	1.29	0.42	0.14	0.07
4 – 5	0.90	0.05	0.53	0.03	0.52	0.05	0.13	1.02	0.48	0.52	0.07	0.02
5 – 6	0.41	0.02	0.21	0.007	0.13	0.02	0.06	0.47	0.19	0.13	0.01	0.02

[a] Refer to figure 3.7-22 for relative location of nodes.

[b] Nomenclature:

x, y, z = axes of coordinate system according to figure 3.7-20

F_i = translational force along the I-axis

M_I = rotational force about the I-axis

3.7.2.1.3 Procedure Used for Modeling

3.7.2.1.3.1 Designation of Systems Versus Subsystems

Major Seismic Category I structures that are considered in conjunction with foundation media in forming a soil-structure interaction model are defined as "seismic systems." Other Seismic Category I structures, systems, and components that are not designated as "seismic systems" are considered as "seismic subsystems."

3.7.2.1.3.2 Decoupling Criteria

Decoupling of systems and subsystems was performed in accordance with the provisions of Section 3.2 of reference 5. Although a simplified model of the NSSS has been incorporated into the lumped parameter analysis of the containment structure to account for potential coupling, the detailed analysis of the NSSS was performed using a decoupled model as discussed in paragraph 3.7.2.2.

3.7.2.1.3.3 Lumped Mass Considerations

A description of the procedure used to locate lumped masses for the seismic analyses of Seismic Category I structures and equipment is provided in Section 3.2 of reference 5.

3.7.2.1.3.4 Lumped Parameter Models for the Containment Structure

The two-dimensional lumped-parameter coupled models of the containment structure and the NSSS used for time-history analyses were developed to obtain response characteristics along the two principal axes of the containment exterior structure and the NSSS. Each model consists of five separate subsystems: Soil, basemat, containment shell, internal structure, and the NSSS.

In considering the interactions between subsystems as mentioned above, it was recognized that the proper geometrical relationships must be maintained. This is extremely important when significant rocking of the structure occurs due to soil-structure interaction. This rocking causes a geometric coupling between the horizontal and vertical motions of points on the structure away from the centerline. If the structure is modeled as a beam, with stiffness and inertia properties lumped at the centerline (elastic axis), the response will be decoupled. Vertical motions computed at the centerline will not account for geometric coupling due to rocking. However, geometric coupling can be accounted for by considering the simple transformation of centerline response to points away from the centerline.

This application has been termed a "multipoint constraint" and is equivalent to the introduction of a rigid massless link. In this manner, the proper geometric relationship may be maintained between subsystems whose interfaces are not on the elastic axis. In addition, coupling between horizontal and vertical motions due to rocking can be accounted for in the model itself. Using the multipoint constraint concept, two-dimensional elements with flexural, shear, and axial stiffness were developed for the basemat, containment shell, interior structure, and the NSSS.

The interface between the containment shell and basemat was made using a set of multipoint constraints that approximated the actual connection. An axisymmetric model of the containment and basemat was used to verify the constraint system. This procedure was repeated for the internal structure and basemat interface.

Soil compliance was incorporated into the model by use of a set of discrete springs attached to the basemat. The spring rates were determined by the soil consultant and were based on data obtained from analysis and the field test discussed in section 2.2 and appendix E of appendix 3.7C. Since the soil structure interaction parameters are strain dependent, different spring rates were used for OBE and DBE inputs. The vertical and horizontal springs were distributed to the nodes in the basemat. The actual stiffness of the spring assigned to each node was determined by multiplying the appropriate total spring rate by a weighting ratio. The weighting ratio for a given node is the ratio of the effective area of the basemat represented by that node divided by the total effective area of all of the nodes. An additional rotational spring rate was applied at the center node. This was necessary since the couple produced by the vertical springs accounts for only a portion of the rotational stiffness. The effective spring rates were checked by applying several static loads to the model.

A beam model of the NSSS, which was considered an adequate representation of the mass and stiffness of the subsystem, was provided by the NSSS supplier. The local deflection characteristics of each interface between the NSSS and the interior structure were studied and then incorporated into the model with an appropriate multipoint constraint. An example of this is the steam generator snubber support. This support is located on a wall panel that has significant local deflection characteristics. A horizontal spring was used to include this effect. The spring rate was determined from static loads applied to a three-dimensional fixed-base finite-element model of the interior structure.

Inertial properties were developed by assigning material density properties to the various beam elements within the structural model and then generating a consistent mass matrix. Additional nodal masses were applied at the appropriate locations to account for the mass associated with floor slabs and equipment.

3.7.2.1.3.5 <u>Axisymmetric Finite-Element Model for the Containment Structure</u>

An axisymmetric finite-element model of the containment structure was developed to obtain the resulting stress distributions within the exterior shell and basemat when subjected to postulated axisymmetric and nonaxisymmetric loading conditions. For the seismic induced loads, the response spectra technique was employed.

For this analysis the interior structure was idealized as an axisymmetric structure in order to account for its stiffness and inertial influence on the total structural response. Figures 3.7-16 and 3.7-17 present a pictorial representation of the computer models used. Damping was incorporated by the use of the composite modal damping technique, wherein the individual modal damping coefficients are based on the predominate response characteristic of a given mode. For example, if the predominate modal response characteristic is soil structure interaction, then the modal damping coefficient is related to soil damping value, and if the predominant modal response characteristic is in the form of differential building motion, then the modal damping coefficient is related to the corresponding structural damping values.

The seismic stress distributions were obtained from a two-component absolute summation technique, considering the worst case response from a single axis horizontal excitation in combination with the vertical excitation, using the design criteria response spectra as input.

3.7.2.1.3.6 Three-Dimensional Finite-Element Model for the Containment Structure

A three-dimensional finite-element model of the containment structure was developed to obtain the resulting stress distributions within the internal structure when subjected to postulated loading conditions. For seismic induced loads, the response spectra technique was employed. Figure 3.7-18 presents a pictorial representation of the computer model used. For this analysis the containment exterior shell was idealized as a single lumped-parameter beam stick in order to account for its stiffness and inertial influence on the total structural response. A pictorial representation of interior containment is shown in figures 3.7-19 and 3.7-20. The basemat flexibility was ignored and the soil-structure interaction was represented by a set of discrete springs that are multipoint constrained to the interior structure basemat interface. Damping was again incorporated by the use of the composite modal damping technique.

The three-component SRSS modal response spectra technique was used to determine the seismic stress distribution.

3.7.2.1.3.7 Three-Dimensional Geometrically Coupled Lumped-Parameter Models

The lumped-parameter geometrically coupled models for the auxiliary building, the fuel handling building, and the diesel generator building used for both time history and response spectra analyses were developed to account for coupling between the various modes of response independent of the orientation of input, and to facilitate the definition of the system physical properties that are required to formulate the equations of motion. The system response is defined by nodal coordinates originating at the center of mass of the various floor levels. This was done since the center of mass for a given floor level can be uniquely defined at a single point independent of the orientation of motion.

The aforementioned results in a geometrically uncoupled mass matrix with diagonal terms that are conveniently evaluated to represent the translational and rotational inertia of the masses tributary to each nodal point. The stiffness matrix, on the other hand, becomes geometrically coupled. It is developed by considering all the resisting assemblies affecting the connectivity between nodal points and transforming these local element stiffnesses to the common nodal coordinate system. This approach permits analysis of the structure as a three-dimensional geometrically coupled system, allows for full consideration of the coupling of translation, torsion, and rocking response, and provides for the evaluation of the coupled natural frequencies. It also permits the representation of partial floors by allowing multiple connectivity between nodal points and affords the use of a single model to study input motion in any direction.

A pictorial representation of the lumped-parameter model for the auxiliary building is shown in figure 3.7-21 and a similar model for the fuel handling building and the diesel generator building is shown in figures 3.7-22 and 3.7-36, respectively.

For these models a diagonal mass matrix was used. The resisting elements to be considered in the formulation of the stiffness matrix are the various shear walls, and to a lesser extent, the columns connecting the nodal points under consideration. These assemblies are treated as three-dimensional elements with flexural, shear, and axial stiffness characteristics. Finite element studies were performed to establish guidelines to be used in determining the effectiveness of specific assemblies and the type of boundary conditions to be assumed. Once resisting assemblies had been identified, and their stiffness effects calculated relative to their local coordinate system with due regard to their directional effectiveness and assumed boundary conditions, the results were transformed and summed with respect to the nodal coordinate system. This was equivalent to introducing a unit displacement in each of the nodal degrees of freedom, performing a rigid-body transformation to the local coordinate system of the resisting assembly, calculating the forces developed in the resisting assemblies, and finally algebraically adding all of the forces about the nodal points.

This whole development was based upon the fundamental definition of the stiffness matrix: Each column of a stiffness matrix was associated with a degree of freedom and represented the vector of forces in every degree of freedom that resulted from a unit displacement imparted to the given degree of freedom.

A similar concept was applied to the soil stiffness characteristics when the modeling was extended to the soil-structure interaction. The discrete springs representing the soil-structure interaction were assumed to act at the geometric center of the basemat, which was not coincident with the basemat nodal point location (center of mass). Therefore, a coordinate transformation was required to incorporate the soil stiffness characteristics into the unconstrained system stiffness matrix of the structural system already defined.

In order to account for all potentially significant interaction phenomena, the model of the fuel handling building also incorporates the hydrodynamic effects of the fluid content in the spent fuel pool. This is accomplished by use of both stationary and oscillatory masses in accordance with the transmissibility characteristics of the fluid.

Utilizing the lumped-parameter model, a modal response spectra analysis was performed to aid in the initial seismic evaluation of the structure and to develop representative stress distributions within the structure. Once the final structural configuration and anticipated member sizes were established, a time-history analysis was performed to develop in structure acceleration time-history records and associated response spectra.

The final step in the seismic analysis of the auxiliary, fuel handling, and diesel generator buildings was to translate the seismic response characteristics defined by the lumped-parameter model into stress distributions within the structure. Specific subsystem finite-element models were developed where necessary to aid in this analysis.

A supplemental lumped-parameter model was developed for the control area of the auxiliary building to account for the potential amplification to the vertical response resulting from the more flexible steel column support system. Typical column lines together with their associated tributary areas were excited with the basemat acceleration time history developed above with due consideration for the geometric rigid-body transformation associated with the location of column bases.

Subsequent to completion of the seismic analysis of the auxiliary building, the concrete walls and roof which were designed to enclose the upper level (elevation 85 feet), over the radwaste area and part of the control area, were deleted. The deletion represents a slight reduction in overall mass and in geometric eccentricity, neither of which significantly affects the seismic response. The validity of the original analysis was confirmed by a partial re-analysis of the building utilizing a mathematical model that incorporated the revised configuration. The re-analysis demonstrated that the dominant soil-structure interaction frequencies were virtually unchanged and that the base shear seismic response was slightly decreased. The results of the re-analysis were used to evaluate the effects of torsional seismic excitation in response to NRC inquiries.

In 1985 evaluations were performed for the addition of a non-safety related building on top of the roof of a part of the existing auxiliary building. The new addition is to be built on top of the "Radwaste Storage Tank Area." The new building is a light-weight structural steel framework covered with light-gage metal sidings and conventional roofing. A new floor system is also added to provide an independent support; separating the building from the existing auxiliary building roof. In order to demonstrate the structural integrity of the existing building a refined 3-dimensional thin shell finite element model that accurately represents the main load carrying shear walls of the auxiliary building was prepared. This model was coupled to the elevated floor subsystem representing the new building addition. Static and dynamic response spectrum analyses were done to evaluate the status of the representative main shear walls. Time-history analyses were also performed to develop floor response spectra at key points for comparison with the original analysis. The new model and the analyses followed the criteria and the basic assumption used in the original analyses of the building. It was demonstrated that the effect of the proposed addition on the dynamic characteristics of the existing structure will be negligible. The evaluation of the main shear walls showed that they have sufficient reserve capacity to resist the effects of adding a new light-weight structure. Comparison of the selected floor response spectra indicated that the original spectra are conservative. Therefore, it was concluded that there will be no discernible adverse effect of the new building addition on the existing structure.

A finite element model (FEM) of the fuel handling building (FHB) was used to evaluate the effects of installing the high density racks in the spent fuel pool. This current FEM is consistent with the original lumped mass model shown in figure 3.7-22. The table 3.7-20A comparison shows that the current FEM behaves very similar to the lumped parameter model. The dynamic characteristic of the current FEM are compared with those stated in table 3.7-10. The two dominant modes for each direction are compared. The model (lumped vs. FEM) comparisons show that the FEM accurately depicts the FHB and the differences in the model frequencies are as expected (more mass - lower frequency). The verified FEM was used to compute the resulting stresses (see table 3.8-7B) from the new spent fuel racks and additional stored fuel for the structural evaluation of the FHB.

3.7.2.1.3.8 Three-Dimensional Finite-Element Subsystem Models

The purpose of the subsystem analysis was to develop the stress distributions within the various subsystem assemblies resulting from the seismic-induced loads. Typical three-dimensional finite-element subsystem models were then developed for the areas of major concern. Appropriate boundary conditions were applied to the structural interfaces of the subsystem models compatible with the physical constraints present in the actual structure. The input data used in this analysis were in the form of modal force and displacement responses developed from the lumped-parameter model using the modal response spectra technique. The specific modal response characteristics such as the relative sign of the various force components within the modal force vectors were preserved by evaluating each mode independently in a mode-by-mode step procedure. The resulting stress distributions from each mode are then combined by the methods described in paragraphs 3.7.2.1.6 and 3.7.2.1.7 and added to the seismic induced inertial effects generated within the subsystem assembly itself.

3.7.2.1.3.9 Three-Dimensional Finite-Element Models

Three-dimensional finite-element models of the safety equipment building, electrical and piping gallery structure, and condensate and refueling tank enclosure structure were developed for use in establishing both time-history acceleration response data and modal response spectra stress distributions. The use of a single model for use in the evaluation of the dynamic response characteristics of a structure was made possible by the incorporation of numerous advanced capabilities of an existing three-dimensional finite element computer code.

For these analyses the structural finite-element meshes are sized to adequately describe the structural response characteristics of the structure and to produce enough data to determine maximum stress levels. Four node quadrilateral plate elements and three node triangular elements were used for this purpose. These elements exhibit both membrane and flexural stiffness characteristics with prescribed material characteristics (i.e., density, modulus of elasticity and Poisson's ratio) and element thickness. Figure 3.7-23 gives a pictorial representation of the mathematical model for the safety equipment building while figures 3.7-25 and 3.7-35 depict a similar pictorial representation for the electrical and piping gallery structure and condensate and refueling tank enclosure structure, respectively. Figure 3.7-24 represents a typical mesh size used in these analyses. The refueling water storage tanks and condensate tanks were modeled as beam elements with masses lumped at the nodes according to the criteria given in reference 8. The "stick model" bases (master nodes) are multipoint constrained to the foundation slab to simulate the effect of tank stiffness upon it.

Due to the varied embedment conditions, the soil-structure interaction characteristics were modeled by a combination of three-dimensional brick elements that were multipoint constrained to a master node and a set of discrete springs attached between the master node and ground. The brick elements were assigned physical parameters consistent with the soil properties defined by the project geotechnical consultant. The set of discrete springs was so proportioned that the series combination of the spring and brick elements will produce the desired soil-structure interaction parameters defined by the project geotechnical consultant. This was verified by applying static loads to the system independently in each of the principal coordinate directions and monitoring the displacement response. For this model, a composite modal damping technique was utilized in both the time-history analysis and the response spectra analysis. The seismic stress distributions were obtained by the methods described in paragraphs 3.7.2.1.6 and 3.7.2.1.7 using the design criteria response spectra as input.

3.7.2.1.3.10 Power Block Analysis

The model used in the analysis of the relative response between adjacent structures is shown in figure 3.7-26. The model takes into account the fact that the site is symmetrical about the east-west centerline and therefore it is necessary to model only one-half of the total site. However, in order to obtain the complete response characteristics, two separate analyses must be performed and the results superimposed. The first analysis incorporates symmetrical boundary conditions along the plane of symmetry, while the second analysis uses the antisymmetrical boundary conditions.

Each structure was modeled as a six degree-of-freedom, rigid body attached to the appropriate soil contact surface. The nodes to which a structure is attached are therefore forced to displace (both in translations as well as rotations and in three-dimensional space) as the master node representing the building. The translational and rotational masses were applied to the building master nodes, at the elevation of the center of gravity for each structure. The soil was modeled in two ways. First a soil grid of 489 by 694 plan dimension and 80 feet deep was modeled using eight-node solid brick elements. The contact surface between the soil and each of the structures was included, in as much detail as possible. Second, the exterior boundary of the soil grid, excluding the plane of symmetry, was multipoint constrained to a master node with a set of discrete springs attached between the master node and ground. The brick elements are assigned physical parameters consistent with the soil properties defined by the project geotechnical consultant. The set of discrete springs is so proportioned that the series combination of the spring and brick elements will produce the desired soil-structure interaction parameters defined by the project geotechnical consultant.

The analyses were performed using composite modal damping and the design criteria free-field response spectra as input. The resulting relative building motions are then obtained through use of the response characteristics for the master nodes of the various buildings. A rigid body transformation is used to translate the individual building responses from the master node location (i.e., center of gravity of the structure) to the desired attachment interface location on the perimeter of the structure. Furthermore, the relative building motions are established on a mode-by-mode step procedure in order to retain the appropriate sign relationship between the various response components. The resulting "modal" relative displacements can then be combined by use of the three-component SRSS combination technique for use in the analysis of piping systems.

Table 3.7-20A
FUEL HANDLING BUILDING
COMPARISON OF MODEL CHARACTERISTICS FOR THE ORIGINAL CONFIGURATION VERSUS THE CURRENT CONFIGURATION[a]

Direction	Frequency (Hz)		Participation Factor		Critical Damping	
	Original	Current	Original	Current	Original	Current
East-West	2.38	2.53	48.6	54.9	9.79	9.72
North-South	2.58	2.67	41.9	34.5	9.87	9.87
Vertical	2.58	2.67	10.0[b]	25.4[b]	9.87	9.87
Vertical	2.99	2.89	83.9[b]	71.5[b]	9.98	9.93
North-South	5.53	4.84	37.4	36.2	9.94	9.21
East-West	5.85	5.16	38.1	38.8	9.87	9.77

Original values in the above table are obtained from Table 3.7-10.

(a) Original Configuration: Original Spent Fuel Storage Racks
Current Configuration: New High Density Spent Fuel Storage Racks

(b) The summation of participation of vertical masses for the original and the current configurations are approximately the same. The frequencies for the two modes are closer spaced for the current evaluation which accounts for the participation shift.

A review of the mode shapes and frequencies from both the symmetrical and antisymmetric models indicated reasonable correlation with those from the individual building analyses. However, it should be emphasized that the results of these analyses were used only to establish inter-building response characteristics. For response characteristics totally within a given structure the separate building analyses are used.

3.7.2.1.4 Soil/Structure Interaction

In general, the methods used to analyze the soil-structure interaction effects are in accordance with section 3.3 and Appendices D and H of reference 5, with other modifiers for geometric configuration and embedment provided by the project geotechnical consultant (see section 3.2 and appendix E of appendix 3.7C). Strain-dependent soil properties are introduced into the analysis by using different rates for OBE and DBE analysis.

The lumped parameter models for the containment time-history analysis utilize beam elements to model the flexibility of the basemat. Vertical and horizontal springs are distributed to the nodes in the basemat. Actual stiffness of the spring assigned to each node is determined by multiplying the appropriate total spring rate by a weighting ratio. The weighting ratio for a given node is the ratio of the effective area of the basemat represented by that node divided by the total effective area of all of the nodes. An additional rotation spring is applied at the center node. This additional spring is necessary since the couple produced by the vertical springs accounts for only a portion of the rotational stiffness. The effective spring rates are checked by applying several static loads to the model.

For three-dimensional geometrically coupled lumped parameter models in which the flexibility of the basemat is not modeled (i.e., auxiliary building and fuel handling building), the discrete springs representing the soil-structure interaction are assumed to act at the geometric center of the basemat, which is not necessarily coincident with the basemat nodal point location (center of mass). Therefore, a coordinate transformation is performed to incorporate the soil stiffness characteristics into the unconstrained system stiffness matrix of the structural system.

For three-dimensional finite-element models (i.e., safety equipment building and piping electrical junction structure), due to the varied embedment conditions, the soil-structure interaction characteristics are modeled by a combination of three-dimensional brick elements that are multipoint constrained to a master node from their exterior boundary and a set of discrete springs attached between the master node and ground. The brick elements are assigned physical parameters consistent with the soil properties. The set of discrete springs is so proportioned that the series combination of the spring and brick elements produce the desired soil-structure interaction parameters. Spring equivalence is verified by applying static loads to the system independently in each of the principal coordinate directions and monitoring the displacement response.

3.7.2.1.5 Development of Floor Response Spectra

The time-history analysis method is used to develop floor response spectra. It is described in Sections 4.2, 4.3, and 5.2 of reference 5.

Independent analyses are performed for each of the principal coordinate directions.

Due to the geometric coupling within the structures, input in any one coordinate direction can produce response in each coordinate direction. Therefore, the response spectra represent an envelope of the response produced from the vertical excitation and a single-axis horizontal input.

The typical in structure response is an envelope of the response obtained from the SRSS combination of the vertical response and either of the single-axis horizontal responses.

3.7.2.1.6 Components of Earthquake Motion

Although independent analyses were performed for each of the three principal coordinate directions, response characteristics used in the design of Seismic Category I structures were established considering several different combination techniques for combining the responses resulting from excitation in the three independent coordinate directions. More specifically, three distinct methods were employed for the combination of seismic response characteristics. The choice of a specific technique evolved as industry and regulatory practice changed. Those structures designed early in the project utilized either a modified two-component SRSS or a two component absolute summation technique, while the structures designed most recently incorporated the three-component SRSS technique.

For the auxiliary building and fuel handling building, the resultant seismic load distributions used in design were established from the direct combination of the individual modal responses resulting from the maximum single axis horizontal excitation and the vertical excitation. This combination of individual modal responses was performed to account for modal superposition of geometrically coupled modes. In this combination technique, the sign relationship between the various response terms was maintained while considering the worst case of either a positive and negative combination of the individual modal response terms. The resulting combined individual responses were then combined by an SRSS technique.

For the following structures, the resultant seismic load distributions used in design were established by a two-component absolute summation technique considering the worst case response from a single axis horizontal excitation in combination with the vertical excitation:

- Intake Structure and Transition Section
- Containment Exterior Shell
- Safety Equipment Building
- Electric and Piping Gallery Structure

For the following structures, the resultant seismic load distributions used in design were established by a three-component SRSS combination technique considering seismic excitation in all three coordinate directions acting concurrently:

- Containment Interior Structure
- Condensate and Refueling Water Tank Enclosure Structure
- Diesel Generator Building
- Offshore Intake Conduit and Auxiliary Intake Structure

For development of in structure response spectra refer to paragraph 3.7.2.1.5.

3.7.2.1.7 Combination of Modal Responses

In general, modal responses are combined as described in Section 4.2.1 of reference 5. The major exception is for the auxiliary building and fuel handling building where an alternate technique was employed. This alternate procedure is discussed in depth in the third paragraph below.

In the application of the modal response spectra technique, the individual modal responses are combined by the SRSS modal summation. This method is based upon probability considerations and provides an excellent approximation of the maximum anticipated response. It takes into account the random nature of the seismic disturbance and the relatively short duration of the response, while at the same time not completely ignoring potential modal superposition. Where modal frequencies are closely spaced, the contribution from these modes are first summed using the sum of their absolute values. These results are then considered as a pseudo-mode when the overall SRSS modal summation is made. The total system response is then established by the methods described in paragraph 3.7.2.1.6.

In the analyses of the auxiliary building and fuel handling building, the individual modal responses from the maximum single axis horizontal excitation and the vertical excitation were directly combined prior to any SRSS combination. This combination of individual modal responses was performed by the algebraic combination of the response terms, considering the worst case of either an in-phase or out-of-phase combination of the various response characteristics. This modal combination technique was employed to account for the superposition of geometrically coupled modes while at the same time preserving the relative sign relationship between the various response terms within a given mode. The resulting combined individual modal responses were then combined by an SRSS technique, as discussed in paragraph 3.7.2.1.6.

3.7.2.1.8 Interaction of Non-Category I structures with Seismic Category I Structures

To ensure that Seismic Category I structures will perform their intended functions after a DBE, non-Category I structures are designed to meet one of the following two conditions:

A. The non-Category I structure, which is not checked for DBE equivalent loads, is sufficiently isolated from Seismic Category I structures so as to preclude interaction.

B. The non-Category I structure is analytically checked to assure that it will not collapse on or otherwise impair the integrity of adjacent Seismic Category I structures when subjected to DBE equivalent loads.

3.7.2.1.9 Effects of Parameter Variations on Floor Response Spectra

Sections 5.2 and 5.3.2 of reference 5 describe the various considerations in the seismic analyses. These include the effects on floor response spectra of expected variations of structural properties, damping, soil properties, soil-structure interaction, etc.

3.7.2.1.10 Use of Static Load Factors

3.7.2.1.10.1 <u>Equivalent Static Analysis for the Intake Structure</u>

In the equivalent static load analysis, the maximum unamplified free-field acceleration levels are input statically into the structure, as equivalent inertia loadings. The structure is idealized by various two-dimensional finite-element models representing typical cross-sections through the structure, taking into account the tributary mass associated with each section. Figure 3.7-27 represents typical models used in the analysis. Soil-structure interaction characteristics are modeled as a set of discrete springs. Seismic-induced lateral soil pressure conditions are also applied. The stress distributions resulting from this analysis are then combined with the various operating loading conditions to establish the reinforcements. Justification for using the maximum unamplified free-field acceleration as the design input is provided in paragraph 3.7.2.1.10.5.

3.7.2.1.10.2 Equivalent Static Analysis for the Offshore Conduits

For the equivalent static analysis of the offshore conduits, the calculated acceleration levels were input statically as equivalent inertia loadings. To obtain the design acceleration levels, a factor of 1.5 was applied to the peak response from the applicable project ground motion response spectra. The operating basis earthquake (OBE) and DBE loadings were determined using structural damping of 4% and 7% of critical, respectively, for the conventionally reinforced concrete sections; and 2% and 5%, respectively, for the prestressed concrete sections.

The pipe sections were analyzed as a closed ring. The stress distributions resulting from the seismic analysis were combined with the various operating loading conditions to establish the reinforcement requirements. Soil structure interaction is not expected to be significant because of the rigidity of the pipe sections, and because the completely buried pipe sections filled with water have similar mass and inertial characteristics as the displaced soil.

3.7.2.1.10.3 Equivalent Static Analysis for the Auxiliary Intake Structure

For the equivalent static analysis of the auxiliary intake structure, the calculated acceleration levels are input statically into the structure as equivalent inertia loads. To obtain the seismic loadings for structural elements subject to oscillatory motion, a factor of 1.5 was applied to the peak response from the applicable project ground motion response spectra. The OBE and DBE loadings were determined using structural damping of 4% and 7% of critical, respectively.

Stress distributions resulting from the equivalent static analysis are combined with the various operating loading conditions to establish the reinforcement requirements. Soil structure interaction will not be significant because of the select gravel backfill, the rigidity of the structure, and the similar mass densities and inertial characteristics of the structure and the backfill.

3.7.2.1.10.4 Equivalent Static Analysis for the Box Conduits

For the equivalent static analysis, the maximum unamplified free-field acceleration levels were input statically to the box conduit cross-section as equivalent inertial loads. Seismically-induced lateral soil pressures were also applied. Seismic loads were combined with the various operating loading conditions and, in using the finite element model, the stresses were calculated and the reinforcing requirements established.

The use of unamplified free-field accelerations is justified for the following reasons: (1) the box conduit is a completely buried structure, filled with water during normal operation, and has similar mass and inertial characteristics as the displaced soil; and (2) the box conduits, being completely buried, are highly damped and thus amplification of the free-field accelerations will be insignificant.

3.7.2.1.10.5 Instantaneous Displacement Profile Analysis

The intent of this analysis is to verify the magnitude and stress distribution obtained in the previous analysis. The critical instantaneous displacement profile (CIDP) is defined as the deflected shape that the structure will assume at an instant during the earthquake, which would cause maximum stresses within the structural elements. The determination of the CIDP is made using a traveling shear-wave finite-element model and evaluating the displacement profile along the base of the structural elements in the finite-element mesh at every instant in time. The critical profile is found using maximum slope change across the profile (maximum bending) as a criterion. In the development of the CIDP, only the gross structural stiffness characteristics are included.

For a more detailed discussion please refer to section 3.5 and appendix H of appendix 3.7C. Once the CIDP has been developed, it is used as a boundary displacement input to a more refined three-dimensional finite-element model. The resulting stress distributions are then combined with the lateral soil pressure conditions and compared to the stress distributions obtained in the equivalent static load analysis. The pictorial representation of the instantaneous displacement profile analysis is shown in figure 3.7-28.

3.7.2.1.11 Method Used to Account for Torsional Effects

Torsional effects are accounted for directly in the modeling of either three-dimensional geometrically-coupled lumped-parameter models or three-dimensional finite-element models.

3.7.2.1.12 Comparison of Responses

A comparison of the results of a modal response spectrum analysis and the modal time-history analysis for the containment structure is given in table 3.7-21.

3.7.2.1.13 Methods for Seismic Analysis of Dams

This section does not apply to this plant since there are no dams which could affect safe shutdown of the plant.

3.7.2.1.14 Determination of Seismic Category I Structure Overturning Moments

The effects of overturning moments are evaluated by the methods shown in Section 4.4 of reference 5.

Vertical and single-axis horizontal responses are combined using the SRSS method.

3.7.2.1.15 Analysis Procedure for Damping

Incorporation of damping into the seismic analysis was accomplished by one of the following procedures. For the lumped parameter time-history analyses, the nonproportional damping technique was used. While for the three-dimensional finite-element analyses, the composite modal damping technique was employed.

The nonproportional damping technique is described in reference 7. For this procedure, the damping characteristics of each major subsystem within a given model is defined independently and is dependent solely upon the physical characteristics of the particular subsystem and the anticipated stress levels. Application of this procedure results in equations of motion that will not uncouple in the generalized modal degrees of freedom, unless the same value of damping has been used in each subsystem. Consequently, the equations of motion must be solved using a direct integration procedure. The Newmark β method was selected for this purpose.

Table 3.7-21
CONTAINMENT STRUCTURE
DBE SEISMIC RESPONSES[(a)]

Elevation (ft)	Horizontal Earthquake						Vertical Earthquake					
	Horizontal Response			Vertical Response			Horizontal Response			Vertical Response		
	SMIS[(b)]	ASHSD[(c)]	% Diff.[(d)]	SMIS[(b)]	ASHSD[(c)]	% Diff.[(d)]	SMIS[(b)]	ASHSD[(c)]	% Diff.[(d)]	SMIS[(b)]	ASHSD[(c)]	% Diff.[(d)]
10.5	23.27	20.67	11.2	20.76	19.03	8.3	0	0	0	21.60	18.74	13.2
35.875	24.15	22.13	8.4	20.76	19.22	7.4	0	0	0	21.69	18.81	13.3
61.25	28.83	25.73	10.8	20.76	19.44	6.4	0	0	0	21.78	18.91	13.2
86.625	33.52	30.22	9.8	20.76	19.61	5.5	0	0	0	21.83	19.03	13.4
112.0	38.06	35.50	6.7	20.76	19.73	5.0	0	0	0	21.91	19.07	13.0
140.39	44.04	41.78	5.1	--	--	--	0	0	0	21.91	19.13	12.7
177.5	52.45	50.41	3.9	--	--	--	0	0	0	21.93	19.39	11.9
Center of Basemat	22.05	20.29	8.0	0.00	0.13	--	0	0	0	21.65	21.29	1.7

(a) Units are feet/second^2

(b) Time-history response data are obtained from computer runs sequence No. F370A1A, FS07AEE and F323HLP.

(c) Response spectrum response data are obtained from computer runs sequence No. F742B65 and F694B20.

(d) With reference to SMIS.

Application of the nonproportional damping technique was restricted conservatively by the selection of soil-damping values to values that result in structural response no less than that resulting from an overall proportional modal damping of 10% for the DBE or 8% for the OBE, even though significantly larger values can be justified (see section 3.0 and appendix D of appendix 3.7C). To ensure this requirement, soil damping values are first selected based upon a comparison of steady-state analyses, using various damping values, and then confirmed by comparison of in structure response spectra from proportional and nonproportional time-history analyses.

As discussed previously, the structural response of all the major structures is dominated by soil-structure interaction modes, and consequently, the overall energy dissipation characteristics of the model are controlled by the damping assigned to the soil subsystem. Therefore, the final damping values used for the soil subsystem are consistent with the preestablished upper-bound proportional damping limit of 10% of the DBE and 8% for the OBE.

The composite modal damping technique is discussed in Sections 3.2 and 3.3 of reference 5. Again damping values are defined independently for each subsystem, based upon the physical characteristics of the particular subsystem and the predicted stress levels, but are then weighted by the response characteristics of the particular modes, which results in an equivalent diagonalized modal damping matrix. By this method, the equations of motion are uncoupled and can be solved using the normal mode solution technique. Damping values used in the soil subsystem again were restricted conservatively to 10% for the DBE or 8% for the OBE.

3.7.2.2 Reactor Coolant System

3.7.2.2.1 Seismic Analysis Methods

The adequacy of seismic loadings used for the design of the major components of the reactor coolant system are confirmed by the methods of dynamic analysis employing time-history techniques. The major components are the reactor, the steam generators, the reactor coolant pumps, the reactor coolant piping, and the pressurizer.

In order to account for possible dynamic coupling effects between the components, a composite coupled model is employed in the dynamic analysis of the reactor, the two steam generators, the four reactor coolant pumps, and the interconnecting piping. The analysis of these dynamically coupled multi-supported components utilizes different time-dependent input excitations applied simultaneously to each support. In addition, the representation of the reactor vessel assembly used in this coupled model includes sufficient detail of the reactor internals to account for possible dynamic interaction between the reactor coolant system and internals. The results of the analysis of the coupled components of the reactor coolant system include an appropriate time-history forcing function for use in a separate analysis of a more detailed model of the reactor internals.

The analysis of the pressurizer employs a separate mathematical model and utilizes the same time-history techniques.

A representation of the coupled components, of sufficient detail to account for possible dynamic interaction effects between the containment internal support structure and the reactor coolant system components, is supplied for use in performing the analysis of the containment internal support structure. The results of the analysis of the containment internal support structure includes the time-history forcing functions for use in the separate analysis of the more detailed model of the coupled components of the reactor coolant system and the pressurizer.

For the time-history analyses, dynamic responses to vertical seismic excitation are found for both the case of initial support displacement upward and the case of initial support displacement downward. The responses are added algebraically at each time step to determine the most severe combinations produced by the effects of seismic excitations in each of the horizontal directions applied simultaneously with seismic excitations in each of the horizontal directions applied simultaneously with seismic excitation in either vertical direction.

Contributions from all significant modes of response are retained in the analyses.

The damping factors used in the seismic analyses of the major components of the reactor coolant system are conservatively selected. Modal damping factors of 1% of critical for OBE and 2% of critical for DBE are used in the seismic analyses of the major components of the reactor coolant system. Allowable damping factors are given in table 3.7-22.

Table 3.7-22

DAMPING RATIOS USED IN ANALYSIS OF CATEGORY I
STRUCTURES, SYSTEMS, AND COMPONENTS

Item	Maximum Damping Ratio (Percent of Critical)	
	Operational Basis Earthquake	Design Basis Earthquake
Equipment and large diameter piping systems, pipe diameter greater than 12 inches	2	3
Small diameter piping systems, diameter less than or equal to 12 inches	1	2
Welded steel structures	2	4
Bolted steel structures	4	7
Prestressed concrete structures	2	5
Reinforced concrete structures	4	7

3.7.2.2.2 Mathematical Models

In the descriptions of the mathematical models that follow, the spatial orientations are defined by the set of orthogonal axes where Y is in the vertical direction, and X and Z are in the horizontal plane, in the directions indicated on the appropriate figure. The mathematical representation of the section properties of the structural elements employs a 12 x 12 stiffness matrix for the three-dimensional space frame models. Elbows in piping runs include the in-plane/out-of-plane bending flexibility factors as permitted in the ASME Section III Code.

A. Reactor Coolant System - Coupled Comments

A schematic diagram of the composite mathematical model used in the analyses of the dynamically coupled components of the reactor coolant system is presented in figure 3.7-29. This model includes 30 mass points with a total of 79 dynamic degrees-of-freedom. The mass points and corresponding dynamic degrees-of-freedom are distributed to provide appropriate representations of the dynamic characteristics of the components, as follows: the reactor vessel with internals is represented by four mass points with a total of 11 dynamic degrees-of-freedom, each of the two steam generators are represented by four mass points with a total of 10 dynamic degrees-of-freedom, each of the four reactor coolant pumps are represented by two mass points with a total of five dynamic degrees-of-freedom, each pump suction and discharge branch of piping is represented by a mass point with three dynamic degrees-of-freedom, and each reactor vessel outlet pipe is represented by a mass point with two dynamic degrees-of-freedom. The representation of the reactor internals is formulated in conjunction with the analysis of the reactor internals discussed in paragraph 3.7.3.14 and is designed to simulate the dynamic characteristics of the models used in that analysis.

The mathematical model provides a three-dimensional representation of the dynamic response of the coupled components to seismic excitations in both the horizontal and vertical directions. The mass is distributed at the selected mass points and corresponding translational degrees-of-freedom are retained to include rotary inertial effects of the components. The total mass of the entire coupled system is dynamically active in each of the three coordinate directions.

The mathematical model employed in the analysis of the pressurizer is shown schematically in figure 3.7-30. This lumped parameter, three-dimensional model provides a multimass representation of the pressurizer and supporting structure, and includes seven mass points with a total of 15 dynamic degrees-of-freedom. Distribution of mass is accomplished in the same fashion as for the coupled components.

B. Excitation Data for Reaction Coolant System (RCS)

The seismic excitations used for the dynamic seismic analysis of the RCS major components are developed as a result of the analysis of the containment structure discussed in paragraph 3.7.2.1.

The information received consists of time histories of the absolute accelerations and relative displacements for the locations in the structure in which the RCS is supported and for the locations in the structure at which the pressurizer is supported. The information contains the horizontal, vertical, and rotational support motions resulting from each of the horizontal directions of ground motions, and the vertical support motions resulting from the vertical ground motion. The supporting structure is observed to exhibit significant rigid body rocking due to the horizontal ground motion, but only vertical motion due to the vertical ground motion.

The data was received as digitized records on magnetic tapes, which were transferred to the C-E data processing system for subsequent computations.

C. Analytical Techniques

As applied in the analysis, the undamped simultaneous equations of motion for linear structural systems can be written: [9]

$$M\ddot{X} + KU = F$$

Where X represented the absolute acceleration of the mass point dynamic degrees-of-freedom, and U represents the displacements of the mass and support point dynamic degrees-of-freedom relative to a datum support that is chosen to eliminate free body motion.

Expanding equation (1) gives:

$$\begin{bmatrix} M_m & O \\ O & M_s \end{bmatrix} \begin{bmatrix} \ddot{X}_m \\ \ddot{X}_x \end{bmatrix} + \begin{bmatrix} K_{mm} & K_{ms} \\ K_{sm} & K_{ss} \end{bmatrix} \begin{bmatrix} U_m \\ U_s \end{bmatrix} = \begin{bmatrix} O \\ F_s \end{bmatrix} \qquad (2)$$

where:

M_m = a diagonal submatrix of the system model lumped masses.

M_s = a submatrix of inertia terms associated with the support joints of the systems. For the purposes of this analysis, $M_s = 0$, because there is no mass lumped at support joints.

F_s = the reaction forces at the system support points due to the response of the system to the motion of the supporting structure.

K = the stiffness matrix of the system model condensed in a manner such that only mass point elements (subscript m) and active, nonreleased, nondatum support elements (subscript s) remain in the matrix. (The method used for this analysis employs the choice of a datum support to eliminate free body motions.)

U_m = displacement of mass point dynamic degrees-of-freedom

U_s = displacement of nondatum support points relative to the datum support.

$\ddot{X}_m$ = absolute acceleration of the mass point dynamic degrees-of-freedom of the model

$\ddot{X}_s$ = absolute acceleration of the system support points

The time-history support motions imposed at the nondatum supports include only such displacements as would tend to cause distortions in the system. Rigid body translation or rotation of the supporting structure would not distort the system being analyzed, therefore rigid body displacements of the supporting structure are removed by computing the nondatum support relative motions as follows:

$$U_s = X_s - X_d - R_s\,\theta \qquad (3)$$

where:

U_s = displacements of nondatum support points relative to the datum support

X_s = absolute displacements of nondatum supports

X_d = absolute displacement of datum support

R_s = a vector of distances from the datum support point to the nondatum support points

θ = rigid body rotational displacement of the supporting structure

The first equation of the set of equations (2) yields:

$$M_m X_m + K_{mm} U_m + K_{ms} U_s = O \qquad (4)$$

A separation of variables can be achieved by defining the absolute acceleration of a mass point in terms of acceleration relative to the datum support, such that:

$$\ddot{U}_m = \ddot{X}_m - \gamma \ddot{X}_{sd} - R_m \ddot{\theta} \tag{5}$$

where:

γ = a vector defining the direction of excitation, such that:
$\gamma = 1$, if the i^{th} dynamic degree-of-freedom is in the direction of support translation, or
$\gamma = 0$, if the i^{th} dynamic degree-of-freedom is not in the direction of support translation

$\ddot{X}_{sd}$ = the absolute acceleration of the datum support in a given direction

R_m = a vector of distances from the datum support point to the mass point

$\ddot{\theta}$ = rigid body rotational acceleration of the supporting structure

Equation (4) then becomes:

$$M_m \ddot{U}_m + K_{mm} U_m = - M_m \gamma \ddot{X}_{sd} - \text{Msubm}\, R_m \ddot{\theta} - K_{ms} U_s \tag{6}$$

At this point it is to be noted that the equations of motion are in a form expressing three-dimensional response of the system mass points, due to multiple support excitations in a single direction. Methods for determination of the responses due to two or more directions of excitation are discussed later in this presentation.

Introducing the normal mode coordinate transformation:

$$U = \Phi q \tag{7}$$

where:

Φ = the matrix of eigenvectors,

Then the equations of motion can be uncoupled and written in the following form including damping:

$$\ddot{q} + 2\xi\omega\dot{q} + \omega^2 q = (\Phi^T M \Phi)^{-1}\left(\Phi^T M \gamma \ddot{X}_{sd} + \Phi^T M R_m \ddot{\theta} + \Phi^T K_{ms} U_s\right) \tag{8}$$

where:

ω^2 = diagonal matrix of eigenvalues,

Φ = matrix of eigenvectors, and

$2\xi\omega$ = diagonal matrix of modal damping terms.

Having the stiffness and mass properties of the model the eigenvalue solution, and the digitized support excitations $\ddot{X}_{sd}$, X_d, X_s, $\ddot{\theta}$ and θ, equation (8) can be solved in closed form for the time histories of the mass point responses, U_m and $\ddot{X}_m$.

3.7.2.2.3 Frequency Analysis

An eigenvalue analysis is performed utilizing the ICES STRUDL II computer code,[10] to calculate the mode shapes and natural frequencies of the composite mathematical models. Modifications to the standard ICES STRUDL II program were implemented by C-E to include a Jacobi diagonalization procedure in the eigenvalue analysis, and to provide appropriate influence coefficients and stiffness matrices for use in the response and reaction calculations.

The calculated natural frequencies and dominant degrees-of-freedom are shown in tables 3.7-23 and 3.7-24 for the reactor coolant system, and the pressurizer.

A description of the ICES STRUDL II computer code is provided in Appendix 3C.

3.7.2.2.4 Mass Point Response Analysis

The time-history of mass point responses to seismic excitation are computed using TMCALC, a C-E code. This code performs a closed form integration of the equations of motion for singly or multiply supported dynamic systems utilizing normal mode theory. For the multiply supported systems, the separate time histories of each support are imposed on the system simultaneously. The results are time-history responses of the mass points.

A description of the computer code TMCALC is provided in Appendix 3C.

3.7.2.2.5 Seismic Reaction Analysis

The dynamically induced loads at all system design points, due to the superimposed time-history support excitations and mass point responses, are calculated utilizing FORCE, a C-E computer code. This code performs a complete loads analysis of the deformed structure at each incremental time step by computing internal and external system reactions (forces and moments) by superposition of the reactions due to the mass point displacements and the nondatum support displacements.

A description of the FORCE computer program is provided in Appendix 3C.

Influence coefficients for each desired reaction are computed for the effect of unit displacements of each mass point and each nondatum support.

There is a complete set of mass point and support influence coefficients for each component of force, moment, stress, or displacement to be computed at the locations of interest throughout the system. The given support displacements and computed mass point displacements at each time step are multiplied by the set of influence coefficients, to perform a complete reaction analysis of the system at each time step.

Table 3.7-23

NATURAL FREQUENCIES AND DOMINANT DEGREES OF FREEDOM
REACTOR COOLANT SYSTEM (Sheet 1 of 2)

Mode No.	Frequency (Hz)	Joint Number	Dominant Degrees of Freedom	
			Direction	Locations
1	2.63	9932	Z	Reactor internals
2	2.63	9932	X	Reactor internals
3	8.43	9902	Z	Reactor internals
4	8.57	9902	X	Reactor internals
5	15.37	3405, 404	X	Top masses of SG 2 & 1
6	15.37	404, 3405	X	Top masses of SG 1 & 2
7	16.02	3412, 412	Z	Internals masses of SG 2 & 1
8	16.05	412, 3412	Z	Internals masses of SG 1 & 2
9	16.36	9996 etc.	Z,X	RV & pump masses
10	17.82	3408, 408 etc.	X	Internal masses of SG 2 & 1
11	19.29	4103, 2103	X	Top masses of pumps 1B & 2B
12	19.70	2103, 1103 4103, 5103	X	Top masses of all pumps
13	19.84	5103, 1103	X	Top masses of pumps 2A & 1A
14	22.54	9932, 9996	Y	Reactor internals & externals
15	22.67	1103, 5103	X	Top masses of pumps 1A & 2A
16	23.27	9932	Y	Reactor internals
17	23.33	3404, 404	Z	External masses of SG 2 & 1
18	23.36	404, 3404	Z	External masses of SG 1 & 2
19	24.09	4103, 2103	Z	Top masses of pumps 2B & 2B
20	24.09	2103, 4103	Z	Top masses of pumps 1B & 2B
21	24.12	5103, 1103	Z	Top masses of pumps 2A & 1A
22	24.12	1103, 5103	Z	Top masses of pumps 1A & 2A
23	24.38	3404, 404	Y	External masses of SG 2 & 1
24	24.87	404, 3404	Y	External masses of SG 1 & 2
25	30.79	2580, 4580	Z,X	CL piping masses
26	31.17	4580, 2580	Z,X	CL piping masses
27	32.27	4103, 2103	Y	Pump top masses
28	32.35	2103, 4103	Y	Pump top masses
29	32.36	1103, 5103	Y	Pump top masses
30	32.37	5103, 1103	Y	Pump top masses
31	33.40	1580, 5580	X,Z	CL piping masses

Table 3.7-23

NATURAL FREQUENCIES AND DOMINANT DEGREES OF FREEDOM
REACTOR COOLANT SYSTEM (Sheet 2 of 2)

Mode No.	Frequency (Hz)	Joint Number	Dominant Degrees of Freedom	
			Direction	Locations
32	33.90	5580, 1580	X,Z	CL piping masses
33	34.76	4580, 2580	Z	CL piping masses
34	35.67	1580, 5580	Z	CL piping masses
35	36.88	3412, 412	X	Internal masses of SG 2 & 1
36	37.04	412, 3412	X	Internal masses of SG 1 & 2
37	37.25	412, 3412	Z	Internal masses of SG 1 & 2
38	37.27	3412, 412	Z	Internal masses of SG 2 & 1
39	39.05	2580, 4580	Z	CL piping masses
40	39.19	4580, 2580	Z	CL piping masses
41	39.26	5580, 1580	Z	CL piping masses
42	40.18	5101, 1580	Z	CL piping masses
43	42.77	5101, 1101	Z	Pump lower masses
44	42.79	1101, 5101	Z	Pump lower masses
45	43.97	2104, 4101	X,Z	Pump lower masses
46	44.16	4101, 2101	X	Pump lower masses
47	47.18	3412, 412	Y	Internal masses of SG 2 & 1
48	47.18	412, 3412	Y	Internal masses of SG 1 & 2
49	48.94	9995	X	RV lower masses
50	49.87	9932	Y	Reactor internals
51	50.47	3408, 408	Z	Internal masses of SG 2 & 1
52	50.47	408, 3408	Z	Internal masses of SG 1 & 2
53	50.67	3408, 408	X	Internal masses of SG 2 & 1
54	51.63	408, 3408	X	Internal masses of SG 1 & 2
55	61.98	9902	Y	Reactor internal
56	68.60	4580	Y	CL piping mass
57	68.60	2580	Y	CL piping mass
58	76.82	5760, 1760	Y	CL piping mass
59	76.85	1760, 5760	Y	CL piping mass

The desired components of reaction (force, moment, stress, or deflection) are computed at each time step as follows:

$$R(t) = C_m U_m(t) + C_s U_s(t), \qquad (9)$$

where:

$R(t)$ = a vector of reaction components at time t

C_m = a matrix of mass point unit displacement influence coefficients (one column per mass point and one row per reaction component)

C_s = a matrix of nondatum support point unit displacement influence coefficients (one column per nondatum support and one row per reaction component)

$U_m(t)$ = a vector of mass point relative displacement at time t

$U_s(t)$ = a vector of nondatum support relative displacements at time t

In a similar manner, the absolute acceleration of any point in the system can be computed by multiplying the mass point and support relative accelerations by the influence coefficients for displacement reactions, and adding in the datum support absolute acceleration and rigid body rotational acceleration as follows:

$$\ddot{R}(t) = \gamma \ddot{X}_{sd}(t) + C_m \ddot{U}_m(t) + C_s \ddot{U}_s(t), + R_p \ddot{\theta}(t) \qquad (10)$$

where:

$\ddot{R}(t)$ = a vector of absolute acceleration components at time t,

$\ddot{X}_{sd}(t)$ = the absolute acceleration of the datum support at time t,

C_m = matrix of mass point unit displacement influence coefficients, for components of displacement reactions,

$\ddot{U}_m(t)$ = a vector of mass point accelerations relative to the datum at time t,

C_s = a matrix of nondatum support unit displacement influence coefficients for components of displacement reactions,

$\ddot{U}_s(t)$ = a vector of nondatum support relative accelerations at time t,

γ = a vector defining the direction of excitation, such that:

γi = 1, if the i^{th} component-of-reaction is in the direction of support motion, or

Table 3.7-24

NATURAL FREQUENCIES AND DOMINANT DEGREES OF FREEDOM PRESSURIZER

Mode Number	Frequency (Hz)	Joint Number	Direction
1	28.71	406	Y
2	34.55	406	X
3	39.50	406	Z
4	60.72	410	X
5	72.53	410	Z

γi = 0 if the i^{th} component-of-reaction is not in the direction of support motion.

R_P = a vector of distances to the reaction points from the datum.

This method therefore permits the calculation of any desired force or moment, or nonmass point motion, on a time-history basis, for singly or multiply-excited structural systems.

Using the linear superposition approach, the simultaneous results from two or more directions of excitation can be combined at each step. Two or more sets or mass point displacement responses and support point displacement excitations are combined at each time step prior to the influence coefficients multiplications.

The support and mass point displacements due to each horizontal and vertical seismic excitations are added algebraically at each time step. The maximum components of each reaction for the reactor coolant system and for the pressurizer for the entire time domain, and its associated time of occurrence, are found in this manner.

3.7.2.2.6 Results

The reactions (forces and moments) at all design points in the reactor coolant system and in the pressurizer obtained from the dynamic seismic analysis are compared with the seismic loads in each component design specification. The results of this comparison are summarized in tabular form for the points of maximum calculated load in table 3.7-25.

The maximum seismic loads calculated by the time-history techniques are the results of a search and comparison over the entire time domain of each individual component of load due to the simultaneous application of each horizontal with either vertical excitation. The maximum calculated components of load for each design location do not in general occur at the same time, nor for the same combination of horizontal and vertical excitation, and therefore result in a conservative worst case.

3.7.2.2.7 Conclusion

All seismic loads calculated by the dynamic seismic analyses are less than or equal to the corresponding loads in the component design specifications. These analyses are performed for the OBE excitation and for DBE excitation and the results are compared with the OBE and DBE design specification loads respectively.

It is concluded that the seismic loadings specified for the design of the reactor coolant system components and supports are adequate.

3.7.3 SEISMIC SUBSYSTEM ANALYSIS

3.7.3.1 Seismic Analysis Methods

The seismic analysis methods used for Seismic Category I subsystems are discussed in Sections 3.0 through 6.0 of Bechtel Topical Report BC-TOP-4A[5] and paragraph 3.7.3.14. Appendix 3.7B describes the methods used for seismic analysis of piping systems.

3.7.3.2 Determination of Number of Earthquake Cycles

3.7.3.2.1 Subsystems Other than the NSSS (Systems, Equipment and Components)

Procedures to determine the number of earthquake cycles for piping during seismic events are discussed in appendix 3.7B. Structures and equipment are designed on the basis of analytical results. In general, the design of structures and the majority of the equipment is not fatigue controlled, since most stress and strain reversals occur only a small number of times. The occurrence of earthquake and design basis accident full-design strains occurs too infrequently and with too few cycles to generally require fatigue design of structures.

The number of earthquake cycles to be used in the design of subsystems is dependent upon three parameters:

A. The significant frequency characteristics of the subsystem and/or supporting media.

B. The duration of the postulated seismic event.

C. The number of seismic events to which the plant might be subjected.

Table 3.7-25

LOAD TABLES FOR REACTOR COOLANT SYSTEM (Sheet 1 of 14)

Seismic Excitation	System Location	Seismic Load[a]		
		Component of Reactions	Calculated Maximum	Specified for Design
Combined North-South and Vertical (OBE)	Steam generator upper key	Fz	9	489
	Steam generator snubbers	Fx	1,213	1,214
	Steam generator support skirt	Fy Fz Mx My Mz	3,377 7 64 295 16,053	3,377 7 72 300 17,628
	Steam generator vertical pad	Fy	1,409 102	1,409 102
	Steam generator horizontal key	Fz	13	301
	Reactor vessel support column base	Fa Fb Fc Ma Mb Mc	4 359 178 2,895 3,342 417	4 360 260 2,900 4,900 500
	Reactor vessel upper key	Fc	495	500
	Reactor vessel lower key	Fc	164	250
	Pump hanger	Fy	195	393
	Pump snubber	Fa	73	73
	Pump upper horizontal column	Fa	159	160
	Pump lower horizontal column	Fa	113	113

←See Figure 3.9-18→

Table 3.7-25

LOAD TABLES FOR REACTOR COOLANT SYSTEM (Sheet 2 of 14)

Seismic Excitation	System Location	Seismic Load[a]		
		Component of Reactions	Calculated Maximum	Specified for Design
Combined East-West and Vertical (OBE)	Steam generator upper key	Fz	489	489
	Steam generator snubbers	Fx	10	1,214
	Steam generator support skirt	Fy Fz Mx My Mz	638 782 39,987 454 605	638 782 40,000 1,380 605
	Steam generator vertical pad	Fy	302 22	1,409 102
	Steam generator horizontal key	Fz	301	301
	Reactor vessel support column base	Fa Fb Fc Ma Mb Mc ←See Figure 3.9-18→	4 348 250 2,245 4,853 477	4 360 260 2,900 4,900 500
	Reactor vessel upper key	Fc	330	500
	Reactor vessel lower key	Fc	244	250
	Pump hanger	Fy	210	400
	Pump snubber	Fa	64	64
	Pump upper horizontal column	Fa	150	150
	Pump lower horizontal column	Fa	119	119

Table 3.7-25

LOAD TABLES FOR REACTOR COOLANT SYSTEM (Sheet 3 of 14)

Seismic Excitation	System Location	Seismic Load[a]		
		Component of Reactions	Calculated Maximum	Specified for Design
Combined North-South and Vertical (OBE)	Reactor inlet nozzle	Fa	364	370
		Fb	35	40
		Fc	226	230
		Ma	1,473	1,480
		Mb	3,814	3,820
		Mc	1,917	2,080
	Reactor outlet nozzle	Fa	490	500
		Fb	110	110
		Fc	4	35
		Ma	155	1,630
		Mb	115	1,130
		Mc	7,020	7,025
Combined East-West and Vertical (OBE)	Reactor inlet nozzle	Fa	126	370
		Fb	35	40
		Fc	152	230
		Ma	1,343	1,480
		Mb	2,494	3,820
		Mc	2,070	2,080
	Reactor outlet nozzle	Fa	127	500
		Fb	9	110
		Fc	33	35
		Ma	1,623	1,630
		Mb	1,126	1,130
		Mc	1,079	7,025
Combined North-South and Vertical (OBE)	Steam generator inlet nozzle	Fa	427	430
		Fs	245	250
		Ma	254	1,255
		M_B	4,906	4,910
	Steam generator outlet nozzle	Fa	42	45
		Fs	59	65
		Ma	1,090	1,140
		M_B	2,397	2,990

Table 3.7-25

LOAD TABLES FOR REACTOR COOLANT SYSTEM (Sheet 4 of 14)

Seismic Excitation	System Location	Seismic Load[a]		
		Component of Reactions	Calculated Maximum	Specified for Design
Combined East-West and Vertical (OBE)	Steam generator inlet nozzle	Fa	104	430
		Fs	78	250
		Ma	1,251	1,255
		M_B	2,109	4,910
	Steam generator outlet nozzle	Fa	22	45
		Fs	55	65
		Ma	1,130	1,140
		M_B	2,904	2,990
Combined North-South and Vertical (OBE) Pump A	Pump inlet nozzle	Fx	93	531
		Fy	712	1,198
		Fz	140	263
		Mx	2,557	4,949
		My	7,837	8,658
		Mz	6,396	9,228
	Pump outlet nozzle	Fa	458	647
		Fb	36	213
		Fc	87	1,015
		Ma	824	4,040
		Mb	6,596	8,815
		Mc	3,544	9,955
Combined East-West and Vertical (OBE) Pump A	Pump inlet nozzle	Fx	104	651
		Fy	806	834
		Fz	182	183
		Mx	4,619	5,594
		My	3,424	6,904
		Mz	2,745	7,339
	Pump outlet nozzle	Fa	158	713
		Fb	24	50
		Fc	36	809
		Ma	747	5,299
		Mb	2,208	2,420
		Mc	2,753	5,642

Table 3.7-25

LOAD TABLES FOR REACTOR COOLANT SYSTEM (Sheet 5 of 14)

Seismic Excitation	System Location	Seismic Load[a]		
		Component of Reactions	Calculated Maximum	Specified for Design
Combined North-South and Vertical (OBE) Pump B	Pump inlet nozzle	Fx	93	640
		Fy	712	981
		Fz	140	778
		Mx	2,557	4,500
		My	7,837	8,027
		Mz	6,396	8,977
	Pump outlet nozzle	Fa	458	461
		Fb	36	45
		Fc	87	547
		Ma	824	2,101
		Mb	6,596	7,800
		Mc	3,544	3,599
Combined East-West and Vertical (OBE) Pump B	Pump inlet nozzle	Fx	104	763
		Fy	806	811
		Fz	182	697
		Mx	4,619	9,829
		My	3,424	5,833
		Mz	2,745	6,622
	Pump outlet nozzle	Fa	158	797
		Fb	24	84
		Fc	36	559
		Ma	747	9,817
		Mb	2,208	5,033
		Mc	2,753	7,443
Combined North-South and Vertical (OBE)	Pressurizer key (joints 81,82,83,84)	Fs	57	57
	Pressurizer support skirt (joint 400)	Fx	106	106
		Fy	192	192
		Fz	7	7
		Mx	2,849	2,849
		My	281	281
		Mz	7,442	7,442

Table 3.7-25

LOAD TABLES FOR REACTOR COOLANT SYSTEM (Sheet 6 of 14)

Seismic Excitation	System Location	Seismic Load[(a)]		
		Component of Reactions	Calculated Maximum	Specified for Design
Combined North-South and Vertical (OBE)(cont)	Pressurizer key level supports (joints 91,98,99,100)	Fa	39	39
		Fc	14	14
		Mb	335	335
	Pressurizer base support (joints 30,35,37)	Fa	62	62
		Fb	103	103
		Fc	7	7
		Ma	1,928	1,928
		Mb	678	678
		Mc	1,577	1,577
	Pressurizer support column	Fx	1	1
		Fy	17	17
		Fz	0	0
		Mx	1	1
		My	0	0
		Mz	47	47
Combined East-West and Vertical (OBE)	Pressurizer keys (joints 81,82,83,84)	Fs	105	105
	Pressurizer support skirt (joint 400)	Fx	27	27
		Fy	193	193
		Fz	153	153
		Mx	4,174	4,174
		My	1,454	1,454
		Mz	5,612	5,612
	Pressurizer key level supports (joints 91,98,99,100)	Fa	13	13
		Fc	105	105
		Mb	2,656	2,656
	Pressurizer base support (joints 30,35,37)	Fa	3	3
		Fb	91	91
		Fc	84	84
		Ma	1,795	1,795
		Mb	296	296
		Mc	2,207	2,207

Table 3.7-25

LOAD TABLES FOR REACTOR COOLANT SYSTEM (Sheet 7 of 14)

Seismic Excitation	System Location	Seismic Load[a]		
		Component of Reactions	Calculated Maximum	Specified for Design
Combined East-West and Vertical (OBE)(cont)	Pressurizer support column	Fx	0	0
		Fy	15	15
		Fz	0	0
		Mx	13	13
		My	0	0
		Mz	1	1
Combined North-South and Vertical (OBE)	Reactor vessel inlet piping	M_i[b]	4,387	8,208
	Reactor vessel outlet piping	M_i	7,020	8,208
	Steam generator inlet piping	M_i	4,903	8,208
	Steam generator outlet piping	M_i	2,228	8,208
	Pump inlet piping	M_i	7,010	8,208
	Pump outlet piping	M_i	7,409	8,208
	Cold leg elbow	M_i	910	8,208
Combined East-West and Vertical (OBE)	Reactor vessel inlet piping	M_i	3,287	8,208
	Reactor vessel outlet piping	M_i	2,166	8,208
	Steam generator inlet piping	M_i	2,146	8,208
	Steam generator outlet piping	M_i	2,624	8,208
	Pump inlet piping	M_i	5,077	8,208
	Pump outlet piping	M_i	2,950	8,208
	Cold leg elbow	M_i	1,207	8,208

Table 3.7-25

LOAD TABLES FOR REACTOR COOLANT SYSTEM (Sheet 8 of 14)

Seismic Excitation	System Location	Seismic Load[a]		
		Component of Reactions	Calculated Maximum	Specified for Design
Combined North-South and Vertical (DBE)	Steam generator upper key	Fz	11	696
	Steam generator snubbers	Fx	1,378	1,378
	Steam generator support skirt	Fy Fz Mx My Mz	4,984 8 313 103 27,970	4,984 8 313 108 35,200
	Steam generator vertical pad	Fx	1,473	1,902
			106	138
	Steam generator horizontal key	Fy	16	858
	Reactor vessel support column base	Fa Fb Fc Ma Mb Mc ←See Figure 3.9-18→	6 628 275 4,344 5,196 710	7 628 409 4,350 7,956 780
	Reactor vessel upper key	Fc	717	717
	Reactor vessel lower key	Fc	255	401
	Pump hanger	Fy	244	494
	Pump snubber	Fa	90	90
	Pump upper horizontal column	Fa	244	292
	Pump lower horizontal column	Fa	163	163

Table 3.7-25

LOAD TABLES FOR REACTOR COOLANT SYSTEM (Sheet 9 of 14)

Seismic Excitation	System Location	Seismic Load[(a)]		
		Component of Reactions	Calculated Maximum	Specified for Design
Combined West-East and Vertical (DBE)	Steam generator upper key	Fz	696	696
	Steam generator snubbers	Fy	12	1,378
	Steam generator support skirt	Fy Fz Mx My Mz	1,160 1,192 62,377 716 886	1,160 1,270 62,400 2,760 888
	Steam generator vertical pad	Fy	546 39	1,902 138
	Steam generator horizontal key	Fz	387	858
	Reactor vessel support column base	Fa Fb Fc Ma Mb Mc ←See Figure 3.9-18→	7 624 409 3,847 7,954 778	7 628 409 4,350 7,956 780
	Reactor vessel upper key	Fc	621	717
	Reactor vessel lower key	Fc	400	401
	Pump hanger	Fy	248	500
	Pump snubber	Fa	83	83
	Pump upper horizontal column	Fa	192	292
	Pump lower horizontal column	Fa	123	205

Table 3.7-25

LOAD TABLES FOR REACTOR COOLANT SYSTEM (Sheet 10 of 14)

Seismic Excitation	System Location	Seismic Load[a]		
		Component of Reactions	Calculated Maximum	Specified for Design
Combined North-South and Vertical (DBE)	Reactor inlet nozzle	Fa	590	600
		Fb	49	50
		Fc	329	330
		Ma	1,851	1,860
		Mb	5,765	5,770
		Mc	2,650	3,150
	Reactor inlet nozzle	Fa	678	680
		Fb	187	190
		Fc	6	50
		Ma	169	2,640
		Mb	130	1,930
		Mc	12,453	12,460
Combined East-West and Vertical (DBE)	Reactor inlet nozzle	Fa	216	600
		Fb	41	50
		Fc	226	330
		Ma	1,503	1,860
		Mb	4,265	5,770
		Mc	3,143	3,150
	Reactor outlet nozzle	Fa	169	680
		Fb	15	190
		Fc	48	50
		Ma	2,639	2,640
		Mb	1,925	1,930
		Mc	1,424	12,460
Combined North-South and Vertical (DBE)	Steam generator inlet nozzle	Fa	605	610
		Fb	319	325
		Ma	263	1,820
		M_B	7,057	7,075
	Steam generator outlet nozzle	Fa	66	670
		Fs	88	95
		Ma	1,494	1,630
		M_B	2,937	3,400

Table 3.7-25

LOAD TABLES FOR REACTOR COOLANT SYSTEM (Sheet 11 of 14)

Seismic Excitation	System Location	Seismic Load[a]		
		Component of Reactions	Calculated Maximum	Specified for Design
Combined East-West and Vertical (DBE)	Steam generator inlet nozzle	Fa	142	610
		Fs	101	325
		Ma	1,813	1,820
		M_B	3,298	7,075
	Steam generator outlet nozzle	Fa	26	70
		Fb	68	95
		Ma	1,622	1,630
		M_B	3,369	3,400
Combined North-South and Vertical (DBE)	Pump inlet nozzle	Fx	94	1,102
		Fy	815	1,020
		Fz	109	710
		Mx	2,850	19,619
		My	13,266	14,953
		Mz	11,209	15,320
	Pump outlet nozzle	Fa	790	837
		Fb	61	232
		Fc	145	1,451
		Ma	1,119	9,268
		Mb	11,531	13,064
		Mc	5,499	8,813
Combined East-West and Vertical (DBE)	Pump inlet nozzle	Fx	109	426
		Fy	908	918
		Fz	180	531
		Mx	6,745	17,266
		My	4,737	13,882
		Mz	3,610	5,522
	Pump outlet Nozzle	Fa	222	378
		Fb	36	245
		Fc	56	982
		Ma	1,181	19,267
		Mb	2,864	13,902
		Mc	3,793	4,865

Table 3.7-25

LOAD TABLES FOR REACTOR COOLANT SYSTEM (Sheet 12 of 14)

Seismic Excitation	System Location	Seismic Load[a]		
		Component of Reactions	Calculated Maximum	Specified for Design
Combined North-South and Vertical (DBE) Pump B	Pump inlet nozzle	Fx	94	964
		Fy	815	950
		Fz	109	863
		Mx	2,850	16,842
		My	13,266	14,544
		Mz	11,209	17,228
	Pump outlet nozzle	Fx	790	795
		Fy	61	556
		Fz	145	431
		Mx	1,119	16,843
		My	11,531	14,544
		Mz	5,499	17,226
Combined East-West and Vertical (DBE) Pump B	Pump inlet nozzle	Fx	109	797
		Fy	908	955
		Fz	180	1,519
		Mx	6,745	12,940
		My	4,737	16,999
		Mz	3,610	4,365
	Pump outlet nozzle	Fa	222	906
		Fb	36	279
		Fc	56	950
		Ma	1,181	9,751
		Mb	2,864	16,999
		Mc	3,793	4,365
Combined North-South and Vertical (DBE)	Reactor vessel inlet piping	M_i	6,792	22,608
	Reactor vessel outlet piping	M_i	12,453	22,608
	Steam generator inlet piping	M_i	7,053	22,608
	Steam generator outlet piping	M_i	2,929	22,608
	Pump inlet piping	M_i	17,339	22,608
	Pump outlet piping	M_i	12,710	22,608
	Cold leg elbow	M_i	1,272	22,608

Table 3.7-25

LOAD TABLES FOR REACTOR COOLANT SYSTEM (Sheet 13 of 14)

Seismic Excitation	System Location	Seismic Load[a]		
		Component of Reactions	Calculated Maximum	Specified for Design
Combined East-West and Vertical (DBE)	Reactor vessel inlet piping	M_i	5,563	22,608
	Reactor vessel outlet piping	M_i	3,656	22,608
	Steam generator inlet piping	M_i	3,694	22,608
	Steam generator outlet piping	M_i	3,099	22,608
	Pump inlet piping	M_i	7,707	22,608
	Pump outlet piping	M_i	4,246	22,608
	Cold leg elbow	M_i	1,607	22,608
Combined North-South and Vertical (DBE)	Pressurizer key Joints 81,82,83,84)	Fs	85	85
	Pressurizer support skirt (joint 400)	Fx Fy Fz Mx My Mz	145 282 11 4,117 311 11,990	145 282 11 4,117 311 11,990
	Pressurizer key level supports (joints 91,98,99,100)	Fa Fc Mb	57 17 439	57 17 439
	Pressurizer base support (joints 30,35,37)	Fx Fy Fz Mx My Mz	85 159 10 2,964 934 2,329	85 159 10 2,964 934 2,329
	Pressurizer support column	Fa Fb Fc Ma Mb Mc	1 22 0 1 0 82	1 22 0 1 0 82

Table 3.7-25

LOAD TABLES FOR REACTOR COOLANT SYSTEM (Sheet 14 of 14)

Seismic Excitation	System Location	Seismic Load[a]		
		Component of Reactions	Calculated Maximum	Specified for Design
Combined East-West and Vertical (DBE)	Pressurizer keys (joints 81,82,83,84)	Fx	105	105
	Pressurizer support skirt (joint 400)	Fx	36	36
		Fy	356	356
		Fz	154	154
		Mx	5,244	5,244
		My	1,462	1,462
		Mz	10,264	10,264
	Pressurizer key level supports (joints 91,98,99,100)	Fx	18	18
		Fz	106	106
		My	2,672	2,672
	Pressurizer base support (joints 30,35,37)	Fx	33	33
		Fy	147	147
		Fz	85	85
		Mx	3,054	3,054
		My	302	302
		Mz	4,080	4,080
	Pressurizer support column	Fx	0	0
		Fy	29	29
		Fz	1	1
		Mx	22	22
		My	0	0
		Mz	1	1

(a) Forces = kips
Moments = inch-kips

(b) Subscripts x, y, z = global coordinates (figures 3.7-29 & 3.7-30).
Subscripts a, b, c = local coordinates, a-axial; b-vertical; c-horizontal and perpendicular to a & b (unless noted otherwise).
Fs = shear force; M_B = bending moment.

$$M_i = \sqrt{Mx^2 + My^2 + Mz^2}$$

Amended: May 2007 TL: E041420

A conservative estimate of the number of design cycles can be established by multiplying the numerical value of each of these three parameters together.

$$N = n \cdot f \cdot d \qquad (11)$$

where:

N = number of earthquake cycles

n = number of seismic events to be considered

f = significant frequency characteristic of the subsystem and/or supporting media

d = duration of the postulated seismic event

Further conservatism is introduced by applying the resulting number of design cycles to the maximum stress range even through most of the actual stress cycles are well below the maximum stress range.

In the application of equation (11) two occurrences of the OBE are assumed to occur over the life of the plant. The resulting number of design cycles is specified in the design specifications for the various subsystems.

3.7.3.2.2 NSSS

The procedure used to account for the fatigue effect of cyclic motion associated with the OBE recognizes that the actual motion experienced during a seismic event consists of a single maximum or peak motion, and some number of cycles of lesser magnitude. The total or cumulative fatigue effect of all cycles of different magnitude will result in an equivalent cumulative usage factor. The equivalent cumulative usage factor can also be specified in terms of a finite number of cycles of the maximum or peak motion. Based on this consideration, Seismic Category I subsystems, components, and equipment are designed for a total of 200 full-load cycles about a mean value of zero with an amplitude equal to the maximum response produced during the entire OBE event.

3.7.3.3 <u>Procedure Used for Modeling</u>

General modeling techniques used for the remainder of the Seismic Category I subsystems are in accordance with the criteria specified in Section 3 of reference 5. Such modeling incorporates either a multi-degree-of-freedom lumped-parameter technique or a finite-element modeling approach. The degree of complexity of the individual models is sufficient to define the dynamic behavior characteristics of the specific subsystem. Modeling of the attachment interface is consistent with the method of mounting the subsystem in its installed condition.

Modeling of internals, fuel assemblies and CEDMs is described in paragraph 3.7.3.14.

3.7.3.4 Basis for Selection of Frequencies

Structural fundamental frequencies ("forcing frequencies") are not selected, but are calculated in accordance with Section 4.2.1 of reference 5 and paragraph 3.7.3.14.

3.7.3.5 Use of Equivalent Static Load Method of Analysis

For piping, refer to appendix 3.7B, section 2.3.2 and appendix D.

The equivalent static load method involves the multiplication of the total weight of the equipment or component member by the specified seismic acceleration coefficient. The magnitude of the seismic acceleration coefficient is established on the basis of the expected dynamic response characteristics of the component. Components that can be adequately characterized as a single-degree-of-freedom system are considered to have a modal participation factor of one. Seismic acceleration coefficients for multi-degree-of-freedom systems, which may be in the resonance region of the amplified response spectra curves, are increased by 50% to account conservatively for the increased modal participation.

3.7.3.6 Components of Earthquake Motion

For all other Seismic Category I subsystems, independent analyses are performed for each of the three principal coordinate directions; however, response characteristics used in design are established considering only two components of earthquake motion occurring simultaneously. More specifically, the total response used in design is taken to be the most severe response resulting from the SRSS combination of the response due to a single axis horizontal excitation in combination with the response from the vertical excitation. Paragraph 3.7.3.14 discusses the components of earthquake motion used in the analysis of internals, fuel assemblies and CEDMs.

3.7.3.7 Combination of Modal Responses

3.7.3.7.1 Subsystems other than the NSSS

Appendix 3.7B describes the criteria used for the piping systems.

For subsystems other than piping and the NSSS, the individual modal responses are combined by the SRSS modal summation in the application of the modal response spectra technique. This method is based upon probability considerations and provides an excellent approximation of the maximum anticipated response. It takes into account the random nature of the seismic disturbance and the relatively short duration of the response, while at the same time not completely ignoring potential modal superposition. Where modal frequencies are closely spaced, the contributions from these modes are first summed using the sum of their absolute values. These results are then considered as a pseudomode when the overall SRSS modal summation is made. The total system response is then taken to be the SRSS combination of the most severe response resulting from a singleaxis horizonal input in combination with the vertical response.

3.7.3.7.2 NSSS

The SRSS method is the procedure normally used for the NSSS to combine the modal responses, when the modal analysis response spectrum method of analysis is employed. The procedure is modified only in two cases:

A. In the analysis of simple systems, where three or less dynamic degrees-of-freedom are involved, the modal responses are combined by the summation of the absolute values method.

B. In the analysis of complex systems, where closely spaced modal frequencies are encountered, the responses of the closely spaced modes are combined by the summation of the absolute values method and, in turn, combined with the responses of the remaining significant modes by the SRSS method. Modal frequencies are considered closely spaced when their differences is less than $\pm 10\%$ of the lower frequency.

3.7.3.8 Analytical Procedures for Piping

Appendix 3.7B describes the design criteria and the analytical techniques applicable to piping systems.

3.7.3.9 Multiply Supported Equipment Components with Distinct Inputs

Section 5.3 of reference 5 describes the approaches used for multiply supported systems. Appendix 3.7B discusses the methods for piping systems.

3.7.3.10 Use of Constant Vertical Static Factors

A constant seismic vertical load factor is not used for the seismic design of Seismic Category I structures, components, and equipment.

3.7.3.11 Torsional Effects of Eccentric Masses

The significant torsional effects of valves and other eccentric masses are taken into account in the seismic piping analysis by the techniques discussed in appendix 3.7B.

Torsional effects are accounted for directly in the modeling for other subsystem analysis similar to the approach discussed in section 3.2 and appendix C of reference 5.

3.7.3.12 Buried Seismic Category I Piping Systems and Tunnels

Section 6.0 of reference 5 discusses the techniques used to calculate the stresses from seismic loadings for buried seismic piping. The buried Seismic Category I piping is designed to remain functional when subjected to seismic loads. This consideration is accomplished by limiting the calculated stresses in the pipe material under all loading combinations, including earthquake, as discussed below.

The sum of the stresses produced by internal and/or external pressure, and those produced by seismic forces, shall not exceed 2.4 (S_h) for the DBE or 1.2 (S_h) for the OBE.

(S_h) indicates the allowable stresses prescribed in tables I-7.1, I-7.2 and I-7.3 of the ASME Boiler and Pressure Vessel Code. When ANSI B31.1.0 is used, the allowable stresses are indicated in tables A-1 and A-2 of appendix A.

3.7.3.13 Interaction of Other Piping with Seismic Category I Piping

Appendix 3.7B describes the techniques used to consider the interaction of Seismic Category I piping with non-Category I piping.

3.7.3.14 Seismic Analysis of Reactor Internals, Core, and Control Element Drive Mechanisms (CEDMs)

Dynamic analyses of the reactor internals, core and CEDMs are conducted to determine their response to horizontal and vertical seismic excitation, and to verify the adequacy of their seismic design. The seismic analyses of the internals and core include the use of modal analysis techniques that utilize both response spectra and time-history accelerograms for linear conditions, and step-by-step integration of the equations of motion for nonlinear impact conditions, such as exist when the gaps between components close. These analyses are conducted in conjunction with the analyses of the RCS. The applicable seismic load, stress and deformation criteria are presented in subsections 3.9.4, 3.9.5, and section 4.2.

3.7.3.14.1 Reactor Internals and Core

The seismic analyses of the reactor internals and core consist of three phases. In the first phase, linear lumped-parameter models are formulated, natural frequencies and mode shapes for the models are determined, and the response is obtained utilizing the modal analyses response spectrum method. The response spectra used are based upon the acceleration of the reactor-vessel supports. The response spectra are modified by a conservative factor to account for possible response amplification between the vessel supports and the reactor internals support. The response spectrum analysis is used to obtain preliminary design seismic loads and displacements.

In the second phase, a more accurate determination of the internals and core response is obtained by the modal analyses time-history method. The input excitation to the internals model is the horizontal and rotational (rocking) time-history response of the reactor vessel at the flange, determined from the RCS analysis. Coupling effects between the internals and reactor vessel are accounted for by including a simplified representation of the internals with the RCS model. This is discussed in subsection 3.7.2.

In the third phase, because the linear horizontal analysis showed that the relative displacements between the core and core shroud and between the core-support barrel and pressure-vessel snubbers are sufficiently large to close the gaps that exist between these components, a nonlinear horizontal analysis is performed. The horizontal nonlinear analysis is divided into two parts. In the first part, the internals and core are analyzed to obtain internals response and the proper dynamic input for the reactor core model. In the second part, the core plate motion from the first part is applied to a more detailed nonlinear model of the reactor core. Because the linear vertical analysis indicates that the response of the core may be sufficiently large to cause it to lift off the core support plate, a vertical nonlinear analysis of the internals was also performed.

In these analyses, the horizontal and vertical components of the seismic excitation are considered separately, and the maximum absolute responses for either horizontal direction are added to the maximum absolute vertical responses.

The horizontal and vertical seismic analyses of the reactor internals are decoupled because the relative displacements of the reactor internal structures are so small that coupling effects are insignificant. Following the completion of the separate horizontal and vertical seismic analyses of reactor internals, the responses of the internal structures were examined to verify that beam column effects are small. The components that experienced the largest horizontal relative displacements were the CEA shrouds. The maximum relative displacement between the top and bottom of the CEA shrouds was found to be less than manufacturing tolerances.

Decoupling of the horizontal and vertical models is also appropriate because the vertical natural frequencies of the internals structures are much higher than the horizontal natural frequencies; e.g., the highest horizontal frequency is lower than the lowest vertical frequency. In a coupled analysis, the computation time step would be determined by the highest vertical natural frequency resulting in excessive computer time. By separating the models, a coarser step is used in the horizontal portion of the analysis. Also, the practical consideration of computation time and computer program capacity limit the number of nodes that can be used in a coupled analysis. By decoupling the horizontal and vertical models, more nodes and consequently more physical detail of internals structures are represented in the separate models.

3.7.3.14.1.1 Mathematical Models

Equivalent multimass mathematical models are developed to represent the reactor internals and core. The linear mathematical models of the internals are constructed in terms of lumped masses and elastic-beam elements. At appropriate locations within the internals and core, points (nodes) are chosen to lump the weights of the structure. A sketch of the coupled internals-core model showing the relative node locations is presented in figure 3.7-37. Figures 3.7-38 and 3.7-39 show the idealized horizontal and vertical models.

The criterion for choosing the number and location of mass concentration is to provide for accurate representation of the dynamically significant modes of vibration of each of the internals components. Between the nodes, properties are calculated for moments of inertia, cross-section areas, effective shear areas, and lengths. Separate horizontal and vertical models of the internals and core are formulated to more efficiently account for structural differences in these directions.

Lumped-mass nodes are positioned to coincide with fuel-spacer grid locations. The core is modeled by subdividing it into fuel assembly groupings and choosing stiffness values to adequately characterize its beam response and contacting under dynamic loading. In order to represent the effect of fuel impacting on internals loads, impacting between the core shroud and peripheral fuel bundles is modeled.

The horizontal nonlinear reactor core model, consisting of one row of 17 individual fuel assemblies, is depicted in figure 3.7-40. Distribution of mass and stiffness values is based upon experimentally determined fuel-assembly vibration characteristics. The 17 fuel assemblies are modeled to properly account for multiple contacting of fuel assemblies. Nonlinear springs are also incorporated between the fuel and core shroud to account for contact with the core shroud. Details of the methodology used to model and analyze fuel under seismic excitation are presented in reference 11.

The impact stiffness and impact damping (coefficient of restitution) parameters for the gap elements used in the coupled internals-core model and the reactor core model are derived from the fuel assembly structural tests described in section 4.2. The impact stiffness used for the analysis represents the stiffness that characterizes the motion of the fuel rods relative to the spacer grid. This stiffness most accurately characterizes the impact between the peripheral fuel row and the core shroud where the peak spacer grid impact load is generated.

The vertical nonlinear model shown in figure 3.7-41 incorporates nonlinear spring couplings to account for the nonlinear behavior of the internals in the vertical direction. The linear portion of the model is basically similar to the linear vertical model of figure 3.7-39, but has been greatly simplified. This is accomplished by dividing the model into subsections and developing a dynamically equivalent system for each subsection.

Reactor internals/vessel interface gaps are included in the internals models. The reactor internal structures are constrained from vertical motion by means of the core support barrel, upper guide structural flanges and holddown ring sandwiched between the reactor vessel head and the support ledge of the reactor vessel. Horizontal positioning of the reactor internals structures relative to the reactor vessel is accomplished by means of four alignment keys at the upper flange location and six snubbers at the lower end of the core support barrel. Precise gaps between alignment features of the reactor vessel and internal structures are obtained from careful installation in the field of the alignment keys and snubbers relative to the reactor vessel. The gap sizes used in the dynamic response analyses are adjusted for temperature effects. The tolerance range on the gaps is held to within a few mils of nominal, however, as-built data is utilized when available. Variations in the gap sizes between the reactor vessel and internals of a few mils cause very small changes in internals responses. Parameter studies have been performed on reactor internals structures, such as the core, confirming very little sensitivity to small changes in gap size.

The damping factors used in the seismic analyses of the reactor internals in accordance with the values in table 3.7-22 are 4% of critical for the DBE and 2% of critical for the OBE. Damping values used for fuel assemblies are based upon the results of the full scale structural tests of the fuel defined in section 4.2.

Additional salient details of the internals and core models are discussed in the following paragraphs.

A. Hydrodynamic Effects

The dynamic analysis of reactor internals presents some special problems due to their immersion in a confined fluid. It has been shown both analytically and experimentally[12] that immersion of a body in a dense-fluid medium lowers its natural frequency and significantly alters its vibratory response as compared to that in air. The effect is more pronounced where the confining boundaries of the fluid are in close proximity to the vibrating body as is the case for the reactor internals. The method of accounting for the effects of a surrounding fluid on a vibration system has been to ascribe to the system the addition of "hydrodynamic mass."

This hydrodynamic mass decreases the frequencies of the system. The hydrodynamic mass of an immersed system is a function of the dimensions of the real mass and the space between the real mass and confining boundary.

Hydrodynamic mass effects for moving cylinders in a water annulus are discussed in references 12 and 13. The results of these references are applied to the internals structures to obtain the total (structural plus hydrodynamic) mass matrix that is then used in the evaluation of the natural frequencies and mode shapes for the model. In the nonlinear lateral internals model, hydrodynamic coupling (off-diagonal terms of the mass matrix) is included.

B. Core-Support Barrel

The core-support barrel is modeled as a beam with shear deformation. It has been shown that the use of beam theory for cylindrical shells gives sufficiently accurate results when shear deformation is included.[14][15]

C. Fuel Assemblies

The fuel assemblies are modeled as uniform beams with rotational springs at each end to represent the proper end conditions. The member properties for the beam elements representing the fuel assemblies are derived from the results of experimental tests of the fuel-assembly load deflection characteristics and fundamental natural frequency.

D. Support-Barrel Flanges

To obtain accurate lateral and vertical stiffness of the upper and lower core-support-barrel flanges and the upper guide structure support-barrel upper flange, finite-element analyses of these regions are performed. As shown in figure 3.7-42, these areas are modeled with quadrilateral and triangular ring elements. Displacements and rotations are applied to the ends of the flange models to obtain member stiffness properties for use in the models.

E. Control Element Assembly (CEA) Shrouds

For the horizontal model, the CEA shrouds are treated as vibrating in unison and are modeled as guided cantilever beams in parallel. In addition, the restraint to relative rotation between the upper guide structure support plate and the fuel alignment plate due to vertical shroud stiffness is modeled. To account for the decreased lateral stiffness of the upper guide structure due to local bending of the fuel alignment plate, a short member with properties approximating the local bending stiffness of the fuel alignment plate is included at the bottom of the CEA shrouds. Since the stiffness of the upper guide structure support plate is large compared to that of the shrouds, the CEA shrouds are assumed to be rigidly connected to the upper guide structure support plate.

F. Upper Guide Structure Support Plate and Lower Support Structure Grid Beams

These grid beam structures are modeled as plane grids. Displacements due to vertical (out-of-plane) loads applied at the beam junctions are calculated through the use of the STRUDL computer program.[10] Average stiffness values based on these results yield an equivalent member cross-section area for the vertical model.

3.7.3.14.1.2 Analytical Techniques

A. Natural Frequencies and Mode Shapes

The mass- and beam-element properties of the models are utilized in the MODSK computer program (see paragraph 3.9.1.2.2.2, item H) to obtain the natural frequencies and mode shapes. The system utilizes the stiffness-matrix method of structural analysis. The natural frequencies and mode shapes are extracted from the system of equations:

$$(\underline{K} - W_n^2 \underline{M})\,\theta_n = O \qquad (12)$$

where:

$\underline{K}$ = model stiffness matrix

$\underline{M}$ = model mass matrix

$W_{(n)}$ = natural circular frequency for the n^{th} mode

θ_n = normal mode shape matrix for n^{th} mode

The mass matrix, $\underline{M}$, includes the hydrodynamic and structural masses.

B. Response Calculation Methods

1. Response Spectra Method

The response spectrum analysis is performed using the modal extraction data and the following relationships for each mode:

a. Nodal Accelerations

$$\ddot{X}_{in} = \gamma_n A_n \Phi_{in} \quad (13)$$

where:

$\ddot{X}_{in}$ = absolute acceleration at node "i" for mode "n".

γ_n = modal participation factor

A_n = modal acceleration from response spectrum

Φ_{in} = mode shape factor at node "i" for mode "n"

b. Nodal Displacement

$$Y_{in} = \frac{\ddot{X}_{in}}{W_n^2} \quad (14)$$

where:

Y_{in} = displacement at node "i" for mode "n" relative to base

W_n = natural circular frequency for n^{th} mode

c. Member Forces and Moments

$$F_n = \frac{(\gamma_n A_n)}{W_n^2} \overline{F_n}$$

(15)

where:

F_n = actual member force for mode "n"

$\overline{F_n}$ = modal member force for mode "n"

The effect of the fluid environment is accounted for by defining the modal participation as follows:

$$\gamma_n = \frac{\sum_{i=1}^{M} W_{si}\,\Phi_{in}}{\sum_{i=1}^{M}\sum_{j=1}^{M} \Phi_{in}\,W_{ij}\,\Phi_{jn}} \qquad (16)$$

where:

W_{si} = structural weight of node "i"

W_{ij} = structural + hydrodynamic weight of node "i"

M = number of masses

The SRSS method is normally used to combine the modal responses. Where modal frequencies are closely spaced, the responses of these modes are combined by the sum of their absolute values. The modal damping factors are obtained by the method of "mass mode weighing", which gives:

$$B_n = \frac{\Sigma M_i\,|\Phi_{in}|\,B_i}{\Sigma M_i\,|\Phi_{in}|} \qquad (17)$$

where:

B_n = modal damping factor

M_i = structural mass of mass node "i"

$|\Phi_{in}|$ = absolute value of the mode shape at mass mode "i"

B_i = damping associated with mass point "i"

2. Modal Time-History Method (Linear Analysis)

The time-history response analysis is performed utilizing the MRI/Stardyne System DYNRE computer program. This program utilizes the "normal mode method" to obtain the time-history response of linear elastic structures. A brief description of the method of solution is described below. Details of the program and the normal mode method are presented in references 16, 17, and 18.

The equations of motion in matrix form for a structural system subjected to dynamic loads in which viscous damping is present are:

$$[m]\{\ddot{x}\}+[C]\{\dot{x}\}+[K]\{x\}=\{p\}f(t) \qquad (18)$$

where:

$[m]$ = mass matrix

$[C]$ = matrix of damping coefficients

$[K]$ = stiffness matrix

$\{x\}$ = displacements at the coordinates of the system

$\{\dot{x}\}$ = velocities at the coordinates of the system

$\{\ddot{x}\}$ = accelerations at the coordinate of the system

$\{p\}$ = spatial distribution of loads

$f(t)$ = time-history of the applied forces $\{p\}$

Application of the normal mode method will result in a set of n independent (decoupled) equations that may be solved individually to obtain the response of each (or any) of the normal modes to the applied forcing functions.

Given a set of normal modes (Φ) for the structure, the following coordinate transformation is applied:

$$\{x\} = [\Phi]\{\eta\} \qquad (19)$$

Where $\{\eta\}$ are the generalized coordinate displacements.

Substitution of the above transformation into equation (17) and simplifying results in the following equations of motion:

$$\ddot{\eta}_n + 2\beta_n \dot{\eta}_n + W_n^2 \eta_n = \frac{\gamma_n f(t)}{M_n} \tag{20}$$

where:

$\gamma_{(n)} = \{\Phi^n\}^T\{p\}$ = n^{th} mode participation factor

$M_{(n)}$ = n^{th} mode generalized mass

$W_{(n)}$ = frequency of the n^{th} natural mode of vibration

β_n = n^{th} mode critical damping ratio

η_n = generalized coordinate displacement

In the STARDYNE computer program Laplace transformation methods are used to solve equation (20) for the generalized coordinate displacements, velocities, and acceleration time-history relative to the base. The true mass-point nodal displacements are obtained from equation (19).

The member-bending moments and shears are obtained from the STAR computer program and are derived from the DYNRE nodal displacement vectors at the times of peak response.

3. Nonlinear Analysis

The nonlinear seismic response and impact forces for the internals are determined using the CESHOCK computer program. This computer program provides the numerical solution to transient dynamic problems by step-by-step integration of the differential equations of motion. The input excitation for the model is the horizontal and rotational (rocking) time-history response of the reactor vessel at the flange.

Input to the CESHOCK computer program consists of initial conditions, nodal lumped masses, linear-spring coefficients, mass moments of inertia, nonlinear spring curves, and the acceleration time-histories. The output from the CESHOCK computer program consists of displacements, velocities, accelerations, impact forces, shears, and moments.

A brief description of the general methods used in the CESHOCK computer program to solve transient dynamic problems can be found in paragraph 3.9.1.2.2.2, item E.

3.7.3.14.1.3 Results.

A. Linear Analysis. The results of the linear analyses are provided in Section 3.3.2.2 of reference 19.

B. Response Loads, Nonlinear Analysis. The maximum loads on the reactor internals and the fuel due to a vertical OBE and DBE are obtained from the CESHOCK code using the nonlinear model of figure 3.7-41 (node locations described in table 3.7-26). The maximum values of shears and moments on the reactor internals due to a horizontal OBE and DBE are obtained using the nonlinear model of figure 3.7-38 (node locations described in table 3.7-27). The adequacy of the reactor internals to accommodate the stresses and deformations resulting from the loads and moments in the analysis is discussed in subsection 3.9.5.

   The fuel loads, including spacer grid impact loads due to a horizontal OBE and DBE, are obtained using the nonlinear core model of figure 3.7-40. Fuel loads and stresses are compared to criteria in section 4.2.

3.7.3.14.2 Control Element Drive Mechanisms (CEDMs)

The pressure-retaining components of the CEDM are designed to the appropriate stress criteria of ASME Code Section III for all loadings specified in the mechanism design specification. The structural integrity of the CEDM when subjected to seismic loadings is verified by a combination of test and analysis. The structural integrity of the CEDM when subjected to the combined effects of design earthquake and postulated pipe breaks (faulted conditions) is verified in section 3.9A.5. Methods of modal dynamic analysis employing response spectrum techniques are supported with experimentally obtained information.

The CEDM is seismically supported by the closure head lift rig assembly through a series of seismic snubbers. (The original configuration was modified during Cycle 5 (Unit 3) and Cycle 6 (Unit 2) refueling outages to replace snubbers with rigid struts as part of the snubber reduction program.) The CEDM and snubbers are described in subsection 3.9.4. To demonstrate the structural integrity of the CEDM and snubber system, a combined analysis and test program was performed. First, a modal dynamic analysis, employing response spectra, was used to study a structural model of the free standing CEDM. Test results for a free standing CEDM verified the analytically derived dynamic characteristics employed in the model. The free standing CEDM analysis demonstrated the need to provide seismic supports for the CEDMs. Following design of the seismic supports, the analytical model was modified to simulate the CEDM, seismic support system, and a final analysis was performed. The dynamic characteristics employed in the supported CEDM analysis model were verified by test of a supported CEDM. This test served also as a qualification test to further demonstrate the structural integrity of the system. The following paragraphs describe the seismic analysis and test program. Results are presented in paragraph 3.7.3.14.2.5 and demonstrate acceptable final maximum stress level and acceptable deflections within the CEDM to permit tripping.

3.7.3.14.2.1 Input Excitation Data

For the dynamic analyses, a response spectra definition of the excitation at the base of the CEDM nozzle is obtained from the seismic analysis of the RCS. The excitation at the head lift rig attachment points for the seismic supports is assumed identical to that at the nozzles.

In the seismic tests, moderate level sine sweep tests were conducted for the purpose of confirming the accuracy of the analytical models for the free standing and seismically supported CEDM. In addition, the seismically supported test CEDM was also exposed to random multi-frequency uniaxial (horizontal) and biaxial input motions with excitation intensities representative of the San Onofre Units 2 and 3 DBE seismic event.

3.7.3.14.2.2 Model Description

A mathematical model consisting of lumped masses and weightless structural members is used in the dynamic analysis of the CEDM and seismic support. The lumped-mass nodal points and member stiffness properties are defined to provide an accurate representation of the dynamically significant modes of vibration within the seismic frequency range. The model provides a three-dimensional representation of the dynamic response of the CEDM plus seismic support.

An analysis using this three-dimensional model and including the reactor vessel head lift rig structure indicated equal natural frequency and mode shape characteristics (symmetry) of the structure in the directions of its principal axes. This result, combined with the fact that the CEDMs are symmetric along their vertical axes provided sufficient justification for performing a two-dimensional analysis for the supported CEDMs. The two-dimensional model representation, figure 3.7-43, was employed for the combined seismic analysis of the reactor vessel head left rig and CEDM structure.

The simplified head lift rig model retains the major natural frequency, mass and stiffness characteristics of the full size head lift rig structure. The 91 CEDMs were modeled by a single CEDM incorporating the stiffness and mass characteristics of all CEDMs together. In this fashion, it was conservatively assumed that all 91 CEDMs had tuned frequencies. Seventeen different analysis cases were run, whereby the model CEDM nozzle length was varied from the shortest to longest actual length. Shear force and moment loading results from all computer runs were enveloped for each CEDM portion before the operational loadings were added. For this analysis, the snubber connections of the CEDMs to the seismic support plate were modeled by a single spring with stiffness properties representative of an inline arrangement of 10 CEDMs.

The CEDM snubbers have been replaced with rigid struts, which are designed to maintain the stiffness and dynamic load carrying characteristics of the CEDM-to-head lift rig support arrangement.

Each snubber or rigid strut may actually have a gap of up to 1/16 inch. This dimension is quite small and, for the purpose of the analysis, it was felt unnecessary to model this gap. The following reasoning adds additional support to this decision.

Table 3.7-26

REACTOR INTERNALS VERTICAL SEISMIC MODEL
NODE AND MEMBER DESCRIPTIONS

Node No.	Description
1	Lower CSB Flange and Core Shroud
2	Bottom of the CSB
3	Top of the CSB
4	Top of the CSP
5	Top of the Lower End Fitting
6	Middle of the Guide Tubes
7	Bottom of the Upper End Fitting
8	Bottom of the Fuel Rods
9	Middle of the Fuel Rods
10	Top of the Fuel Rods
11	Fuel Alignment Plate
12	Top of the CEA Shrouds
13	UGS and CSB Flanges
14	Reactor Vessel Flange
Spring No.	Description
1	CSB Lower Flange
2	CSB Axial Spring-Rate
3	CSB Upper Flange
4	Lower Support Structure Spring-Rate
5	Fuel Bundles Lower End Fitting
6	Guide Tubes Axial Spring-Rate
7	Guide Tubes Axial Spring-Rate
8	Fuel Rods Axial Spring-Rate
9	Fuel Rods Axial Spring-Rate
10	Fuel Rods Axial Spring-Rate
11	Fuel Rods Axial Spring-Rate
12	Fuel Holddown Springs
13	CEA Shrouds Axial Spring-Rate
14	UGS Flange
15	CSB Upper Flange and Comp Ring

Table 3.7-27

REACTOR INTERNALS HORIZONTAL SEISMIC MODEL
NODE LOCATIONS (Sheet 1 of 2)

Node No.	Node Location Description
1	Bottom of Pressure Vessel
2	Pressure Vessel at Snubber Elevation
3	Pressure Vessel
4	Pressure Vessel
5	Pressure Vessel
6	Pressure Vessel
7	Pressure Vessel
8	Pressure Vessel
9	Pressure Vessel
10	Pressure Vessel - Internals Interface Location
11	Bottom of Core Support Barrel
12	Core Support Barrel
13	Core Support Barrel
14	Core Support Barrel
15	Core Support Barrel
16	Core Support Barrel
17	Core Support Barrel
18	Core Support Barrel
19	Core Support Barrel
20	Centerline of Core Support Plate (top of LSS)
21	Core Shroud
22	Core Shroud
23	Core Shroud
24	Core Shroud
25	Core Shroud
26	Centerline of Fuel Alignment Plate
27	Control Element Assembly (CEA) Shrouds
28	Upper Guide Structure (UGS) Support Plate
29	CEA Shroud Extensions

Table 3.7-27

REACTOR INTERNALS HORIZONTAL SEISMIC MODEL
NODE LOCATIONS (Sheet 2 of 2)

Node No.	Node Location Description
30 31 32 33 34	18 Fuel Bundles Along the Periphery of the Core Assumed to Impact with the Core Shroud
35 36 37 38 39	181 Central Fuel Bundles No Impacting Assumed
40 41 42 43 44	18 Fuel Bundles Along the Periphery of the Core Assumed to Impact with the Core Shroud

Assuming a hypothetical case where all gaps of a CEDM line will accumulate, the maximum deflection of any CEDM at the seismic support elevation will be less than 10/16 inch. This level of deflection, however, is small when compared to acceptable deflections of greater than 4 inches for the OBE event. In terms of CEDM stress intensities, the 10/16-inch deflection of the CEDM will apply less than 16% of the OBE stress allowable and less than 8% of the DBE stress allowable on the limiting component, the CEDM nozzle. From table 3.7-28, however, it is seen that the available load margins by far exceed these hypothetical increases in stress.

Scramability of the CEDMs was verified to lateral deflections of 6 inches. A 10/16-inch increment added to the maximum computed deflections of table 3.7-29, therefore, can be easily accepted during both seismic events.

The structural analysis of the CEDM is based on a critical damping ratio of 2%. This value was confirmed for all significant vibration modes of the free standing CEDM type. The analysis does not credit the structure with the damping capacity inherent in the seismic snubbers.

Sketches of the actual CEDM and seismic support structure are shown in figures 3.9-31 and 3.7-44.

Table 3.7-28
CEDM NOZZLE STRESS

	Nozzle Stress (k/in.^{2})	
	OBE	DBE
Allowable	23.30	55.93
Calculated	16.25	20.50

3.7.3.14.2.3 Analysis

A dynamic analysis of the mathematical structural model is performed using the ICES STRUDL II computer program. Natural frequencies and mode shapes of the composite mathematical model are calculated first. These values are verified through test. Where necessary, the model is modified to reflect the test results. Using the mode shapes and natural frequencies, a modal response analysis using a response spectrum technique is performed. The response at each node is calculated and compared with design criteria. The loads imposed by the CEDM through the seismic support to the head lift rig (HLR) are verified to be less than specification allowable. The CEDM nozzle loads are also verified against design allowable. A discussion of the evaluation of the CEDM and HLR for the faulted condition is provided in Appendix 3.9A.

3.7.3.14.2.4 Tests

Testing of the CEDM employed two configurations: a free standing CEDM and a seismically supported CEDM.

For the free standing configuration, pluck tests and forced vibration (sine sweep) tests were conducted to verify the free standing CEDM analytical model. Natural frequencies and modes shapes were determined and compared to analytical results and modal critical damping ratio parameters were identified. The results of these tests and the comparison of test results with analysis are provided in paragraph 3.7.3.14.2.5.

For the seismically supported configuration, forced vibration (sine sweep) tests and multi-frequency input tests were conducted to verify the combined CEDM/lift rig model and to further verify the structural integrity of the CEDM seismic support system. Figure 3.7-45 shows a schematic representation of the test fixturing employed for the supported CEDM test. This fixture was used to simulate the support characteristics, which are provided in plant by the seismic snubber arrangement and tie-in to the closure head lift rig structure. The support fixture and associated struts were designed to provide a rigid support structure at the seismic snubber elevation. The test CEDM was connected to the support fixture by a single seismic snubber in series with a leaf spring. The characteristics of the leaf spring were selected to simulate the dynamic effects of the closure head lift rig. Lateral stability was achieved by tying CEDM shroud to a low-friction, linear bearing shaft system to force a linear response motion. To identify the dynamic characteristics of the CEDM during the various test phases, the CEDM was instrumented with 17 accelerometers, 12 strain gauges, and 2 linear variable differential

Table 3.7-29

DEFLECTIONS OF SAN ONOFRE UNITS 2 AND 3 CEDMS UNDER SEISMIC LOADING - COIL STACK AND SHROUD

Height Along CEDM (in.)	RSS Deflections Under OBE Loading (in.)	RSS Deflections Under DBE Loading (in.)
25.3	0.045	0.088
30.5	0.052	0.101
35.5	0.064	0.113
39.5	0.072	0.123
44.7	0.082	0.136
52.7	0.095	0.153
70.7	0.117	0.180
106.7	0.135	0.216
141.9	0.142	0.253
175.3	0.179	0.318
214.7	0.258	0.443
232.8	0.322	0.540

transformers. The results of the supported CEDM tests and a comparison of the results with analysis are provided in paragraph 3.7.3.14.2.5.

3.7.3.14.2.5 Results

The responses (forces, moments, and deflections) at all design points in the system were compared with the load and deflection restrictions of the design specification. The most critical loads for all CEDMs, with differing nozzle lengths, were found to be within the allowable of the design specification. Tables 3.7-30 and 3.7-31 show loads along the CEDM and at the CEDM nozzle. In addition to seismic, these loads include both deterministic and random vibrational loads. Stresses resulting from these loads were determined to be well within stress allowable as described below. Deflections determined by the analysis were well within the values for which the tripping capability of the mechanism has been demonstrated.

For the pressure-retaining components of the CEDM structure and CEDM nozzles, a stress analysis was performed in accordance with the ASME Boiler and Pressure Vessel Code, Sections II and III. Four loading conditions, design (normal plus upset), emergency, faulted, and test, were considered. Five critical locations in the housing wall and the CEDM nozzles were examined for primary stresses. All omega seals and threaded connections were also examined. These critical locations and interface areas are indicated in figure 3.7-46. Tables 3.7-28, 3.7-32, 3.7-33, and 3.7-34 summarize the various computed stress intensities and compare these to the stress allowable.

Scramability of the CEDM was demonstrated under static and dynamic (pluck test) type of deflection conditions of the three most significant modes of the free standing CEDM. Actual static and initial dynamic deflection conditions were selected conservatively high (maximum deflection of CEDM was 4 inches) during these tests. Maximum RSS deflection value for the San Onofre Units 2 and 3 CEDM is calculated as 0.5 inches. The scram time did not change up to 3 inches deflection values and the maximum increase of the entire test series remained within 10% of the undeflected CEDM. Figure 3.7-47 presents the average extension shaft location as a function of time during pluck tests of each of the three modes studied. In all cases, scram time allowable were satisfied. Tables 3.7-28 and 3.7-35 summarize the RSS deflections for the San Onofre Unit 2 and 3 CEDMs.

Forced sinusoidal vibration testing of the free standing CEDM demonstrated that its major natural frequencies and mode shapes closely coincide with those predicted by analysis. Table 3.7-36 provides the comparison. Critical damping ratios for all significant resonance modes of the free standing CEDM were found to be in excess of the 2% value used in analysis.

Acceleration controlled, sinusoidal vibration testing of the supported CEDM demonstrated that its major natural frequencies and mode shapes closely coincide with those predicted by analysis. Table 3.7-37 provides the comparison. The test clearly demonstrated that the response of the CEDM at its lowest resonance mode (5.6 Hz) is effectively curbed by the seismic snubber system. This experimental frequency is comparable to the analytical modes of 4.7 and 7.2 Hz, which combines into one single mode when the drive shaft inertia is modeled less conservatively. The CEDM response at the 10.8 Hz resonance is considered negligible. The 13.8 Hz resonance compares well with the analytical frequency of 14.4 Hz and yields the highest nozzle loadings since, in this mode, the CEDM shroud reveals a modal point close to the support elevation. The fourth mode was considered a support structure table resonance and did not contribute significantly to the nozzle loading. Critical damping ratios determined by the test were well above the 2% used in analysis. The seismic support snubber was found to contribute to the damping when the CEDM was excited at its lowest natural frequency and less so when the CEDM was vibrating at the 13.8 Hz resonance (minimum ratios of 4.5 and 2.5% of critical damping, respectively).

The supported CEDM was exposed to random, multi-frequency (1/6 octave spacing) horizontal excitation tests and biaxial excitation tests (with equal input motions in the horizontal and vertical directions). Test response spectra enveloped the required response spectra over the applicable frequency range. Table 3.7-38 compares the results of a typical test to analysis. Input intensities averaged 11% above the DBE values. For these input conditions, the measured CEDM nozzle stresses, including drive shaft impacting, were only slightly above (10-15%) the computed values and well within nozzle allowable. The maximum relative displacement of the snubber ends during the simulated DBE remained below 0.2 inches. The test further demonstrated that the snubber always returns to its neutral position, during and following the seismic event.

Table 3.7-30

CEDM LOADS - PRESSURE HOUSING AND NOZZLE

Height Along CEDM (in.)	Axial Force Mechanical (lbs)	Shear Force (lbs)			Bending Moment (in.-lbs)		
		Mechanical	OBE	DBE	Mechanical	OBE	DBE
-22.7	4173	561	1353	1974	15150	52055	76286
11.5	4173	561	1353	1974	13990	32022	48978
17.7	3881	446	1301	1897	12874	24462	38110
19.7	3881	446	1301	1897	12530	22132	34560
20.3	4131	416	1250	1823	12391	21550	33681
25.3	3978	411	1152	1678	10809	15780	25813
30.5	3605	460	1152	1678	9303	11770	19462
35.5	3154	437	980	1424	7798	9385	16231
37.5	2803	431	742	1104	7116	8626	14990
39.5	2265	582	1246	1818	6431	8022	14000
44.7	2265	819	1391	2667	5671	11330	17363
51.8	1674	638	1391	2667	2684	4660	8791
54.8	1258	193	216	329	2261	4450	8330
59.1	1258	193	216	327	1993	4143	7791
95.0	1017	53	93	172	764	2418	3604
128.7	920	59	74	136	1093	2275	3582
162.4	768	50	59	80	1496	2790	5406
192.5	560	43	58	89	1093	2430	4780
196.2	560	52	79	127	1193	2407	4769
204.5	297	36	79	147	974	2066	4165
232.8	297	35	73	147	0	0	0

Table 3.7-31

CEDM LOADS - COIL STACK AND SHROUD

Height Along CEDM (in.)	Axial Force Mechanical (lbs)	Shear Force (lbs)			Bending Moment (in.-lbs)		
		Mechanical	OBE	DBE	Mechanical	OBE	DBE
25.3	1252	37	16	28	407	571	945
30.5	1252	58	103	171	423	626	1011
35.5	1252	72	159	295	113	121	198
39.5	1252	233	579	983	233	626	1121
44.7	1252	757	1807	2860	975	2429	4033
52.7	1252	757	1807	2860	4454	10374	16220
70.7	1278	126	182	290	3487	12923	18890
106.7	1257	111	120	197	4820	15615	23044
141.9	1193	120	112	215	4864	15550	23286
175.3	1050	162	287	472	5811	13813	22451
214.7	252	116	287	472	1305	2615	4066
232.8	0	74	145	226	0	0	05

Table 3.7-32
COMPARISON OF COMPUTED CEDM STRESS INTENSITIES
WITH STRESS ALLOWABLE
(OMEGA SEAL STRESSES IN LB/IN.^{2})

Location	Conditions	Design (Normal plus Upset)	Emergency[a]	Test
Seal A	Stress Intensity	10,852	9,760	13,580
	Pm Allowable	Sm = 16,600	1.2 Sm = 20,256	0.9 Sy = 19,260
Seal B	Stress Intensity	11,735	10,554	14,636
	Pm Allowable	Sm = 16,600	1.2 Sm = 20,256	0.9 Sy = 19,260
Seal C	Stress Intensity	11,735	10,554	14,686
	Pm Allowable	Sm = 16,600	1.2 Sm = 20,256	0.9 Sy = 19,260
Seal D	Stress Intensity	11,735	10,554	14,686
	Pm Allowable	Sm = 23,300	1.2 Sm = 27,960	0.9 Sy = 36,820

[a] Stress intensity also applies to the faulted condition; however, faulted allowable exceed emergency allowable and thus are not shown.

Table 3.7-33
COMPARISON OF COMPUTED CEDM STRESS INTENSITIES
WITH STRESS ALLOWABLE
(SCREW THREAD STRESSES IN LB/IN.^{2})

Location	Conditions	Design (Normal plus Upset)	Emergency[a]	Test
Thread A	Stress Intensity	1,701	1,933	1,672
	Allowable	0.6 Sm = 9,960	0.6 Sm = 10,128	0.6 Sm = 11,520
Thread B	Stress Intensity	1,954	2,044	1,961
	Allowable	0.6 Sm = 9,960	0.6 Sm = 10,128	0.6 Sm = 11,520
Thread C	Stress Intensity	4,603	4,226	5,097
	Allowable	0.6 Sm = 9,960	0.6 Sm = 10,128	0.6 Sm = 11,520
Thread D	Stress Intensity	2,281	2,103	2,398
	Allowable	0.6 Sm = 13,980	0.6 Sm = 13,980	0.6 Sm = 13,980

[a] Stress intensity also applies to the faulted condition; however, faulted allowables exceed emergency allowables and thus are not shown.

Table 3.7-34
COMPARISON OF COMPUTED CEDM STRESS INTENSITIES
WITH STRESS ALLOWABLE
(CRITICAL WALL SECTION STRESSES IN LB/IN.^{2})

Location	Conditions	Design (Normal plus Upset)	Emergency[a]	Test
Section I	Stress Intensity	9,957	9,198	12,407
	Pm Allowable	Sm = 16,600	1.2 Sm = 20,256	0.9 Sy = 14,742
Section II	Stress Intensity	13,977	18,658	13,820
	Pm Allowable	Sm = 16,600	1.2 Sm = 20,256	0.9 Sy = 19,260
Section III	Stress Intensity	14,091	12,674	17,633
	Pm Allowable	Sm = 18,900	1.2 Sm = 23,016	0.9 Sy = 21,510
Section IV	Stress Intensity	24,462	22,578	30,446
	Pm Allowable	Sm = 29,900	1.2 Sm = 36,468	0.9 Sy = 64,215
Section V	Stress Intensity	11,352	10,245	14,177
	Pm Allowable	Sm = 23,300	1.2 Sm = 27,960	0.9 Sy = 26,820

[a] Stress intensity also applies to the faulted condition; however, faulted allowables exceed emergency allowables and thus are not shown.

Table 3.7-35

DEFLECTIONS OF SAN ONOFRE UNITS 2 AND 3 CEDMS UNDER SEISMIC LOADING - PRESSURE HOUSING

Height Along CEDM (in.)	RSS Deflection Under OBE Loading (in.)	RSS Deflection Under DBE Loading (in.)
-22.7	0.000	0.000
11.5	0.027	0.053
17.7	0.035	0.069
19.7	0.038	0.074
20.3	0.039	0.075
25.3	0.045	0.088
30.5	0.054	0.101
35.5	0.064	0.113
37.5	0.068	0.118
39.5	0.072	0.123
44.7	0.082	0.136
51.8	0.095	0.153
54.8	0.100	0.160
59.1	0.108	0.170
95.0	0.173	0.327
128.7	0.286	0.533
162.4	0.352	0.650
192.5	0.342	0.626
196.2	0.338	0.616
204.5	0.325	0.590
232.8	0.322	0.540

Table 3.7-36

COMPARISON OF COMPUTED AND MEASURED NATURAL FREQUENCIES FOR FREE STANDING CEDM

Significant Natural Frequencies (Hz)	
Analytical	Experimental
2.95	2.73
11.80	10.50
14.50	14.25
17.30	--

Table 3.7-37

COMPARISON OF NATURAL FREQUENCIES FOR THE SUPPORTED CEDM (ANALYTICAL VS. EXPERIMENTAL)

Frequencies as Computed for SCE Plant (Hz)	Frequencies as Computed for Test Configuration (Hz)	Frequencies as Determined by Test (Hz)
4.78[a]	4.73[a]	
7.33[a]	7.23[a]	5.6[a]
11.18	12.15	10.8
13.14	13.14	--
14.36[a]	14.51[a]	13.8[a]
17.05[a]	17.2[a]	--
20.22	--	20.7
32.35	31.1	--

[a] Indicates high modal participation.

Table 3.7-38

COMPARISON OF SIGNIFICANT ANALYTICAL AND EXPERIMENTAL RESULTS FOR CEDM UNDER DBE LOADING CONDITIONS

Parameter	CEDM Supported By Head Lift Rig[a] (RSS)	CEDM Supported By Test Fixture (RSS)	Test Results[b] (Peak Amplitudes)
Nozzle load-bending moment due to seismic	75.7 inch kips	78.9 inch kips	~89.6 inch kips
Displacement: at snubber level, at bottom of shroud, at top of shroud	0.273 inch 0.136 inch 0.538 inch	0.255 inch 0.145 inch 0.472 inch	0.354 inch ----- -----
Max. deflection: on shroud, on pressure housing	0.538 inch 0.548 inch	0.472 inch 0.525 inch	----- -----

(a) Analysis performed for nozzle length employed in test.

(b) Note that test spectrum was considerably above R.R.S. and that nozzle stresses include impact stresses caused by lateral shifting of CEDM components. (High Frequency)

3.7.3.15 Analysis Procedure for Damping

The analysis procedure for damping of Seismic Category I subsystems is given in Section 3.2.1 of reference 5 and section 3.7.3.14, appendix 3.7B.2.4 describes the damping of the piping systems.

3.7.4 SEISMIC INSTRUMENTATION PROGRAM

3.7.4.1 Comparison with NRC Regulatory Guide 1.12, Revision 2, (March, 1997)

The seismic instrumentation program is consistent with the recommendations of NRC Regulatory Guide 1.12, Revision 2.

3.7.4.2 Location and Description of Instrumentation

The following instrumentation and associated equipment are used to measure plant response to earthquake motion.

A. Four remote triaxial time/history strong-motion accelerographs (SSA-1)

B. Two seismic switches (Integral part of 2UA-8020)

C. Personal Computer with special software.

D. Three strong motion accelerometers (FBA-3)

E. Annunciator (2UA-8020)

F. Three Solid State Accelerographs (SSA-3)

The location of seismic instrumentation is outlined in table 3.7-39. Seismic instrumentation is not installed at Unit 3, because Unit 3 is identical in design to Unit 2 and is located on the same soil foundation.

3.7.4.2.1 Strong-Motion Accelerographs

Strong-motion accelerographs produce a record of the time-varying acceleration at the sensor location. The records will be used directly for comparison with calculated motions determined from the design model for the same location and subsequently converted to response spectra form for comparison with design response spectra.

Each sensor unit contains three accelerometers mounted in a mutually orthogonal array. The principal axes of all accelerometers are oriented with one horizontal axis parallel to a major horizontal axis assumed in the seismic analysis.

There are three FBA-3 type strong motion accelerometers in the SSA-3 system. These are located at the containment base in the tendon gallery, containment operating deck vertically above the unit in the tendon gallery, and adjacent to the reactor coolant pump base.

The three accelerometers (FBA-3) in the SSA-3 system are activated by built-in triaxial seismic triggers. Each FBA-3 unit sends a signal to the SSA-3 recording unit, located in panel 2/3L-167.

The remaining four SMAs are in the SSA-1 system and are located at the auxiliary building base and roof, safety equipment building base slabs, and a free field. These units, with the exception of the free field, are activated by integral triaxial seismic triggers. These particular accelerographs store the event data in reliable CMOS memory in the unit itself which must be retrieved from the field to access the stored data. The free field accelerograph is connected to a telephone modem and the stored data can be retrieved either locally using a portable computer or at the seismic analysis computer at panel 2/3 L-167 using the telephone modem.

The selection of these locations is based on the requirements of Regulatory Guide 1.12, Revision 2.

Table 3.7-39
DESCRIPTION OF SEISMIC INSTRUMENTATION (Sheet 1 of 3)

Item	Component	Location	Elevation (ft)	Elevation (in.)	Setpoint (g)	Operating Range
1[(a)]	Strong-motion accelerometer, 2XT-8020C	Adjacent to reactor coolant pump motor on the wall of same base	52	0	--	-2 to +2g
2	Strong-motion accelerometer, 2XT-8020A	Containment base in tendon gallery	(-)6	6	--	-2 to +2g
3[(a)]	Strong-motion accelerometer, 2XT-8020E	Containment operating level	63	6	--	-2 to +2g
4	Strong-motion accelerograph, 2XT-8020F	Auxiliary building radwaste area basement	9	0	0.019 Vert 0.019 Horiz	-2 to +2g
5	Strong-motion accelerograph, 2XT-8020G	Auxiliary building roof	85	0	0.019 Vert 0.019 Horiz	-2 to +2g
6	Strong-motion accelerograph, 2XT-8020I	Safety equipment building base slab	(-)15	6	0.019 Vert 0.019 Horiz	-2 to +2g

Table 3.7-39
DESCRIPTION OF SEISMIC INSTRUMENTATION (Sheet 2 of 3)

Item	Component	Location	Elevation (ft)	Elevation (in.)	Setpoint (g)	Operating Range
7	a) Seismic switch (containment operating deck) (input from 2XT-8020E)	Part of 2UA-8020 annunciator located in Item 12	63	6	0.50 horiz 0.45 vert	-2 to +2g
	b) Seismic switch (containment base in the tendon gallery) (input from 2XT-8020A)	Part of 2UA-8020 annunciator located in Item 12	(-)6	6	0.40 horiz 0.50 vert	-2 to +2g
8	Solid state accelerograph 2XR-8020A (Input from Item 2)	Installed in Item 12	--	--	0.019g	--
9	Seismic alarm annunciator, 2UA-8020 (with seismic switch electronics items 7a and 7b). Items 2 and 3 are sensors.	Installed in Item 12	--	--	--	--
10	Solid State Accelerograph 2XR-8020C (Input from Item 1)	Installed in Item 12	--	--	0.019g	--
11	Solid State Accelerograph 2XR-8020E (Input from Item 3)	Installed in Item 12	--	--	0.019g	--

Table 3.7-39
DESCRIPTION OF SEISMIC INSTRUMENTATION (Sheet 3 of 3)

Item	Component	Location	Elevation (ft)	Elevation (in.)	Setpoint (g)	Operating Range
12	Seismic event recording panel, 2/3 L-167	Control building (auxiliary building) control room cabinet area	30	0	--	--
13	Strong-motion Accelerograph, 2XT-8020L	Site free field, west of AWS building	20	0	0.019 vert 0.019 horiz	-2 to +2g

[a] Instruments inside the containment.

3.7.4.2.2 Seismic Switches

The signals from two of the strong-motion accelerometers, located on the containment operating deck support and containment base in the tendon gallery, provide seismic switch outputs for actuating visual and audible annunciators in the control room if the operating basis earthquake (OBE) is exceeded at either of the two accelerometer locations. The selection of these locations is based on the requirements of Regulatory Guide 1.12 Revision 2.

3.7.4.2.3 Solid State Accelerographs

The Solid State Accelerographs mounted in panel 2/3L-167 are manufactured by Kinemetrics, model SSA-3. This unit is a digital solid state recorder that will record the accelerometer output data from the FBA-3 accelerometers at the Tendon Gallery (2XT-8020A), adjacent to reactor coolant pump motor base on the wall (2XT-8020C) and containment operating deck (2XT-8020E). The SSA-3 recorders are linked to a local seismic computer that will access the information in their RAM and use software to generate a response spectrum. The SSA-3 is utilized for its data integrity and ease of playback. There is no loss of data due to compression and playback is achieved by utilization of a PC communications program. Time of event, peak acceleration, and duration of each event are available in each event header.

The SSA-3 is powered by a SSA-3 power supply (2XY-8020) also located in panel 2/3L-167. This unit provides indicators for "AC on" for power to the component and event exceedance when the recorder is triggered (at 0.019g). This unit has a reset switch to turn off the event indicator and a DC volt meter switch to test and verify the backup battery voltage.

3.7.4.2.4 Recording and Playback Console

A console in the control room cabinet area houses the recording units for the three containment SMAs and a computer for all SMAs. The seismic analysis computer is used in conjunction with the FBA-3 strong motion accelerometer sensors, to produce a time-history record of the earthquake. This console houses the digital solid state accelerograph. It also contains audible and visual annunciators associated with the seismic switches, audible and visual annunciators wired to display initiation of the SSA-3 recorders, and the power supply components for all equipment in the console.

3.7.4.3 <u>Control Room Operator Notification</u>

Activation of either seismic trigger causes audible and visual annunciation in the control room to alert the plant operator that an earthquake has occurred. These triggers cause initiation of the SSA-3 recording system at horizontal or vertical acceleration levels higher than the expected background level.

Audible and visual annunciators are provided in the control room to indicate if OBE accelerations have been exceeded at the containment foundation or at the containment operating level.

The peak acceleration level experienced on the containment base slab and other locations is available immediately following the earthquake. This level is obtained by playing back the recorded SMA data from the three SSA-3 recording units and reading the peak value for this data from the seismic analysis computer.

After a seismic event, data is retrieved electronically from the SSA-3 and SSA-1 RAMs and stored in the local seismic computer. This data is then used to generate response spectrums for comparison of earthquake data to design data. The information stored in the local computer as well as the raw data stored in the SSA-1 (free field) and SSA-3 is available to other computers via a modem link to the telephone system.

3.7.4.4 Comparison of Measured and Predicted Responses

Initial determination of the earthquake level is performed after the earthquake by comparing the measured response spectra for the containment base slab with the OBE response spectra for the corresponding location. If the measured spectra exceed the OBE response spectra, action will be taken consistent with the requirements of 10CFR100, Appendix A.

When an earthquake occurs and the level is equal to or greater than 0.05g, the data from all seismic recorders are retrieved and reviewed in accordance with ANSI Standards. Basically, the data from the instruments are analyzed to obtain the seismic accelerations experienced at the location of major Seismic Category I structures and equipment. The measured responses from the strong-motion accelerograph and the peak recording accelerographs are compared to the design response spectra at the location of each Seismic Category I structure and system to determine whether the structure or system is still capable of performing its function. If the measured responses are less than the values used in the design and qualification of the Seismic Category I structures, systems, and equipment, the structure, system, or equipment is considered adequate for future operations. Otherwise, a more detailed evaluation of the individual components that had measured responses exceeding design values will be performed to establish the operability of the plant. This evaluation will account for actual margins of safety established with respect to design and qualification levels, the susceptibility of the components to damage by severe seismic motion, and the actual role of the component related to the safe operation of the plant.

3.7.5 REFERENCES

1. Newmark, N. M. and Hall, W. J., "Seismic Design Criteria for Nuclear Reactor Facilities," Proceedings, 3rd World Conference on Earthquake Engineering Vol 2, Santiago, Chile, 1969.

2. Jennings, P. C., Housner, G. W., and Tsai, N. C., "Simulated Earthquake Motions," Earthquake .Engineering Research Laboratory, California Institute of Technology, April 1968.

3. Tsai, N. C., "Spectrum-Compatible Motions for Design Purposes," Journal of Engineering Mechanics Division, ASCE, Vol 98, EM2, April 1972.

4. McNeill, R. L., "Machine Foundations: The State-of-the-Art," Proceedings of Specialty Session 2, Seventh International Conference on Soil Mechanics and Foundation Engineering, Mexico city, Mexico, August 1969.

5. "Seismic Analyses of Structures and Equipment for Nuclear Power Plants," BC-TOP-4A, Revision 3, Bechtel Power Corporation, San Francisco, California, November 1974.

6. "Final In-Structure Response Spectra Analysis for the Containment and Interior Structure, San Onofre Nuclear Generating Station Units 2 and 3; Bechtel Power Corporation, LAPD, August 1973.

7. "Methods of Direct Application of Element Damping, San Onofre Units 2 and 3," Bechtel Power Corporation, Los Angeles office, January 1972.

8. "Nuclear Reactors and Earthquake," TID 7024, U.S. Atomic Energy Commission, Division of Technical Information, August 1963. Distributed by National Technical Information Service, U.S. Department of Commerce.

9. Przemieniecki, J. S., "Theory of Matrix Structural Analysis," Chapter 13, McGraw-Hill Book Company, New York, New York, 1968.

10. ICES STRUDL-II, "The Structural Design Language Engineers Users Manual," MIT Press, Cambridge, Mass., 1968.

11. "Structural Analysis of the 16 x 16 Fuel Assembly' for Combined Seismic and Loss of Coolant Accident Loading," Combustion Engineering, Ins., CENPD-178P, October 1976.

12. Fritz, R. J., "The Effect of Liquids on the Dynamic Motions of Immersed Solids," Journal of Engineering for Industry, Paper No. 71-VIB-100.

13. McDonald, C. K., "Seismic Analysis of Vertical Pumps Enclosed in Liquid Filled Containers," ASME Paper No. 75-PVP-56.

14. Pahl, P. J., "Modal Response on Containment Structures," Seismic Design for Nuclear Power Plants, MIT Press, Cambridge, Mass.

15. Forsberg, K., "Axisymmetrical and Beam-Type Vibrations of These Cylindrical Shells," AJAA Journal, Volume 7, February 1969.

16. MRI/STARDYNE - Static and Dynamic Structural Analysis System: User Information Manual, Control Data Corporation, June 1, 1970.

17. MRI/STARDYNE User Manual, Computer Methods Department, Mechanics Research, Inc., Los Angeles, California, January 1, 1970.

18. Hurty, W. C. and Rubenstein, M. F., Dynamics of Structures, Chapter 8, Prentice Hall, Inc., Englewood Cliffs, New Jersey, 1970.

19. "Seismic Category I Criteria and Implementation Program," December 1975, submitted on San Onofre Units 2 and 3, Dockets 50-361 and 50-362.

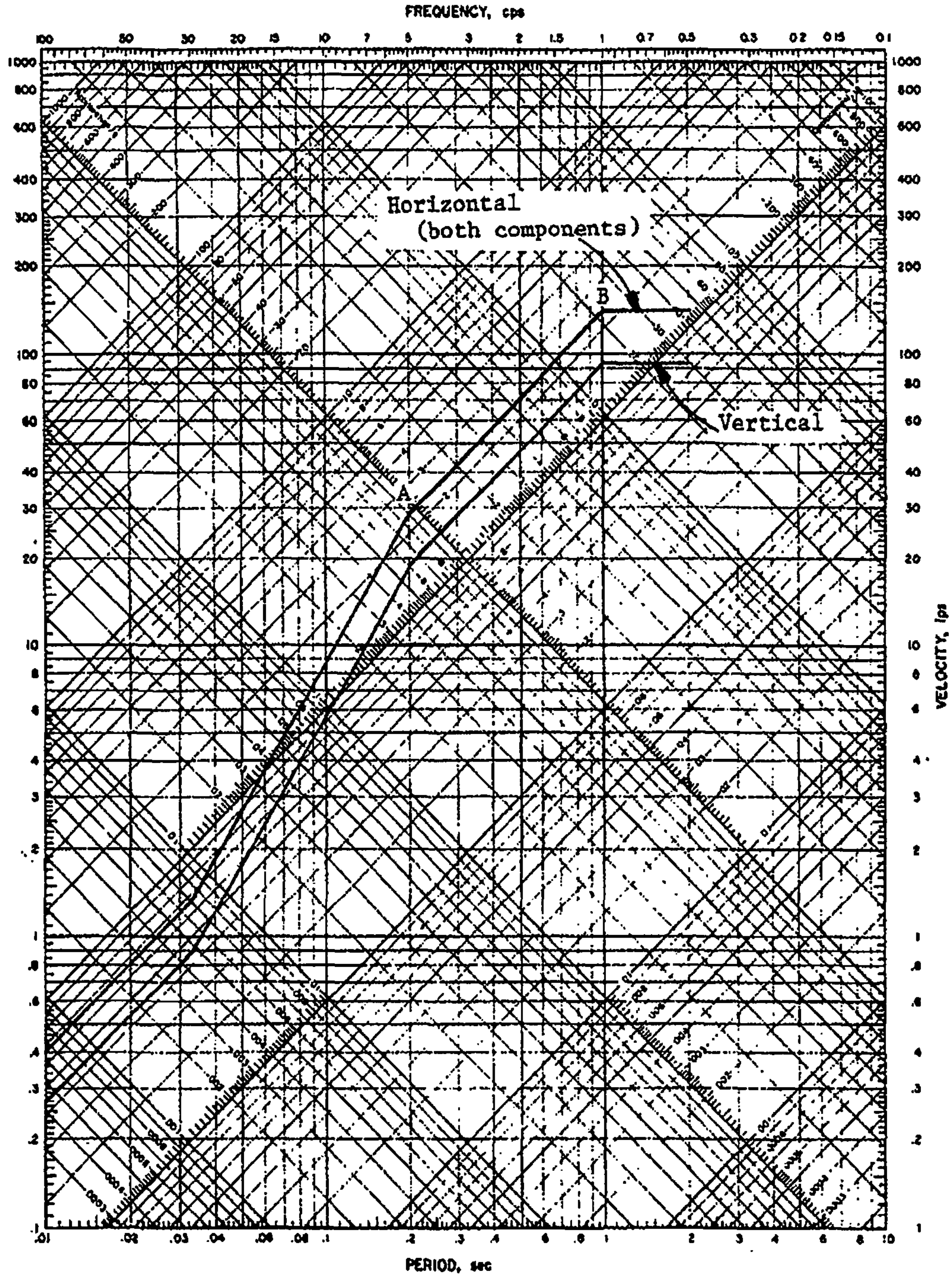

SAN ONOFRE
NUCLEAR GENERATING STATION
Units 2 & 3

SITE SPECIFIC DESIGN RESPONSE
SPECTRA FOR 2% DAMPING

Figure 3.7-1

10079-11D-570
12AU6

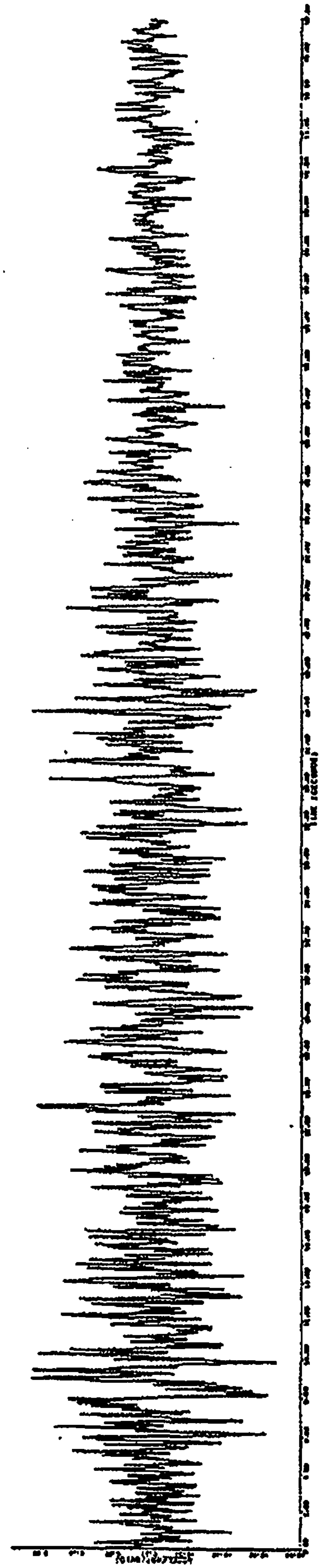

10079-11D-571
12AU6

SAN ONOFRE
NUCLEAR GENERATING STATION
Units 2 & 3

DBE ACCELERATION
TIME HISTORY

Figure 3.7-2

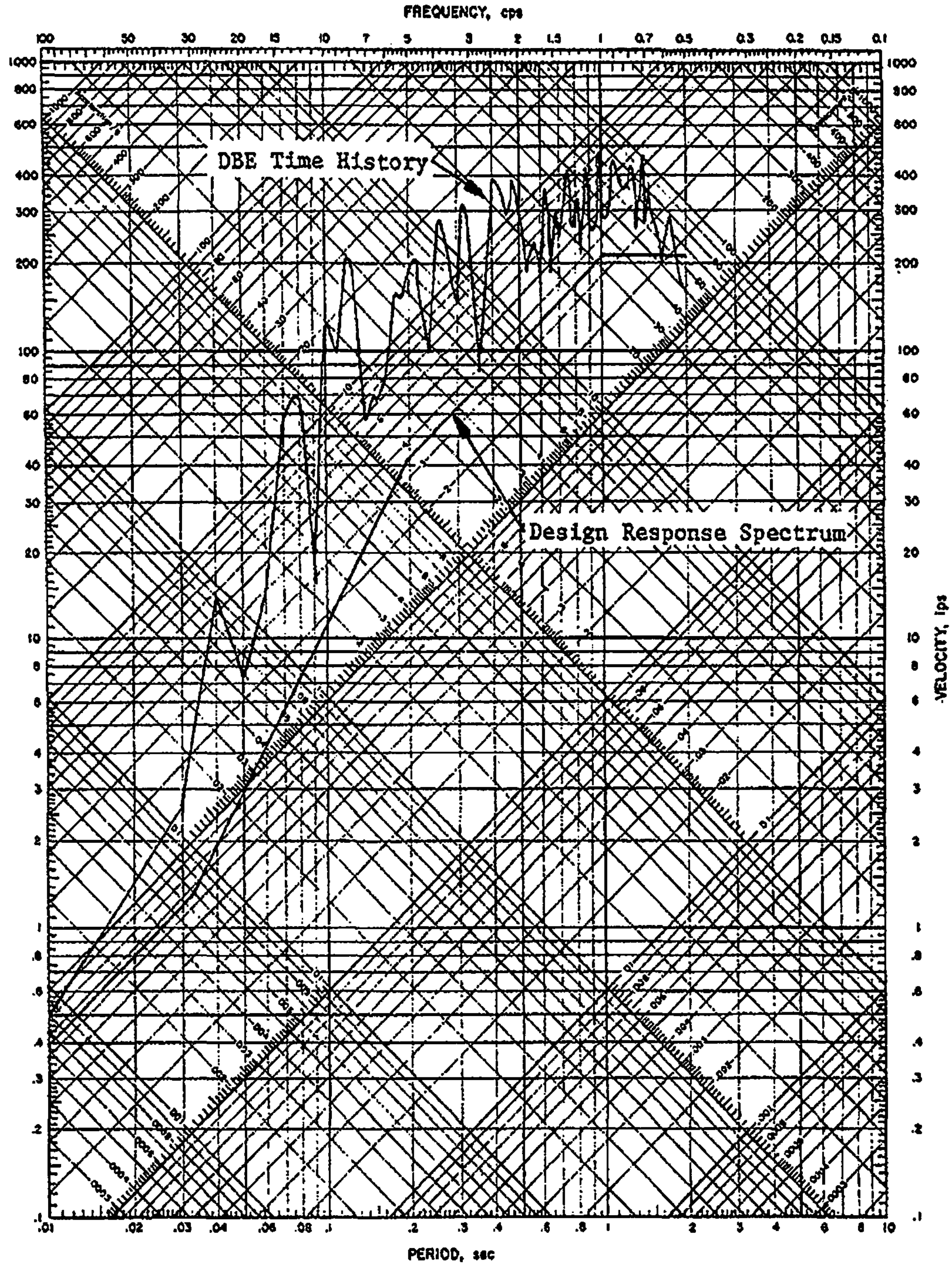

SAN ONOFRE
NUCLEAR GENERATING STATION
Units 2 & 3

DESIGN AND TIME-HISTORY SPECTRA
0% DAMPING

Figure 3.7-3

10079-11D-572
12AU6

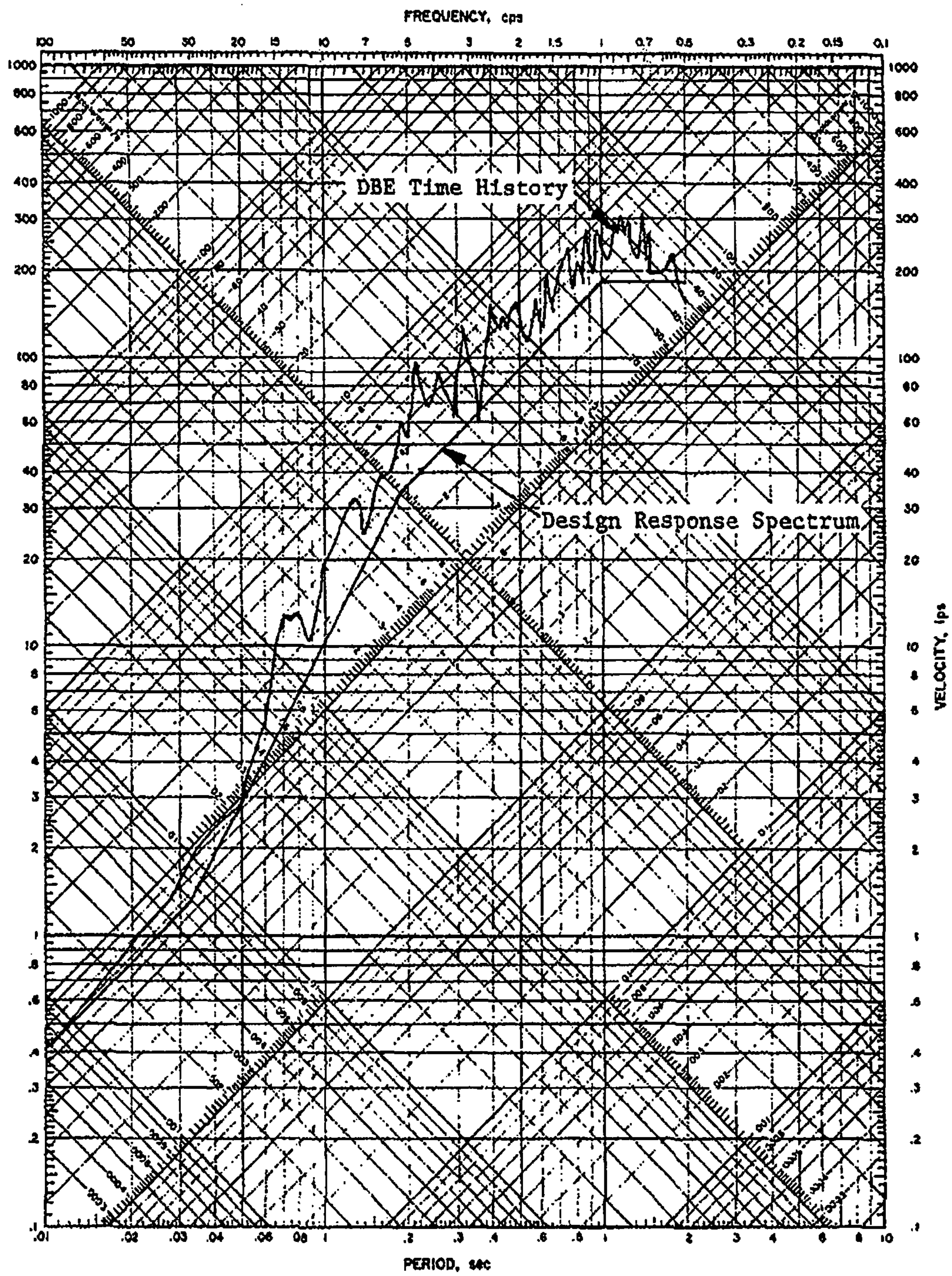

SAN ONOFRE
NUCLEAR GENERATING STATION
Units 2 & 3

DESIGN AND TIME-HISTORY SPECTRA
0.5% DAMPING

Figure 3.7-4

10079-11D-573
12AU6

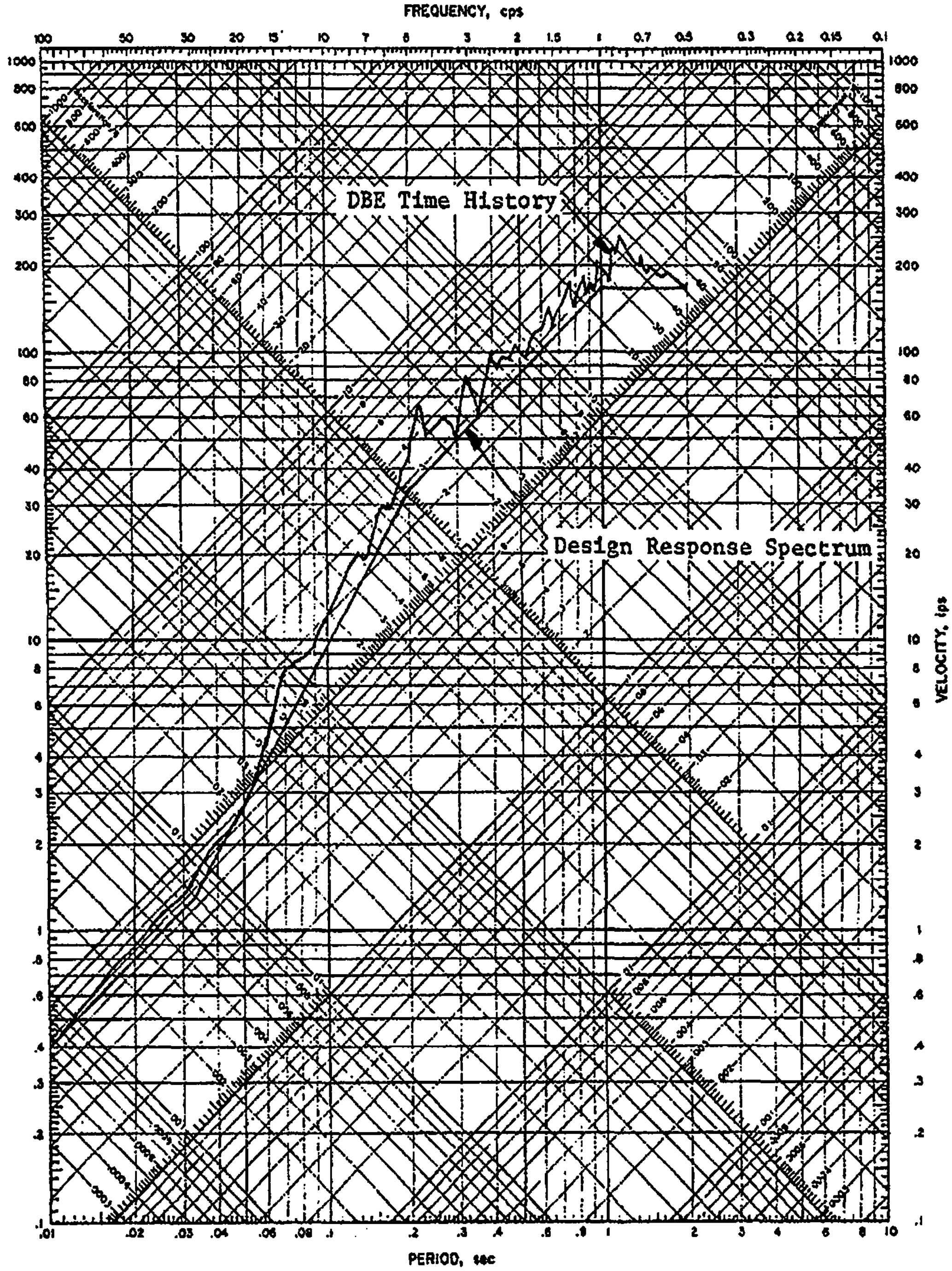

SAN ONOFRE NUCLEAR GENERATING STATION Units 2 & 3
DESIGN AND TIME-HISTORY SPECTRA 1% DAMPING
Figure 3.7-5

10079-11D-574
12AU6

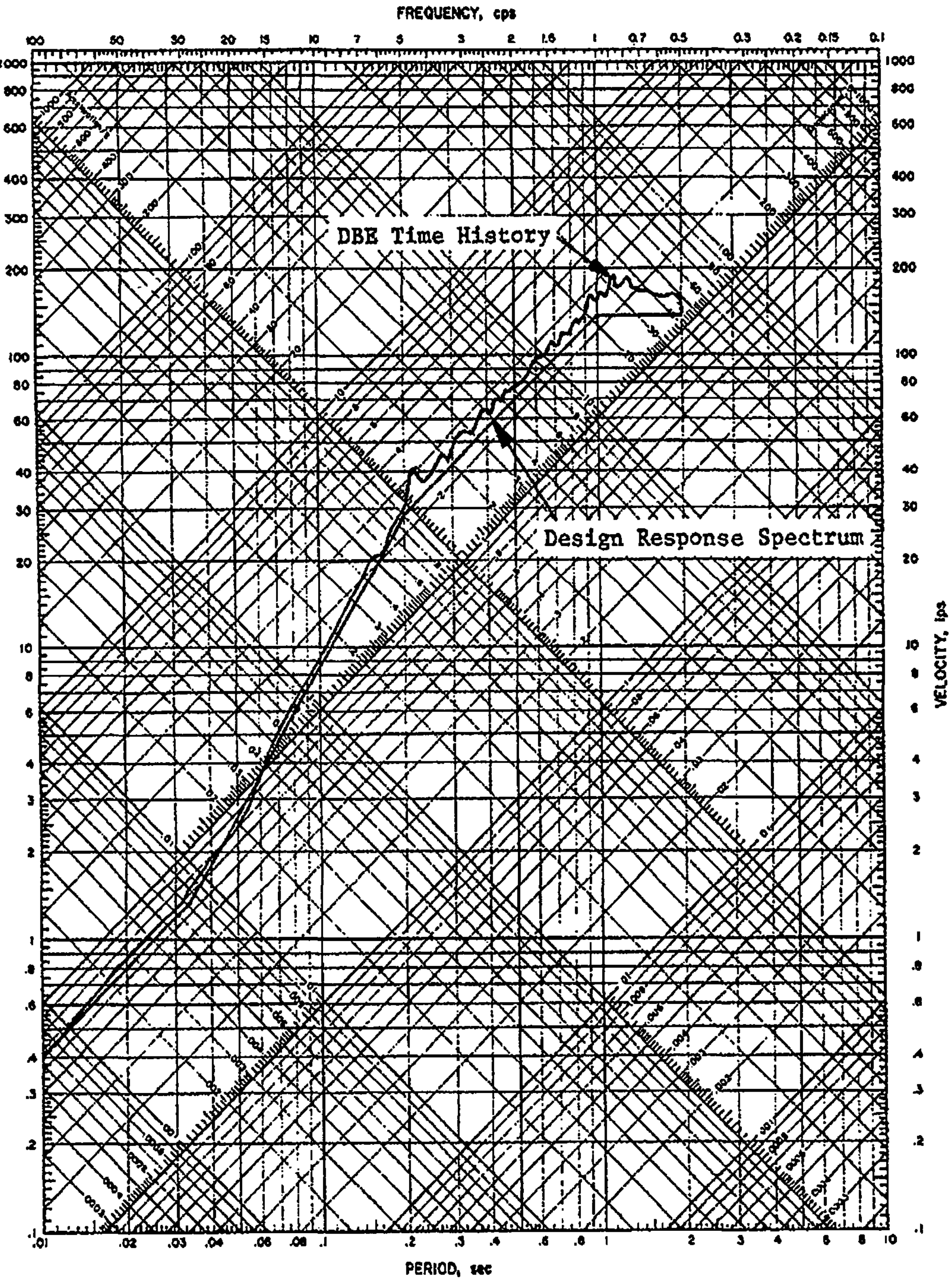

SAN ONOFRE
NUCLEAR GENERATING STATION
Units 2 & 3

DESIGN AND TIME-HISTORY SPECTRA
2% DAMPING

Figure 3.7-6

10079-11D-575
12AU6

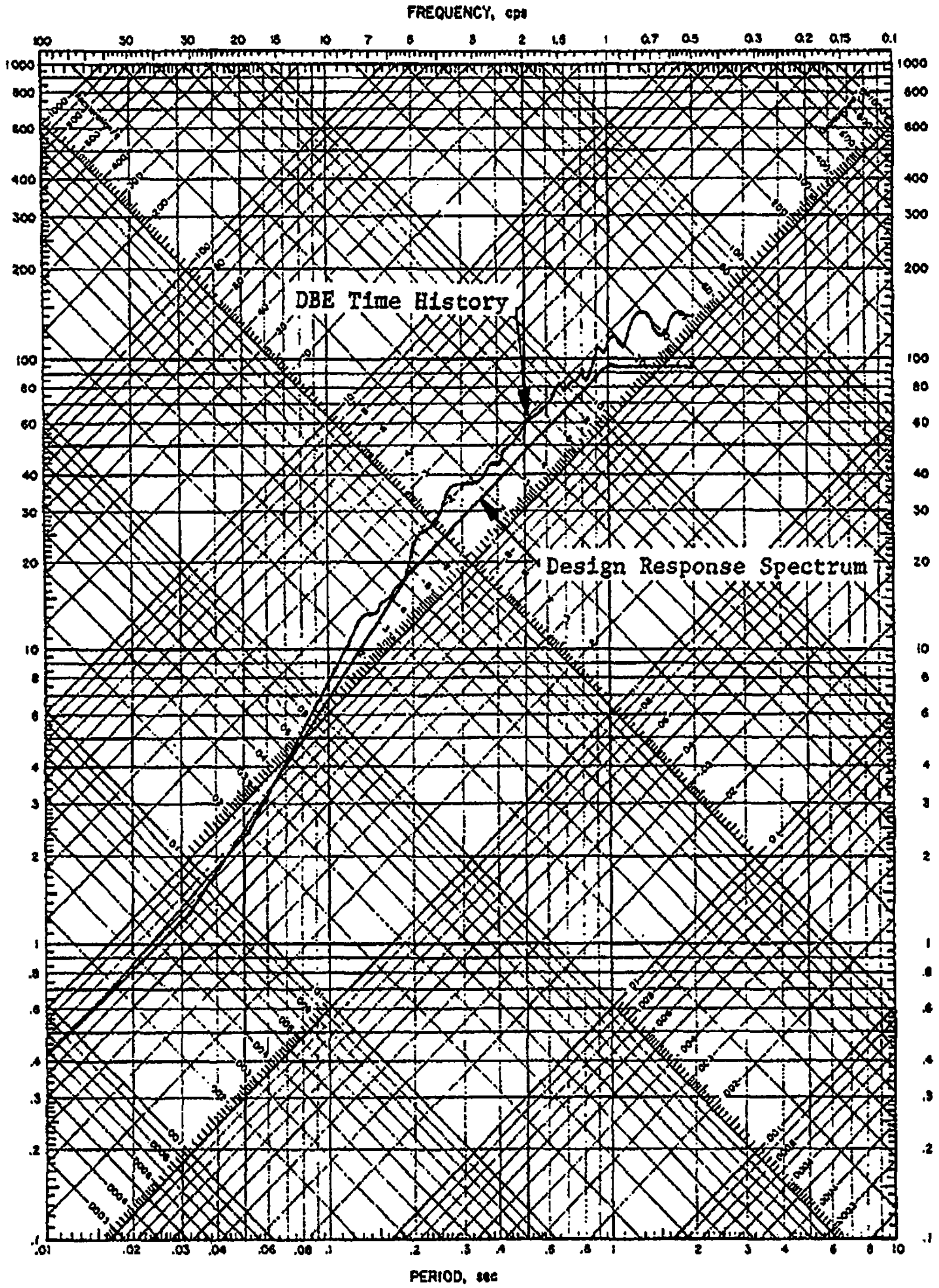

SAN ONOFRE
NUCLEAR GENERATING STATION
Units 2 & 3

DESIGN AND TIME-HISTORY SPECTRA
5% DAMPING

Figure 3.7-7

10079-11D-576
12AU6

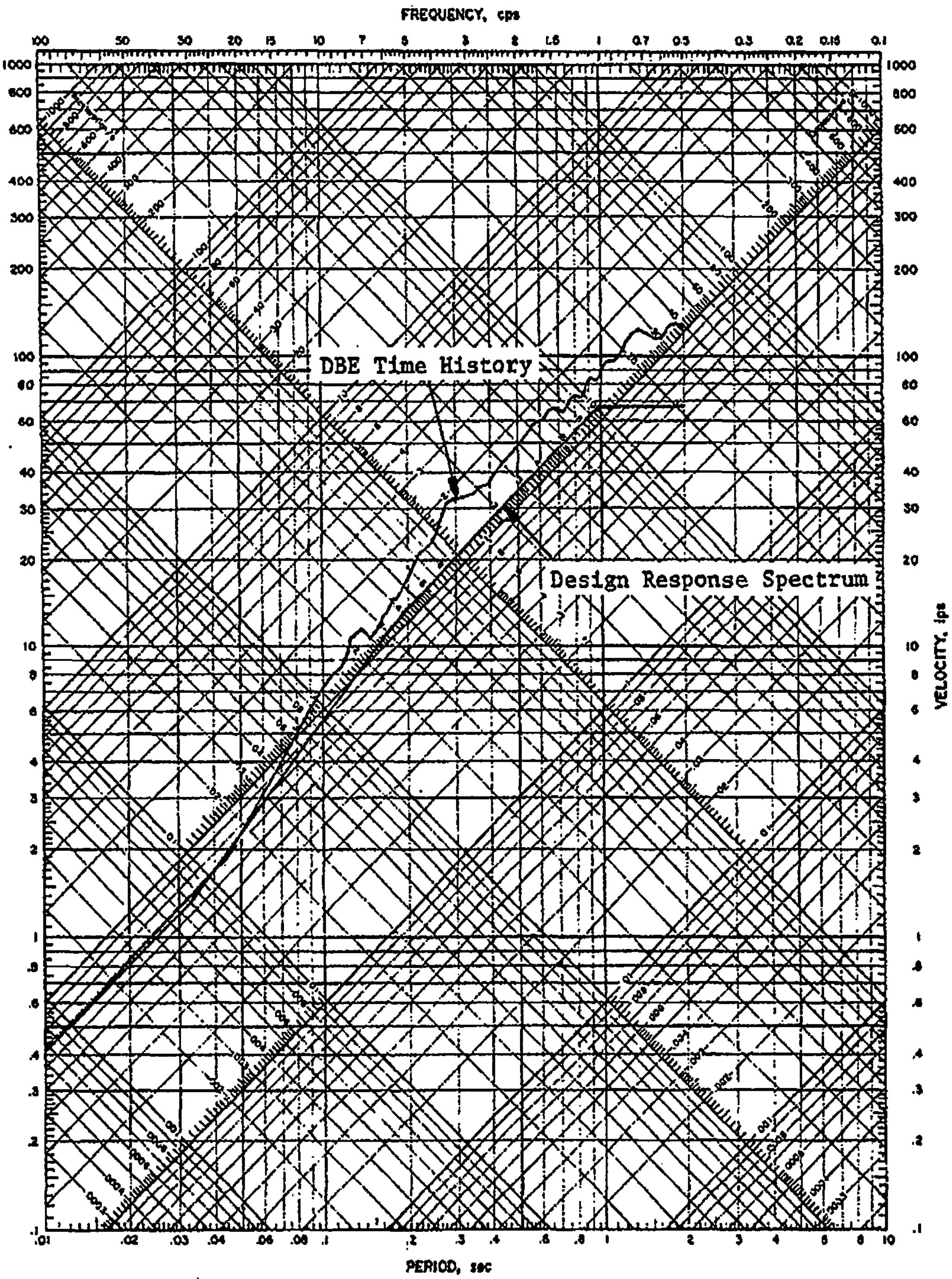

SAN ONOFRE NUCLEAR GENERATING STATION Units 2 & 3

DESIGN AND TIME-HISTORY SPECTRA 7% DAMPING

Figure 3.7-8

10079-11D-577
12AU6

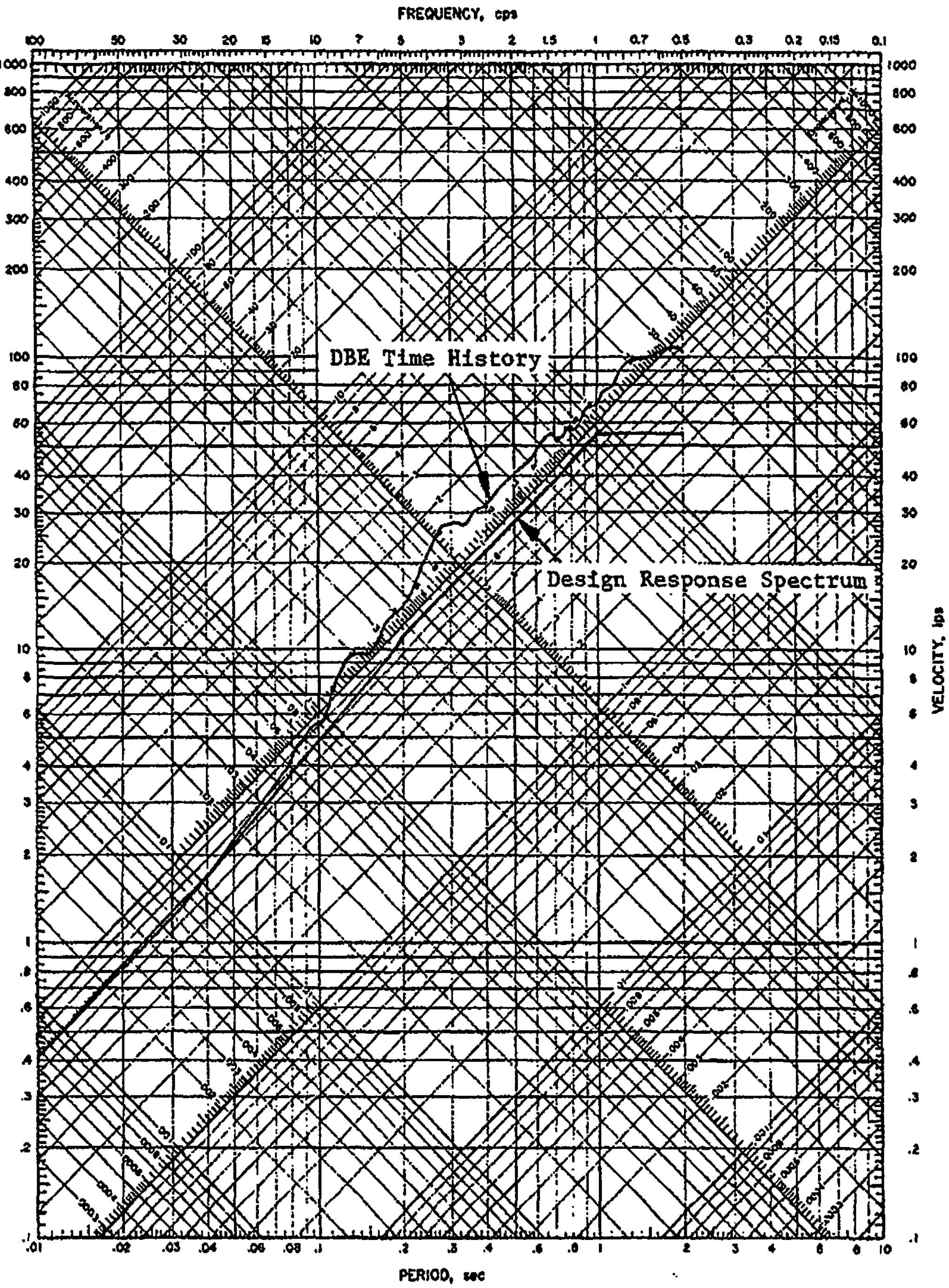

SAN ONOFRE
NUCLEAR GENERATING STATION
Units 2 & 3

DESIGN AND TIME-HISTORY SPECTRA
10% DAMPING

Figure 3.7-9

10079-11D-578
12AU6

3.7A APPENDIX 3.7A

SEISMIC RESPONSE SPECTRA

The SONGS design seismic response spectra are provided in the following figures:

- 3.7A-1 Design Basis Earthquake Vertical Acceleration Response Spectra, Parallel to Hot Leg Reactor Vessel Column Support
- 3.7A-2 Design Basis Earthquake Horizontal Acceleration Response Spectra, Parallel to Hot Leg Reactor Vessel Column Support
- 3.7A-3 Design Basis Earthquake Horizontal Acceleration Response Spectra, Parallel to Hot Leg Reactor Vessel Base Shear Key
- 3.7A-4 Design Basis Earthquake Horizontal Acceleration Response Spectra, Parallel to Hot Leg Reactor Vessel Nozzle Restraint
- 3.7A-5 Design Basis Earthquake Vertical Acceleration Response Spectra, Parallel to Hot Leg Steam Generator Base Support
- 3.7A-6 Design Basis Earthquake Horizontal Acceleration Response Spectra, Parallel to Hot Leg Steam Generator Snubber Support
- 3.7A-7 Design Basis Earthquake Vertical Acceleration Response Spectra, Parallel to Hot Leg RCP Base Support
- 3.7A-8 Design Basis Earthquake Horizontal Acceleration Response Spectra, Parallel to Hot Leg RCP Lower Horizontal Support
- 3.7A-9 Design Basis Earthquake Horizontal Acceleration Response Spectra, Parallel to Hot Leg RCP Upper Horizontal Support
- 3.7A-10 Design Basis Earthquake Horizontal Acceleration Response Spectra, Parallel to Hot Leg RCP Snubber Support
- 3.7A-11 Design Basis Earthquake Vertical Acceleration Response Spectra, Parallel to Hot Leg Pressurizer Base Support
- 3.7A-12 Design Basis Earthquake Horizontal Acceleration Response Spectra, Parallel to Hot Leg Pressurizer Base Support
- 3.7A-13 Design Basis Earthquake Horizontal Acceleration Response Spectra, Parallel to Hot Leg Pressurizer Shear Key Support